UNIVERSITÀ DEGLI STUDI DI MILANO

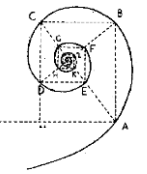

SCUOLA DI DOTTORATO

IN MEDICINA MOLECOLARE E TRASLAZIONALE

CICLO XXX

TESI DI DOTTORATO DI RICERCA

Settore Scientifico Disciplinare **MED/26**

AUTOLOGOUS INTRAMUSCULAR TRANSPLANTATION OF ENGINEERED SATELLITE CELLS INDUCES EXOSOME-MEDIATED SYSTEMIC EXPRESSION OF FUKUTIN-RELATED PROTEIN AND RESCUES DISEASE PHENOTYPE IN A MURINE MODEL OF LIMB-GIRDLE MUSCULAR DYSTROPHY TYPE 2I

Dottorando: **Paola FRATTINI**

Matricola N° **R11152**

Tutor: Prof. Giacomo Pietro COMI

Co-Tutor: Prof. Yvan TORRENTE

Coordinatore del dottorato: Prof. Riccardo GHIDONI

Anno Accademico 2016/2017

A Roby e papà,
Siate come il mare che infrangendosi contro gli scogli,
trova sempre la forza di riprovarci

SOMMARIO

Le α-dystroglycanopatie rappresentano un gruppo molto eterogeneo di distrofie muscolari, causate da un deficit di glicosilazione della proteina α-distroglicano. Dal momento che i domini glicosilici dell'α-distroglicano favoriscono il legame tra le proteine della matrice extracellulare e le proteine del citoscheletro della miofibra, l'ipoglicosilazione della proteina causa una rottura di questo legame, con conseguente sviluppo di fragilità della membrana sarcolemmatica e necrosi della miofibra. Ad oggi, non esistono terapie risolutive applicabili alle α-distroglicanopatie. Sono stati identificati diversi geni principali coinvolti nello sviluppo del fenotipi clinico; tutti questi geni codificano per glicosiltransferasi: enzimi coinvolti nella glicosilazione dell'α-dystroglycano. Tra questi, la mutazione del gene FKRP comporta l'insorgenza di un ampio spettro di fenotipi distrofici: da forme lievi quali la distrofia muscolare dei cingoli di tipo 2I (LGMD2I), a forme molto severe con possibile coinvolgimento del sistema nervoso, quali la distrofia muscolare congenita di tipo 1C (MDC1C), la sindrome di Walker Warburg (WWS), e la distrofia conosciuta come Muscle-Eye-Brain (MEB). La proteina FKRP esercita la sua funzione di glicosiltransferasi trasferendo un gruppo ribitolo fosfato da una molecola di CDP-ribitolo all' α-dystroglycano. Studi recenti hanno dimostrato che, cellule seminate in vitro, posso secernere l'FKRP nel loro terreno di coltura. Benchè il pathway di glicosilazione delle proteine avvenga a livello intracellulare, in accordo con quanto osservato in vitro, è stata riportata la presenza di glicosiltransferasi circolanti, genericamente definite ''glicosiltransferasi extracellulari''. Queste ultime possono circolare liberamente nel torrente circolatorio o, in alternativa, all'interno di una sottopopolazione di microvescicole di dimensioni nanometriche fisiologicamente secreta dalle cellule: gli esosomi. Partendo da queste osservazioni, abbiamo ipotizzato che la proteina FKRP, sia libera nella circolazione sanguigna che trasportata dagli esosomi, possa raggiungere ed esercitare la sua funzione glicosiltransferasica anche in siti molto distanti da quello di secrezione. In primo luogo, sono state isolate le cellule staminali multipotenti CD133+ dal sangue di un paziente MDC1C e le cellule satelliti da un modello murino di LGMD2I: il topo L276I^{KI}. Le cellule sono state ingegnerizzate con un vettore lentivirale esprimente la forma wild-type del gene FKRP umano. Inoltre, l'espressione della proteina esogena è stata valutata anche negli esosomi rilasciati dalle due popolazioni di cellule infettate. Successivamente, è stato eseguito un trapianto intramuscolare autologo delle cellule SCs infettate nel modello murino ed è stato valutato il recupero di espressione della proteina e il ripristino della sua attività glicosiltransferasica nei muscoli iniettati. Per valutare la presenza di FKRP nel torrente circolatorio, gli esosomi del plasma dei topi trapiantati sono stati isolati e caratterizzati. Gli esosomi sono risultati positivi per l'espressione della glicosiltransferasi. Inoltre, è stato evidenziato che la distribuzione sistemica di FKRP veicolata dagli esosomi favorisce il recupero di espressione della proteina in siti distati da quello del rilascio, determinando un recupero della glicosilazione dell'α-distroglicano in altri distretti muscolari (ad esempio il cuore) e un conseguente incremento della forza muscolare e della performance dei topi trapiantati, come dimostrano i risultati ottenuti dai test funzionali. L'utilizzo di un bioreattore per microfluidica ha permesso di mimare i processi di diffusione degli esosomi fra le cellule, fornendo dettagli importanti sulla cinetica di distribuzione propria degli esosomi e sui meccanismi alla base dell'interazione fra cellule target ed esosomi. I dati ottenuti supportano la possibilità di sviluppare un approccio terapeutico

trivalente, basato sulla combinazione di terapia cellulare e genica, che fisiologicamente promuovono lo sviluppo di una terapia esosoma-mediata. Il trapianto autologo di cellule staminali ingegnerizzate potrebbe simultaneamente favorire il recupero di espressione della proteina e un effetto di rigenerazione del tessuto distrofico, superando così il limite di un approccio basato solo sulla terapia genica. Inoltre, gli esosomi secreti dalle cellule staminali ingegnerizzate e trapiantate nel muscolo, potrebbero mediare un effetto terapeutico sistemico ottenendo un generale miglioramento del fenotipo distrofico. L'approccio basato sull'uso di esosomi è estremamente pioneristico e promettente, soprattutto nel campo delle miopatie metaboliche e delle distrofie muscolari la cui insorgenza è dovuta a deficit enzimatici e non a deficit di proteine strutturali.
Infatti, esosomi che trasportano target terapeutici (quali enzimi di natura esogena), diffondono rapidamente nel torrente circolatorio e raggiungono le cellule target, determinando un effetto terapeutico molto rapido, favorito da un recupero immediato dell'attività enzimatica.

ABSTRACT

α-Dystroglycanopathies are a group of heterogeneous dystrophic phenotypes associated to reduced levels of α-DG glycosylation.
Since the glycosylated domains of α-DG exert a key role in extracellular matrix proteins (ECM) binding to the myofiber cytoskeleton, the hypoglycosylation leads to the disruption of this linkage and, consequently, to sarcolemma fragility and myofiber necrosis. To date, any successful therapeutical approach has been developed in the field of α-dystroglycanopathies. Many genes have been found to be implicated in the α-DG glycosylation process; all these genes encode for glycosyltransferase enzymes. Of note, mutations occurring in one of these genes, the fukutin related protein (FKRP) give rise to different subtypes of clinical phenotypes, ranging from the mild limb girdle muscular dystrophy 2I (LGMD2I), to the severe congenital muscular dystrophy 1C (MDC1C), to Walker-Warburg Syndrome (WWS) and Muscle-Eye-Brain disease (MEB). FKRP glycosyltransferase exerts its glycosyltransferasic function by conveying a ribitol phosphate group from a CDP – ribitol to α-DG. Recent findings have reported cells ability to release FKRP in vitro. In line with this evidence, it has also been reported that some glycosyltransferases, generally referred to as ''extracellular glycosyltransferases'', freely circulate in the bloodstream or, alternatively, packed with a subpopulation of microvesicles (MVs) physiologically secreted by cells, named exosomes. Thus, we hypothesize that freely or exosome-carried FKRP might circulate as an extracellular glycosyltransferase, reaching distal compartments and acting as a "glycan remodeller". Interestingly, we firstly established a successful transduction of blood-derived CD133+ multipotent stem cells isolated from an MDC1C patient and FKRP L276I^{KI} murine satellite cells, exploiting a lentiviral vector expressing the wild-type isoform of human FKRP gene. Furthermore, we reported FKRP expression in infected LV-FKRP cells- derived exosomes. Subsequently, we performed an autologous intramuscular transplantation of LV-FKRP infected SCs in the L276I^{KI} mouse model and we evaluated the recovery of the exogenous protein expression and function. Similarly, we investigated the presence of FKRP positive exosomes in the plasma of transplanted FKRP L276I^{KI} mice. The exosome-mediated systemic distribution of FKRP glycosyltransferase favoured its rescue at distal sites, determining an overall recovery of α-DG glycosylation and improved muscle strength, as suggested by functional measurement performances. An in vitro model based on an optically accessible microfluidic bioreactor allowed us to mimic the exosome diffusion between cells in vivo, providing further details of functional kinetic and mechanisms underlying exosome uptake. Overall, observed data suggest the possibility to develop a trivalent therapeutical approach, based on the combination of: cell therapy, gene therapy, leading to a physiological exosome-mediated therapy. The autologous transplantation of engineered stem cells would simultaneously provide the recovery of the wild-type isoform of the mutated protein and tissue regeneration, thus overcoming the limits related to single gene therapy. Moreover, intramuscularly transplanted engineered cells- derived exosomes would allow toobtain a systemic amelioration of the dystrophic phenotype. This exosome-based approach is extremely pioneering and promising, particularly in the field of metabolic myopathies and all muscular dystrophies presenting an enzymatic defect, rather than a structural protein disruption. Indeed, vesicles carrying the exogenous

therapeutic enzyme rapidly diffuse through the bloodstream reaching target cells and promoting a fast response mediated by the stabilization of the enzymatic activity.

INDEX

1 INTRODUCTION

1.1 The skeletal muscle

1.1.1 Origins and Structure

Skeletal muscle has two key roles in the human body: it guarantees movements by attaching the skeleton through tendons, thus producing force. Moreover, it also provides the body thermoregulation, generating heat.
In vertebrates, the skeletal muscle develops in the embryo from the somites, which are mesoderm paraxial bodies, localizing parallel to the neural tubes and the notochord [13]. The skeletal muscle progenitors are multi-potent stem cells, localizing in the hipoaxial dermamyotome (one of the two components constituting the somites, together with the sclerotome). These multi-potent stem cells migrate from the dermamyotome to developing limbs, tongue and diaphragm after delamination [14, 15]. The myogenic commitment is a deeply regulated mechanism which is primary determined by Wnts and sonic hedgehog (Shh). Wnts and Shh are secreted by axial structures [16] and stimulate both Paired Box (Pax) genes and directly MRFs (Myogenic Regulation Factors). Oppositely the process of delamination, determining the formation of migratory myoblasts, is regulated by HGF (hepatocyte growth factor), which is in turn initiated by c-met. C-met function is fundamental for the migration of muscle progenitor cells and it is administered by Pax3 and its paralogue, Pax7 [17, 18]. Then, the activation of Notch, a regulator factor released by different cell populations including myoblasts, favours proliferation and inhibits the premature differentiation of myoblasts. The process of differentiation is extremely dynamic and principally orchestrated by MRF genes. MRF genes pertain to the bHLH (basic helix-loop-helix) protein family, comprehending the Myogenic Factor 5 (Myf5), Myoblast Determination protein (MyoD), Muscle specific Regulatory Factor 4 (MRF4) and Myogenin (Myog) [19]. At first, Myf5 and MyoD are activated to induce differentiation, probably driven by Pax3 and Pax7 [20,

21]. Myog is targeted by MyoD and coordinates the transition of myoblasts to myocytes and myotubes by directly activating structural muscle genes. Finally, MRF4 has a fundamental role in the last stages of differentiation [22, 23]. Muscle is constituted by many elements and multiple structural systems. The whole muscle is enclosed by a membrane called epimysium. The total structure is constituted by a variable number of fasciculi and each fasciculus is enveloped by a connective sheath, named perimysium. Then, each fasciculus can be further subdivided in fibers (representing muscle cells), which are surrounded by endomysium [24]. Muscle fibers are multinucleated cells and all these nuclei localize in the periphery of the cell. Fibers are connected to an extensive and complex membrane network. The sarcolemma (corresponding to the plasmalemma) represents the main membrane system, directly surrounding each fiber. The sarcolemma is composed of three layers: the plasmalemma, the basal lamina and collagenous fibrils. Then, the transverse tubular system (T-system) and the sarcoplasmatic reticulum (SR) are complex membranous systems with a fundamental role in the communication of the external stimulus determined by the motoneuron inward to the myofiber [24]. Thus, these two structures are responsible for the excitation-contraction coupling. Briefly, the T-system is composed of plasmalemma membranes which invaginate into the inside of the cell and associate to the SR. SR forms two terminal cisternae, running parallel to the T-system and constituting the triad. The excitation stimulus spreads along the T-system to the SR. When SR receives the stimulus, calcium ions are released along the whole fiber and contraction is activated. The contractile basic unit of muscle fibers is the sarcomere: serial sarcomeres are the unique generators of shortening and force. Sarcomeres are made of thick and thin filaments, which are principally composed of two contractile proteins: myosin and actin. Moreover, other regulatory proteins (tropomyosins and troponins) and scaffold proteins (such as titin and nebulin) contribute to the sarcomere contractile function [25].

1.1.2 Muscle Regeneration

Although adult skeletal muscle is a stable tissue, characterized by a restricted nuclear turnover [26], it has the potential to fast regenerate when damaged. This process is based on the equilibrium between pro- and anti-inflammatory events; this equilibrium is fundamental for determining a successful repair of the damage allowed by new fibers substitution, and the consequent recovery of muscle contractility. Independently from the origin of the damage (i.e. direct trauma, tissue ischemia, genetic defects or aging), the process of muscle regeneration undergoes three steps: degeneration, repair and maturation. Failing of one of these steps turns out in reduced muscle performance and muscle wasting [27, 28]. Degeneration of muscular tissue consists in muscle fibers necrosis and consequent disruption of the sarcolemma, causing an increase of some proteins in the serum, such as creatine kinase and myoglobin [29, 30]. In the starting phase of the damage, the affected muscle stimulates an inflammatory response orchestrated by T helper Th1 cytokines, such as tumor necrosis factor (TNF) and Interferon (INF). Soon after, neutrophils and macrophages intervene and contribute to further induce muscle membrane lysis and eliminate cellular debris with their phagocytic activity [26]. Subsequently, the quiescent Pax7+ myogenic stem cell population, the satellite cells (SCs), activation is promoted by insulin-like growth factor 1 (IGF-1) and fibroblast growth factor 2. Once activated, SCs start to proliferate and migrate to the site of damage [31]. SCs were firstly identified in 1961 by electron microscopy and described as an apparently quiescent population of stem cells localizing on the surface of the myofiber, beneath its basement membrane [32]. After muscle damage these stem cells are able to activate and eventually form new fibers, thus exerting the role of myogenic precursors.

During this migration step, satellite cells differentiate into proliferating MyoD+ and Myf5+ myoblasts. Pro-inflammatory macrophages (M1) are replaced by

anti-inflammatory macrophages (M2) stimulated by Th2 cytokines, such as interleukin 4 (IL-4), 10 (IL-10) and 13 (IL-13) [33].

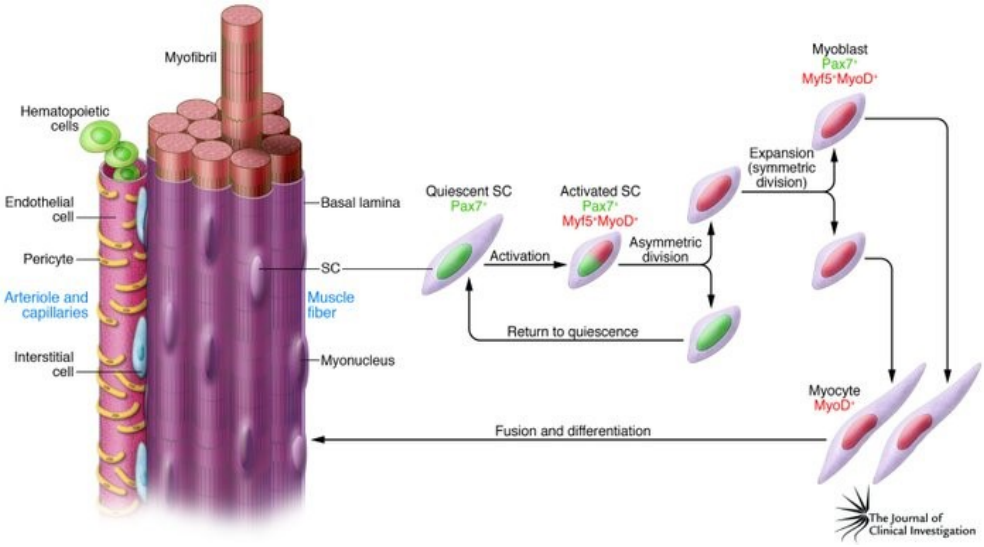

FIGURE 1. *Once activated, satellite stem cells undergo an asymmetric division (Tedesco et al.; The Journal of Clinical Investigation, 2010) [5].*

When the SC proliferation phase is concluded, Myog and MRF4 expression is upregulated and myoblasts leave the cell cycle and conclude their differentiation: they fuse with fibers thus replenish the injured muscle cells [26].

1.1.3 Myogenic Stem Cells

Adult stem cells can be generally depicted as characterized by two main functions: self-renewal and multi-lineage differentiation. Multi-lineage differentiation provides the classification of totipotent, pluripotent, multipotent progenitors and precursors. In the course of the first stages of development, a totipotent zygote originates a completely differentiated adult organism. Following this totipotency, pluripotent cells give rise to 3 germ layers and then multipotent cells produce the whole organism. Multipotent cells still

reside in adult tissues, were they activate and proliferate prompted by environmental signals.

In healthy adult tissues stem cells exert a key role in homeostasis maintenance: tissue waste is immediately counterbalanced by injured cells substitution, favoured by an asymmetric stem cell division. These cells give rise to one cell undergoing differentiation and an identical daughter stem cell. This way, stem cells guarantee the development and replenishment of both tissues and organs [34]. Satellite cells (SCs) act as a heterogeneous subpopulation of stem cells with a fundamental role in muscular tissue growth, regeneration and maintenance. As previously mentioned, SCs localize in niches beneath the sarcolemma and the basal lamina and they represent approximately the 90% of post-natal muscle progenitors in muscle [35]. SCs are normally quiescent, but during muscle regeneration SCs activate and proliferate undergoing a self-renewal process, which is characterized by both asymmetric division and stochastic differentiation. Although SCs represent the main muscular resident stem cells, other skeletal muscle resident cells, which can differentiate into skeletal muscle, may contribute to muscle regeneration under physiological or pathological conditions.

Muscle-derived cells (MDSC)

In 1999, Gussoni and his group identified for the first time a pluripotent stem cell population localized in the skeletal muscle. These cells, identified as a side population (SD), were able to differentiate into variable lineages when systemically transplanted in vivo into host mice [36]. Moreover, they exhibited a hematopoietic differentiation capacity [37]. This cell population, together with other precursor cells successively identified in the bone marrow [38], the neuronal compartment [39] and different mesenchymal tissues [40], were all capable to differentiate into the myogenic lineage and were all Pax7-. This observation suggested the existence of progenitor cells, other than satellite cells, displaying a myogenic potential. In 2002, Qu-Petersen's group

identified 3 populations of muscle-derived stem cells (MDSC), in accordance with their proliferation behaviour and adhesion characteristic [41]. Briefly, after enzymatic dissociation, the muscle extract was seeded on a collagen-coated dish; different unique populations were isolated on the basis of their adhesion features. The first pre-plating passage (PP1) represented primary fibroblasts; heterogenous population of myogenic and not-myogenic cells were obtained in the following passages (PP2-PP6, 24 hours intervals). PP2 and PP3 desmin+ cells were re-plated in combination with PP4 and PP5 and they represented the EP population. PP6 cells were seeded 72 hours after PP5 passage. These cells were recognized as LP population. LP half-life was about 1-2 weeks; surviving cells formed clonal colonies, called MDSC [41]. The early pre-plate cells (EPs) and the late pre-plate cells (LPs) were recognized as satellite cells due to their patterns of myogenic markers expression. EPs were desmin, m-cadherin and myogenin positive and, similarly to SCs, they showed fast proliferation and differentiation into myotubes when cultured in vitro. On the contrary, the role of LPs remained unclear: these cells demonstrated a limited capacity to proliferate and differentiate. The third population, the quintessential MDSCs likely deriving from myofibers, represented a novel type of pluripotent stem cells. MDCS were highly proliferating cells, showing good self-renewal capacity in vitro. When injected in vivo, MDCSs demonstrated their multipotent nature. When transplanted in the *mdx* mouse model of Duchenne Muscular Dystrophy (DMD), they were able to deliver dystrophin to targeted myofibers and restore the histology of dystrophic muscle for at least three months after transplantation. Moreover, they exhibited an immune-privileged behaviour, probably due to MHC-I lack of expression on their surface; no CD4+ or CD8+ lymphocytes were identified in the transplanted muscles after injection. Overall, if compared to EP cells treatment, MDCS transplantation produced better outcomes [34, 41, 42]. The advantage of MDCS for muscle regeneration has been linked not only to their proliferation, self-renewal and

multipotent differentiation capabilities, but also to their resistance to hypoxic and oxidative stress [43].

Myo-endothelial cells

In 2007, Zheng and his colleagues examined the correlation between myogenic and endothelial cells in human skeletal muscle (Zheng et al, 2007). Previous studies had shown that some MDSCs, displaying endothelial cell markers on their surface, differentiated into endothelial cells after injection in the skeletal muscle [41, 43, 44]. They proved the existence of a stem cell population co-expressing endothelial and myogenic markers (CD56+, CD34+, CD144+). This cell population was called ‘’myo-endothelial’’. When cultured in vitro, myo-endothelial cells showed the same regeneration capability upon extended culture as myogenic (CD56+CD34-CD144-) cells and endothelial (CD56-CD34+CD144+) cells; however their proliferation and resistance to oxidative stress were extremely higher. Moreover, when these cells were injected intramuscularly into an immuno-deficient mouse model (SCID), in which skeletal muscles were injured by cardiotoxin, they were able to regenerate muscle similarly to endothelial cells but more efficiently than committed myogenic cells [41, 42]. According to Dr. Zheng observations, regenerated myofibers nuclei were all of human origin, thus underlining that these cells exerted their role by fusing each other. Moreover, donor-derived cells were all localized beneath the sarcolemma, thus suggesting an additional function in replenish satellite cells compartment [45].

Mesoangioblasts

Mesangioblasts (MABs) are multipotent precursors for vascular and extravascular mesodermal tissues. They physically localize within the embryonic dorsal aorta in both avian and mammal species. When isolated and cultured in vitro, mesangioblast clones express early endothelial markers (Flk1+CD34+vascular-endothelialVE-cadherin+) and a variable number of cells co-express α-smooth muscle actin (α-SMA), generally found on the

surface of skeletal myoblasts. If cell clones are seeded onto collagen-coated flasks added with horse serum and chick embryo extract, they also express Myf5 and MyoD myogenic regulator factors and thus differentiate into skeletal muscle cells [46]. Thanks to their myogenic differentiation potential, MABs have been extensively exploited for the regeneration of injured muscular tissue in animal models of muscular dystrophy. MABs isolated from embryonic dorsal aorta (murine D16 MABs) were systemically transplanted in an α-sarcoglycan (α-SG) null mouse model; cells restored the wild-type protein expression in 20% of the muscle fibers and favoured a decrease in fibrosis, thus determining an amelioration of the animals endurance [47, 48]. Moreover, it was proved that these MABs express specific receptors on their surface, favouring their homing and engraftment to damaged tissues. The overexpression of these receptors deeply increases the outcome of MABs transplantation [49]. The main limit related to embryonic MABs is the difficulty of the isolation procedure. The isolation of MABs from human aorta during by-pass surgery may be a promising source; however it has been recently discovered that a population closely similar to mesangioblasts can be also isolated from the skeletal muscle, the bone marrow [50] and the atria and ventricles of the heart [51]. Skeletal-muscle isolated MABs display a short half-life and no self-renewal capability. In 2006, Sampaolesi's group exploited skeletal muscle's MABs to rescue dysferlin expression in a dysferlin-deficient mouse model. The systemic cell transplantation allowed the recovery of the protein expression in 9-12% of total myofibers [52]. According to these observations, skeletal muscle-derived MABs were also isolated, genetically corrected and intra-arterially transplanted in dystrophic animal models of Duchenne muscular dystrophy: the mdx mouse model and the GRMD dogs. MABs were able to determine the restoration of dystrophin in a variable percentage of myofibers in both the two experiments [52, 53]. Finally, in 2015, Cossu and his group reported the first phase I, IIa clinical trial based on MABs transplantation. Cells were isolated from HLA-matched

donors; 5 DMD patients were treated. Escalating doses of MABs were systemically transplanted after immunosuppressive therapy. Although a boy reported a thalamic stroke without clinical consequences, the study was considered as safe. MRI demonstrated that 4/5 showed a slight amelioration of the disease, but without functional progression [54].

Pericytes

Pericytes localize around the vascular tube, interdigitating with endothelial cells in the basement membrane of the vessels. Physiologically, they play a key function in the support of microcirculation. Even though they originally demonstrated a mesenchymal-stem cell nature, showing the capability to differentiate into osteoblasts and adipocytes, recent studies demonstrated that they had also a good capacity of myogenic differentiation [55]. Human skeletal muscle blood vessels- derived cells were found to express pericytes markers: NG2 proteoglycan and ALP alkaline phosphatase. These cells showed a good proliferation rate in vitro and the ability to spontaneously fuse to form myotubes with high efficiency. After transplantation into the SCID/mdx mouse model, they were able to generate a high percentage of human dystrophin+ myofibers. These cells were also isolated from Duchenne patients, engineered with the human mini-dystrophin and transplanted in vivo. Once again, they showed a myogenic potential and the capability to restore the human mini-dystrophin expression in SCID/mdx muscles [55]. In 2009, it was also observed that in the case of focal injury, pericytes are released from their position to exert an immunomodulatory function [56].

CD133+ cells

In 2004, Torrente and his group isolated a population of human skeletal muscle-derived stem cells positive for CD133 antigen. These stem cells were defined as multipotent precursors, as they were able to differentiate into myogenic, hematopoietic and endothelial cells when cultured in vitro in the

presence of certain cytokines [57]. The expression of CD133+ antigen was also observed in a subpopulation of circulating stem cells, showing a myogenic potential too. This cell population was isolated and characterized in vitro: cells were positive for several myogenic precursors: Myf5, Pax7 and M-cadherin. As they were not spontaneously able to differentiate into myogenic cells, they were induced to undergo myogenesis when co-cultured with myogenic cells or in the presence of a specific myogenic signalling. Moreover, human circulating CD133+ cells were intra-arterially and intra-muscularly transplanted in a dystrophic immunodeficient mouse model: the SCID/mdx mice. Their capacity to rescue dystrophin expression and to replenish the SCs pool was then evaluated. It was found that up to 10% muscle fibers were positive for human dystrophin expression; injected cells partially localized beneath the basal lamina and co-expressed M-cadherin, thus suggesting a replenishment of SCs pool. Furthermore, RT-PCR analysis of injected fibers demonstrated the expression of myogenic markers, evidencing that blood-derived CD133+ cells profoundly contributed to the regeneration of dystrophic muscle [57]. In 2007, Torrente' group extended previous observations investigating the therapeutic potential of a combined cell and gene based therapy. Following the isolation of CD133+ cells from DMD patients' blood and muscle, they engineered dystrophic cells exploiting the exon-skipping technique to restore the correct reading frame of mutated dytrophin and finally they intramuscularly transplanted engineered cells in the SCID/mdx mouse model. They demonstrated that both skipped blood- and muscle- derived CD133+ cells could differentiate in vivo into satellite cells and mature myofibers. These myofibers were human dystrophin positive but expressed also α- and β-sarcoglycans, thus suggesting the recovery of the dystrophin-associated protein complex. However, the intramuscular transplantation produced a local regeneration, whereas DMD disease compromises the whole skeletal muscle system. Thus, they performed a systemic transplantation of muscle-derived CD133+ stem cells

and they observed an amelioration of muscle morphology and consequently of SCID/mdx mice endurance [58]. The same year, the safety of an autologous transplantation of muscle-derived CD133+ cells in 8 Duchenne boys in a 7-month double- blind phase I clinical trial was tested. Produced data demonstrated the absolute safety and feasibility of these stem cells transplantation. Treated patients showed an increase in muscle fibers vascularization and in fast myosin myofibers [59].

Mesenchymal stem cells (MSCs)

One of the main problems related to cell therapy is associated to immune rejection. In the field of muscular dystrophies, the process of rejection accelerates the dystrophic progression, causing an increased inflammation. To this aim, MSCs cell therapy has shown promising results. Mesenchymal stem cells are generally considered as adherent, non-hematopoietic cells, positive for CD90, CD105, CD73 and negative for CD14, CD34, and CD45 markers. They were originally isolated from the bone marrow; however they have been identified also in many other tissues: adipose tissue [60], heart [61], peripheral blood [62], dental pulp [63], cord and menstrual blood [64]. MSCs are pluripotent stem cells, with a well-known ability to differentiate into condro, adipo and osteo lineages [65]. However, it has been observed that they are also able to differentiate into cells-resembling neurons [66], muscle [67], hepatocytes [68] and pancreatic islets [69]. The regenerative capacity of MSCs has been extensively investigated in post-myocardial infarct models, stroke [70], pulmonary fibrosis [71], kidney damage [72], as well as muscular dystrophy [73]. MSCs are able to restore full-length dystrophin in dystrophic myotubes by directly fusing with dystrophin-/- cells. MSCs exert a fundamental role in controlling inflammation. Firstly, they express specific receptors determining their homing towards injured tissues. Then, they inhibit macrophage activation [74], Th1 and Th17 generation [75] and they suppress NK and T cytotoxic cell function [76] within these damaged tissues. Recently,

it has been discovered that the therapeutic effects of MSCs may be related not only to their proper regenerative and immunomodulatory ability, but also to the release of paracrine factors, such as cytokines and extracellular microvesicles, which cooperate with cells to exert their role, inhibiting apoptosis, stimulating endogenous cell proliferation and activating resident stem cells in the damaged tissue [77].

1.2 The Congenital Muscular Dystrophies (CMDs)

1.2.1 Generalities and Clinical Phenotypes

Muscular dystrophies (MDs) include a clinically and genetically heterogeneous group of inherited muscle diseases. To date, MDs have been classified in six groups: Duchenne Muscular Dystrophy (DMD, 310200), Becker Muscular Dystrophy (BMD, 300376), Limb Girdle Muscular Dystrophies (LGMDs), Fascioscapular Muscular Dystrophies (FCMDs), Myotonic Muscular Dystrophies (MMDs), Dystal Myopathies (DMs) and Congenital Muscular Dystrophies (CMDs). Recent epidemiological data suggest that the prevalence for CMDs seems to be between 2,6 – 4,5 in 10000 [10], identifying CMDs as the most popular autosomal recessively inherited neuromuscular diseases [78]. CMDs are principally characterized by skeletal muscle diffused weakness, usually presenting from infancy. Infants are generally defined as ‘‘floppy’’, with very low muscle tone and poor spontaneous movements [79]. Muscle alterations occurring in CMD patients depend on an anomalous muscular structure due to mutations occurring in genes encoding mainly for structural components of the extracellular matrix. Affected children may present delayed or arrested motor development and they can develop joint and spinal rigidity. They usually encounter feeding difficulties, leading to poor nutrition. Muscle weakness may worsen or stabilize. The worst consequences of muscle weakness are respiratory insufficiency and cardiac involvement, which can deeply influence patients’

quality of life and life span. Moreover, these diseases may involve also the central nervous system (CNS), eyes and connective tissue [79].

1.2.2 Classification of CMDs

So far, different classifications of CMDs have been proposed. Originally, CMDs have been classified on the basis of patients' clinical phenotype. However, pathological phenotypes due to various mutations in different genes are significantly overlapping. Mutations occurring within a specific gene are able to give rise to a wide spectrum of disorders. For this reason, nowadays the clinical classification of CMDs is based on the genes in which the pathogenic mutation occurs and the cellular localization of the involved mutated protein [79] [1] [80]. Extracellular matrix protein mutations, such as Laminin alpha-2 (LAMA2, 156225) and Collagen VI (COL6A1, 120220, COL6A2, 120240, COL6A3, 120250), respectively lead to the development of merosin-deficient CMD (MDC1A, 607855) and Ulrich CMD (UCMD, 254090)/Bethlem myopathy [81]. External sarcolemmal protein mutations, such as integrin α7 (ITGA7, 600536) and integrin α-9 (IGTA9, 603963), cause integrin α7 and integrin α-9 –related CMDs [82].

Defects of α-dystroglycan glycosylation, depending on mutations occurring in genes encoding for glycosyltransferases, such as fukutin (FKTN, 607440), fukutin-related protein (FKRP, 606596), glycosyltransferase-like protein large1 (LARGE1, 603590), O-linked mannose β1,2-n-Acetylglucosaminyltransferase (POMGNT1, 606822), protein-O-mannosyltransferase1 (POMT1, 607423), protein-O-mannosyltransferase2 (POMT2, 607439), isoprenoid synthase domain-containing protein (ISPD, 614631), lead to the development of different forms of dystroglycanopathies. Defects of proteins residing in the endoplasmic reticulum, such as selenoprotein-N (SELENON, 606210), cause rigid spine syndrome (RSMD1, 602771) and defects of proteins localized in the nuclear envelope lamin A/C (LMNA, 150330) cause the Dropped-head syndrome, (EDMD, 310300).

Finally, mutations arising in sarcolemmal and mitochondrial membrane proteins, such as choline kinase β (CHKB, 612395), give rise to protein-related muscle disease-CMD [83].

Other less common CMD subtypes have been identified (i.e. SYNE1-related CMD caused by SYNE1 mutation encoding enaptin protein, a nuclear envelope protein, 608441), as well as ‘’CMDs of unknown origin’’ caused by unknown mutations of genes [84] [79]. However, data for all CMDs are still inadequate to define a specific genotype/phenotype correlation and a consequent concluding prognosis.

1.2.3 Diagnosis, Treatment and Surveillance

The diagnosis of CMDs is principally based on clinical findings, brain and muscle imaging, molecular genetics analysis, immunohistochemical staining and biopsy histology. Muscle biopsies are fundamental for the evaluation and precise diagnosis of congenital muscular dystrophies. Correlation with the clinical picture is necessary to have a correct biopsy interpretation, given the variability of similar morphologic findings, the variability in the performance of commercial antibodies to detect protein deficiency by immunohistochemistry and the absence of specific stains in some subtypes of CMDs. Muscle biopsies may appear very heterogeneous; for instance each subgroup of disorders, previously identified in CMDs classification, presents unique features.

For example, MDC1A muscle biopsy exhibits a high heterogeneity in fiber size with connective tissue proliferation and fat infiltration in specific muscle areas; the immune staining (IS) must underline the complete absence of laminin-α2 expression. UCMD biopsy shows changes from mildly myopathy, with limited fibers size variability, to a profound dystrophic phenotype, with prominent connective and fat tissue infiltrations and replacement of muscular tissue; IS shows no signal for collagen VI protein staining. Among α-dystroglycanopathies, the differences in muscle biopsies are related to the

amount of residual glycosylation of α-dystroglycan (α-DG). The lower α-DG is glycosylated, the more compromised is the muscle. In RSMD1, fiber size variability and type-1 fiber predominance are the main features and sometimes multiple core-like areas of sarcoplasmic disorganization associated with mitochondrial depletion may be found in muscle biopsy analysis. The presence of basophilic fibers underlines the regenerative activity, but not all basophilic fibers are also regenerating. The analysis of foetal and neonatal myosis may be very helpful. Moreover, other abnormalities may be found, including different types of vacuoles. [85].

So far, no decisive therapeutic approaches for CMDs have been found. Treatments just allow the amelioration of the development of the disorder and focus on the prevention of pulmonary and cardiac failure. Multi-disciplinary medical care aims to the improvement of patients' quality of life and longevity: respiratory insufficiency always requires assisted cough devices, supplemented oxygen and non-invasive ventilation via tracheostomy. Physical therapy, based on stretching exercise, is suggested to avoid contractures and to promote mobility; mechanical devices including wheelchairs are generally exploited to support children mobility. Sometimes, surgical intervention for preventing and treating spinal and limb deformities is required. Throughout the pathology course, surveillance is mandatory for constantly monitoring the respiratory functions, the orthopaedic complications, and the cardiac and neurological functions.

1.3 Alpha-Dystroglycanopathies

1.3.1 DAG1 gene and Dystroglycan protein

After its discovery in 1987 as a new laminin-binding protein in the plasma membrane of different cell types [86], dystroglycan (DG) and its corresponding gene (*DAG*1, 128239) were deeply characterized by the group of Kevin Campbell from the beginning of the 90s. The dystroglycan

gene (*DAG*1) localizes in human chromosome 3p21. The coding sequence of the gene is organized in two exons, the first consisting of 285 pair bases and the second incorporating the rest of the coding sequence (2400 pair bases). The two exons are divided by a single large intron. The cDNA encodes for a 97 KDa precursor protein (895 amino acids), which goes through a post-transcriptional cleavage, thus producing two independent subunits: α-dystroglycan (a 156 KDa highly glycosylated protein) and β-dystroglycan (a 43 KDa transmembrane protein). mRNA is 5.8 Kb and its expression has been found to be positive in many different muscular and non-muscular tissues [87]. α-DG possesses three domains: an N-terminal, a serine-threonine-rich mucin-like and a C-terminal domain. This highly glycosylated peripheral membrane functionally interacts with extracellular matrix (ECM) proteins, such as laminin, biglycan, neurexin, perlecan, agrin, pikachurin and slit [88]. α-DG C-terminal domain binds with high affinity the N-terminus of β-dystroglycan. β-DG, in turn, has a unique transmembrane domain; its cytoplasmic C-terminus domain associates with the last 15 amino acids to the cys-rich domain of dystrophin [89]. This domain is also proline-rich and includes a Tyr- phosphorylation site. The cytosolic domain of β-DG acts also as a junction to other proteins, such as rapsyn, caveolin-3 and Grb2 [90]. This linkage is considered as fundamental in sustaining the integrity and stability of the sarcolemma from mechanical stress induced by skeletal muscle. α-DG N-terminal region is cleaved by proteases after the glycosylation process is concluded. α-DG has a wide tissue distribution throughout human body, with high expression in muscle, in the CNS and peripheral nervous system (PNS), in the epithelial and endothelia [91]. The massive presence of α-DG suggests a key function not only in supporting muscle fibers structure and functionality, but also in neuronal migration, axon guidance, neuromuscular junction formation, and in the formation of optic tissue [92].

The main feature of a functional α-DG, starting from the physiological development of the embryo, is a tissue specific glycosylation. For this reason, even though the amino acid sequence predicts a 74 KDa core protein, α-DG looks like a smear in SDS-PAGE analysis with a variable molecular weight of about 156 KDa in skeletal muscle and 120 KDa in brain and peripheral nerves, thus suggesting a tissue-specific pattern of glycosylation. By electron microscopy, α-DG is a dumbbell-shaped molecule characterized by two globular domains divided by a rod-like region corresponding to its mucin domain.

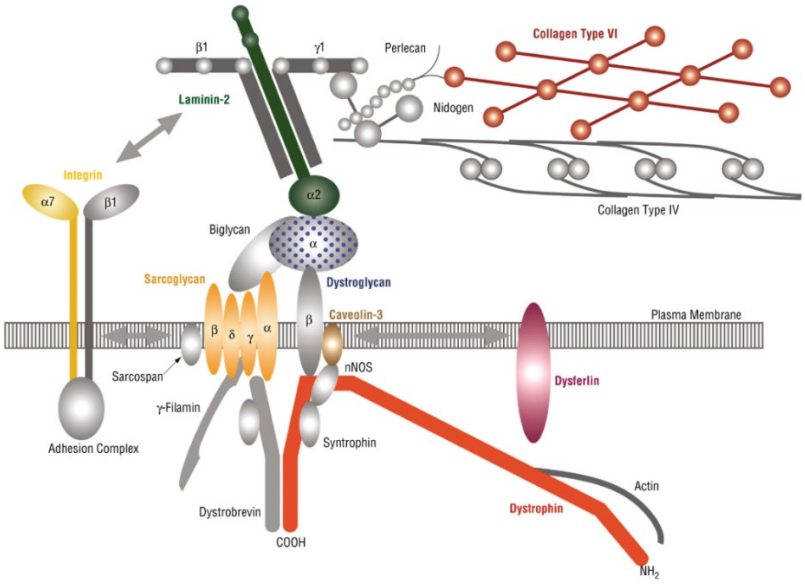

FIGURE 2. *Representation of the DCG complex and other proteins involved in the development of dystrophic phenotypes (J. Kirschner and C. G. Bönnemann; The Archives of Neurology, 2004)[12].*

This central region contains more than 40 Ser/Thr residues that constitute an O-glycan cluster. α- and β- DG proteins were initially classified as components of the dystrophin-glycoprotein complex (DCG), together with sarcoglycans, dystrobrevins, syntrophins and sarcospan. DCG represents an essential component of the sarcolemma, which has a key role in the structural stability of the cytoplasmic membrane. The loss of function of any

protein belonging to DGC leads to the disruption of the whole complex and causes the instability of the linking between extracellular matrix and intracellular cytoskeleton, and the consequent development of muscular dystrophies.

1.3.2 α-Dystroglycan Glycosylation

There are three main categories of sugar-peptide linkages; N-linked, O-linked glycans and glycosaminoglycans (GAGs), found on proteoglycans. N-linked glycans and various O-linked glycans have been found on α-dystroglycan. In this latter, the reducing terminal sugar is usually N-acetylgalactosamine (GalNAc), which associates to the hydroxyl group of serine (Ser) and threonine (Thr). Aside from GalNAc, O-linked mannose linkage plays a significant role for α-dystroglycan functionality, favouring its connection to extracellular matrix proteins. O-mannoglycosylation begins in the endoplasmic reticulum with protein-O- mannosyltransferase 1 (POMT1) and 2 (POMT2) exerting their function [89, 93]. These two proteins share the same hydropathy profiles and they are predicted to be integral membrane proteins with multiple transmembrane domains. POMT1 needs to interact with POMT2 for exerting its enzymatic function. These two proteins are present in all human tissues, with a predominance of POMT1 expression in foetal brain, testis and skeletal muscle and POMT2 in testis. The complex cooperates to form a β-1,2 linkage with N-acetylglucosamine (GalNAc) to catalyze O-mannosylation of proteins. O-linked mannose β1,2-N-acetylglucosaminyltransferase 1 (POMGnT1) operates by transferring a GlcNAc from UDP-GlcNAc to O-mannosyl glycoproteins, demonstrating a specific O-mannose β1,3-N-acetylglucosaminyl transferase activity. POMGNT1 can be further branched by GlcNac and/or elaborated by galactose, fucose or sialic acid to generate the M1 and M2 glycans [94, 95]. A small group of O-Man modified domains on α-DG is extended in the endoplasmic reticulum by a GalNac in a beta- 1,4 linkage by O-linked

mannose β1,2-N-acetylglucosaminyltransferase 2 (POMGNT2, 614828) and forms the M3 glycans [95]. Subsequently, GlcNAcβ1-4Man is further modified and transformed into a trisaccharide by β1,3-N-acetylgalacosaminyltransferase 2 (B3GALNT2, 610194) and the protein kinase-like POMK, a specific O-mannose kinase [95]. Processes leading to the constitution of GalNAcβ1-3GlcNAcβ1-4(phosphate-6)Man occur in the ER. Following unknown elaboration of the phospho-trisaccharide in a phosphodiester linkage, β-1,4-Glucuronyltransferase 1 (B4GAT1, 605517) adds a glucuronic acid (GlcA) in a beta 1,4 linkage to a β-linked xylose [94, 96]. This mechanism functions as a primer for glycosyltransferase-like protein LARGE (LARGE) enzyme. LARGE acts as a bifunctional glycosyltransferase, generating polymers of alternating xylose (Xyl) and glucoronic acid (GlcA), by producing units in this sugar moiety acting as receptors for ECM proteins [94, 97]. The precise mechanism by which the xylosyl-glucoronyl polysaccharide is attached to α-DG is still unknown, but recent evidences suggest the formation of a linkage via phosphorylate O-mannosyl structures. LARGE is widely expressed in brain, heart and skeletal muscle whereas LARGE2, a paralogue of LARGE, is highly expressed in placenta and kidney. In 2016, Well's group reported a M3 glycan structure with a phosphodiester linked ribitol on which transmembrane protein 5 (TMEM5, 605862), B4GAT1, and LARGE act to generate the functional receptor for ECM proteins. They identified isoprenoid synthase domain-containing protein (ISPD) protein as a CDP-ribitol pyrophosphorylase, an enzyme that can synthesize CDP-ribitol from ribitol-phosphate and CTP. Moreover, they also speculated that TMEM5, a xylose transferase, is further elongated by B4GAT1 and acts as a primer for LARGE addition of matriglycan [94]. Recently, the group of Toda et al., identified also a mechanism by which ISPD, fukutin (FKTN) and fukutin-related (FKRP) proteins sequentially act as ribose-5-phosphate (Rbo5P) transferases, exploiting CDP-Rbo as a substrate [98].

1.4 α-Dystroglycan Hypoglycosylation

Muscular dystrophies characterized by hypoglycosylation of α-dystroglycan, due to O-mannosylation lacking, are generally referred to as dystroglycanopathies. Alpha-dystroglycanopathies are group of disorders, extremely heterogeneous from both a clinical and genetical point of view, presenting with various phenotypes ranging from severe disorders of CMDs to milder LGMD forms, with and without CNS involvement and often characterized by optical damage.

FKRP: fukutin related protein	FKTN: fukutin	POMGnT1	POMT1: protein O-mannosyl transferase 1	POMT2: protein O-mannosyl transferase 2	glycosyiltransferase "like": LARGE
LGMD2I[197]	FCMD[199]	MEB[16]	WWS[205]	WWS[156]	two patients with severe CNS involvement: MDC1D[208] and WW[209]
MDC 1C[152]	WWS[200]	WWS[50]	MDC with mental retardation, microcephaly, structural brain changes, muscle hypertrophy and eventual myopia[206]	MEB[171]	
WWS[198]	MEB[50]	LGMD2? with severe myopia and normal intelligence[50,203]	MEB[50]	MDC with microcephaly, severe mental deficiency, possible ocular changes[171,172]	
MEB[198]	Myocardiopathy, minimal or absent muscle weakness, normal ntelligence[201]	MDC with brain malformations without ocular abnormalities[204]		MDC and cerebellar involvement[50]	
MDC with cerebellar cysts[151]	LGMD2M[202]			LGMD2? mild, with normal intelligence and inflammatory changes on muscle biopsy[207]	
MDC with variable cortical, cerebellar and pontine dysplasic changes[149]				LGMD2? with mental retardation[50]	

FCMD: Fukuyama congenital muscular dystrophy; LGMD: limb girdle muscular dystrophy; MDC: muscular dystrophy, congenital; MEB: muscle-eye-brain; POMGnT1: protein O-manose beta1,2-N-acetylglucosaminyltransferase; WWS: Walker-Warburg syndrome.

TABLE 1. Genotype and phenotype correlations alpha-dystroglycanopathies (U.C. Reed; Arquivos de Neuro-Psiquiatria, 2009)[10].

Similar phenotypes can be determined by mutations in different genes: various mutations localizing in the same gene are able to give rise to heterogeneous phenotypes [1, 88, 99].

For this reason, a classification of these disorders has been proposed based on the age of the onset of the weakness, the presence or absence of structural brain abnormalities/ mental retardation and eye involvement, rather than the specific gene mutation or the original clinical entity [100].

Fukuyama Congenital Muscular Dystrophy (FCMD)

FCMD (Muscular dystrophy-dystroglycanopathy type A, 4: MDDGA4, 253800) is reported as one of the most prevalent autosomal recessive disorders of childhood muscular dystrophies in Japan [101]. FCMD is due to a mutation in the FUKUTIN gene on chromosome 9q31. It is a very severe form of CMD, characterized by brain abnormalities such al polymicrogyria of the cerebrum, lissencephaly and hypomyelination, leading to severe to mild mental retardation. 80% of patients may have epileptic attacks or suffer from insomnia. Decreased foetal mobility may occur in utero, and in the neonatal period patients are weak and floppy. Clinical manifestations range from contractures appearing in the first year of age, to muscle hypertrophy of tongue and calf in FCMD patients. Usually, they are not able to walk, and if they walk, severe scoliosis brings to the loss of ambulation. Most patients die by 20 years, due to cardiomyopathy and cardiac failure.

Muscle-Eye Brain (MEB) disease

MEB (Muscular dystrophy-dystroglycanopathy type A, 3; MDDGA3, 253280) pathology is an autosomal recessive disease primary caused by loss-of-function mutations occurring within the POMGnT1 gene on chromosome 1p34-p32. Mutations in other genes including POMT1, POMT2, FKTN and GMPPB can also lead to the development of the pathology.

MEB is considered the second most severe type of alpha-dystroglycanopathy. The hallmarks of MEB patients include brain defects (hypoplastic cerebellar vermis and cerebellar hypoplasia). MEB patients present a severe hypotonia in the neonatal period and an impaired motor development. They show very severe optic symptoms such as retinal defects, optic atrophy, glaucoma and congenital myopia. The life expectancy of MEB patients is 10-30 years. Nowadays, FCMD and MEB are referred to as a unique phenotype, since there is a significant overlapping of these two disorders.

Walker-Warburg Syndrome (WWS)

WWS is typically considered as the most compromising form of dystroglycanopathy. It is inherited as an autosomal recessive disorder, caused by mutations generally occurring in the POMT1 gene (chromosomal locus 9q34.1) (Muscular dystrophy- dystroglycanopathy type A,1; MDDGA1, 236670) or the POMT2 gene (chromosomal locus 14q24.3) (MDDGA2, 613150), causing an identical clinical phenotype. However, also mutations in FKTN, FKRP, LARGE, ISPD, B4GAT1, B3GALNT2, POMK, DAG1, POMGNT and TMEM5 genes have been found to be associated to the development of this pathology [88]. The onset usually begins at early foetal phase, with profound abnormalities in the CNS, such as lissencephaly, hydrocephalus or cerebellar hypoplasia, representing dangerous complications [102].

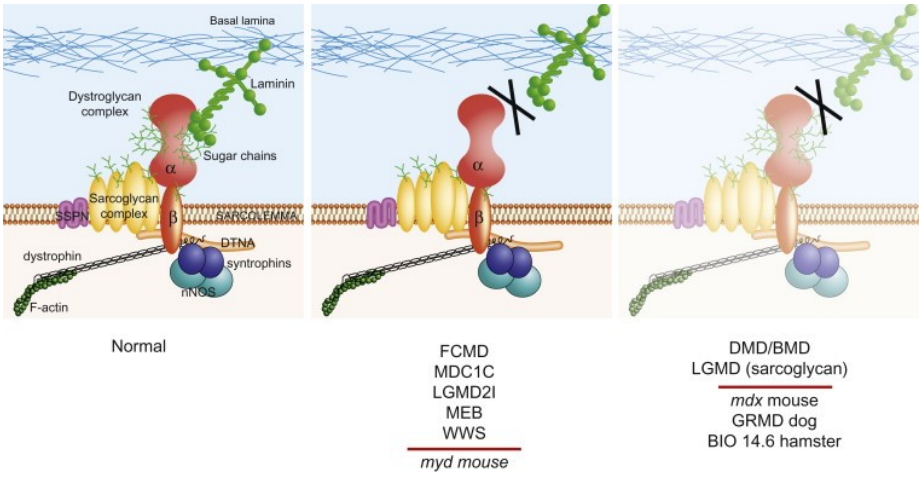

FIGURE 3. *Disruption of the subsarcolemma cytoskeleton-extracellular matrix link in dystrophin-glycoprotein complex-related muscular dystrophies (Y.M. Kobayashi; Neuromuscular disorders, 2012) [8].*

WWS patients always show severe intellectual disabilities and ocular abnormalities, such as microphthalmia, cataracts and myopia. At birth, WWS patients present absence of spontaneous movements, notable hypotonia and inability to see. Life expectancy is generally less than 3 years, due to the insurgence of systemic complications like pneumonia and heart failure [88].

In addition to these principal pathological phenotypes, other minor forms of α-dystroglycanopathies have been identified: the Congenital Muscular Dystrophy Type 1D (MDC1D) (Muscular Dystrophy-Dystroglycanopathy Type B, 6; MDDGB6, 608840), caused by a mutation in LARGE gene, encoding for a putative glycosyltransferase [80], and the Congenital Muscular Dystrophy Type 1C, linked to a mutation in the FKRP gene.

1.5 Congenital Muscular Dystrophy Type 1C (MDC1C) and Limb-Girdle Muscular Dystrophy type 2I (LGMD2I)

1.5.1 MDC1C and LGMD2I clinical features

MDC1C disorder (Muscular Dystrophy-Dystroglycanopathy Type B, 5; MDDGB5, 606612) is due to a mutation occurring within the FKRP gene. FKRP mutations lead to the development of a wide range of disorders, including both severe forms of muscular dystrophy (MDC1C, WWS, MEB), some of which affecting the central nervous system, and a milder disease classified as limb girdle muscular dystrophy type 2I (LGMD2I) (Muscular Dystrophy-Dystroglycanopathy Type C, 5; MDDGC5, 607155).

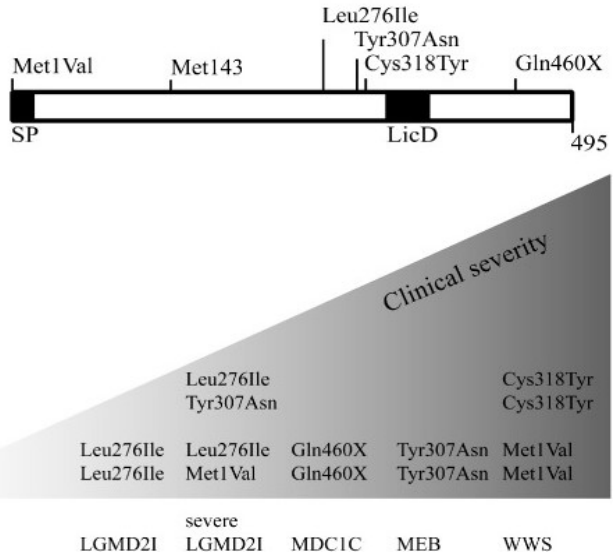

***FIGURE 4**. FKRP mutations and correlated clinical spectra (J. van Reeuwijk; Clinical Genetics, 2010) [2]*

MDC1C patients exhibit an acute muscle weakness compromising also the respiratory muscles. Immediately after birth, they present severe hypotonia and feeding complications. Hypertrophy occurs in the calf muscles and other lower limb muscles. The progressive dystrophic process hampers motor milestones and children never acquire normal functional ambulation. Although FKRP is expressed also in the brain, MDC1C patients may either show or not an involvement of central or peripheral nervous system associated with mental retardation. Microcephaly, mild mental retardation and cerebellar cystis can sometimes occur [103]. Usually, death occurs in the first decade or shortly thereafter, due to pulmonary dysfunction or cardiac failure. The muscle symptomology is undistinguishable from other CMDs phenotypes; MDC1C muscle shows a marked depletion of α-DG glycosylation, as determined by immunocytochemistry analysis.

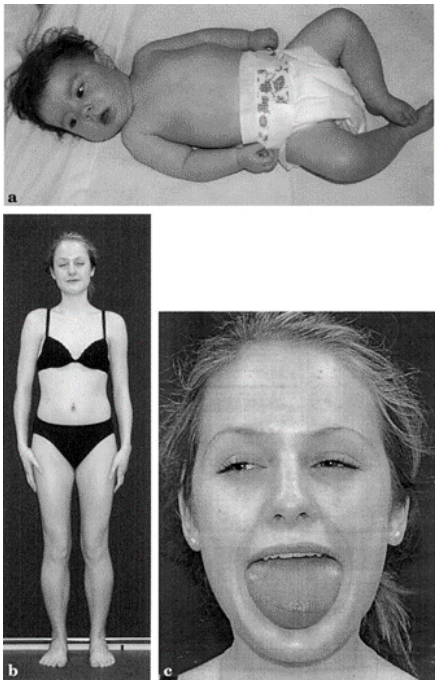

FIGURE 5. *MDC1C (a) and LGMD2I (b, c) phenotypes (E.Mercuri; Annals of Neurology, 2003) [1].*

In addition, the muscular biopsies of some patients carrying specific mutations (such as 1387A>G, N463D) also show a reduced immunoreactivity to β-dystroglycan, α-, β-, -γ sarcoglycans, underlining a widespread pathological effect of FKRP mutation causing a disruption of the dystrophin glycoprotein complex (DCG) [104]. LGMD2I is one of the most frequent autosomal recessive forms of LGMDs forms of limb dystrophy, especially in Northern Europe [105]. While in CMDs the onset of symptoms is usually at birth or within the first 6 months of life, in LGMD it usually occurs in late childhood, adolescence or even adult life. Although this peculiar difference, it is now clear that LGMD and CMDs clinically and genetically overlap, thus suggesting that these pathologies follow a similar pathway. In LGMD2I, patients' muscle weakness results in frequent falls and 'wadding gait' with difficulties in specific exercises, such as running or climbing stairs. With the progression of the disease, these symptoms slowly increase. As well as lower limb weakness, also shoulders and arms are interested. LGMD2I subject's life expectancy and quality of life depend on the early identification and treatment of the pathology. Reports show that a majority of LGMD2I patients display cardiomyopathies. Specifically, they may have a reduced left ventricular ejection fraction, visualized by cardiovascular magnetic resonance imaging (CMR), cardiac conduction failure and dilated cardiomyopathy. CMR analysis also identifies a progressive fatty deposition and fibrosis in the septum and inferior wall. However, it seems that the severity of the cardiac defects is not directly correlated to the severity of clinical skeletal muscle or the involvement of brain. Unfortunately, LGMD2I patients often die because of left ventricular failure [106] [107].

1.5.2 Fukutin- Related Protein gene and protein

In 2011, Brockington and his group identified for the first time a new gene, encoding for a member of the fukutin-protein family: the fukutin-related protein (FKRP).

The 12-Kb FKRP gene maps on chromosome 19q13.3 between markers D19S219 and D19S606, thus suggesting that MDC1C and LGMD2I may be allelic disorders [108]. The gene is composed of three non-coding exons and a single large coding exon of 3.8-kb, containing part of the 5′ untranslated region (5'UTR), the whole open reading frame, and 3′ untranslated region (3'UTR). Biochemical analysis shows a transcript of ~4.0-kb in all body tissues. The protein is principally expressed in skeletal muscle, placenta, and heart; however it has been also weakly detected in the remaining tissues, such as brain [109]. The cDNA encodes for a 495 amino acids protein, with a corresponding molecular weight of 54.6 KDa. However, in the majority of reported studies, immunobiochemical analysis highlighted a protein molecular weight of ~58 KDa. These observations suggest that FKRP undergoes a post-translational modification of ~3.5 KDa: the protein contains two putative N-gycosylation sites: AsnValSer (NVS) and AsnLeuSer (NLS), at amino acid positions 172 and 209. N-linked glycans may explain the slight shift observed in the previous analysis [9]. FKRP sequence analysis predicts the presence of a hydrophobic transmembrane-spanning region (amino acids 4–28), followed by a "stem region" and a catalytic domain. The protein N-terminus contains a hydrophobic Golgi signal anchor sequence (amino acids Met1-Asn33) [110], coinciding with the transmembrane region. This region includes a *RxxR-motif* (amino acids Arg2 to Arg5).

As a similar molecular organization was found in several Golgi-resident glycosyltransferases, even though the exact role of FKRP was initially poorly understood, the protein was immediately considered as a putative glycosyltransferase. The putative glycosyltransferasic DxD-motif is localized from amino acid 362 to 364. Murine and human FKRP gene sequences show 94% of identity. FKRP protein localization is very controversial. Previous studies have examined the localization of fukutin related protein both in cultured cells and tissues, underlining a variable detection in the Golgi apparatus [9, 110], the endoplasmic reticulum [111], or the perinuclear region

[112]. In 2011, Nillsen's group performed immunobiochemical analysis of lysates from FKRP positive cells under reducing conditions; these experiments revealed for the first time a specific FKRP detection both as a monomer (58 KDa), as well as an additional band at ~116 KDa. Thus, they investigated if FKRP was able to interact with other proteins or with itself by performing a co-immune precipitation experiment, discovering that FKRP protein is able to form dimers depending on an N-terminal interaction interface and a Cys6-Cys6 disulfide linkage [9]. Recent works suggest that different mutations occurring in the FKRP gene may influence its position within the cell, thus explaining the wide range of clinical phenotypes.

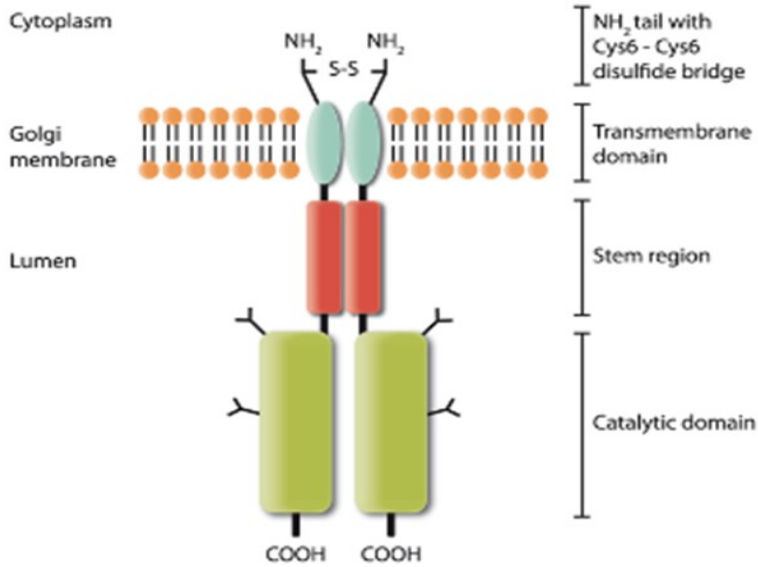

FIGURE 6. *Representation of FKRP hypothetic localization in the Golgi cisternae of muscle fibers. The protein forms disulfide-linked homodimers via an N-terminus Interaction (M.Alhamidi; Plos One, 2011) [9].*

For example, the severe MDC1C phenotype has been associated with mutations causing a retention of the protein in the ER compartment [110]. However, in 2005 Muntoni and his group reported an indistinguishable localization of FKRP in the muscle of MDC1C and LGMD2I patients surrounding the myo-nuclei [112]. Moreover, this observation was confirmed

with *in vitro* experiments, suggesting that FKRP protein localization is dependent on cell type rather than specific mutations [113]. In 2007, Campbell's group firstly reported FKRP localization in the sarcolemma of both wild-type and dystrophic mice skeletal muscles.

They suggested that an FKRP-DGC association might represent a sort of protein complex, hypothesizing a unique role in DCG stable expression [114]. FKRP sequence analysis suggests that its transmembrane domain is a signal peptide associated to the protein secretion [115]. According to this observation, fukutin, which shares high sequence homology with FKRP, can be secreted into culture media. Although the exact physiological role of the secreted FKRP is still unknown, it is noteworthy that glycosyltransferase modifications, such as the proteolytic cleavage leading to secretion as a soluble isoform of the protein, might be useful processes to modify the enzymes activity. For example, β 1,6-N-acetylglucosaminyltransferase V (GnT-V), a glycosyltransferase released by human colon carcinoma cells, has a fundamental role in tumor angiogenesis in a glycosylation-independent way, thus demonstrating that secreted glycosyltransferase might exert precise functions [116]. Patients harbouring mutations in FKRP have a secondary deficiency of laminin-α2 and a significant decrease of α-dystroglycan immunostaining [108]. In addition, the molecular weight of α-DG is reduced in muscle, suggesting that FKRP gene mutations inevitably entail abnormal glycosylation of α-DG. Recent reports demonstrate that the precise structure necessary for the complete functional maturation of α-DG is Rbo5P-1Rbo5P-3GalNAcb1,3 GlcNAcb1,4Man(6P)- O [98, 117]. Rbo5P tandem repeats are fundamental components of the post-phosphoryl moiety and they are extremely necessary for a correct binding of α-DG to ECM proteins.

In 2016, Kanagawa and his group focused on isoprenoid synthase domain-containing protein (ISPD), fukutin, and FKRP genes and their putative involvement in Rbo5P glycosylation. It was found that ISPD protein acts as

a CDP-Rbo synthase, exploiting Rbo5P and CTP [98, 117]. Thus, the intracellular levels of Rbo5P and CTP directly regulate Rbo5P-mediated modification of α-DG. Fukutin and FKRP are expected to convey a ribitol phosphate group to an acceptor, so that a phosphodiester link is generated. Thus, fukutin and fukutin-related proteins are both Rbo5P transferases, taking advantage of CDP-Rbo as a common donor substrate. These two enzymes are able to transfer ribitol phosphate groups from CDP-ribitol to α-DG both *in vitro* and *in vivo,* since patients with mutations in either FKRP or FKNT show a deficiency in mature α-DG glycosylation. FKTN acts independently of FKRP and FKRP also transfers ribitol phosphate independently from FKTN [117]. As these two enzymes are not able to convey Rbo5P directly to GalNAc or to the first Rbo5P residue, the assemblage of a tandem Rbo5P structure needs to be achieved in a sequential way [98, 117].

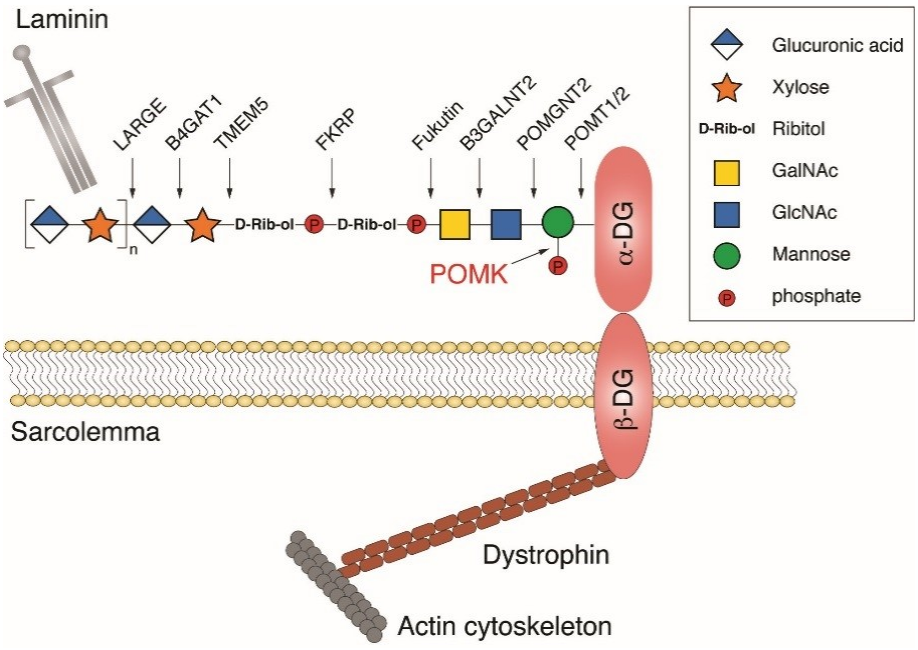

FIGURE 7. *Schematic representation of α-DG structure and glycosyltransferasic enzymes involved in α-DG glycosylation (Q. Zhu et al.; eLife, 2016) [6].*

As previously described, mutations in FKRP gene underlie both MDC1C and LGMD2I, and are associated to a wide spectrum of clinical severity. In 2004, Muntoni's group identified for the first time three broad categories of patients, correlating FKRP mutations, α-DG hypoglycosylation and patients' phenotype.

Children presenting the acute clinical spectrum of MDC1C are compound heterozygote between a null allele and a missense mutation or carry two missense mutations and show a marked depletion of α-DG glycosylation. Patients with LGMD2I, displaying DMD-like phenotype, have a moderate hypoglycosylation of α-DG and are compound heterozygotes between C826A (Leu276Ileu) mutation and either missense or a nonsense mutation. Finally, individuals with the milder form of LGMD2I are almost all homozygous for the Leu276Ileu FKRP mutation and exhibit a less severe hypoglycosylation of α-DG [109]. Until 2010, no homozygous or compound heterozygous null mutations were identified in FKRP, suggesting that null mutations could result in embryonic lethality. However, it was also reported the example of two siblings carrying an homozygous mutation in the starting codon of FKRP, resulting in the complete absence of the protein function. The siblings showed a typical Walker-Warburg syndrome phenotype [2].

1.5.3 Animal Models of MDC1C /LGMD2I

Nowadays, the knowledge of the molecular mechanisms underlying FKRP function is continuously increasing. However, the need to develop a universally recognized animal model resembling MDC1C and LGMD1C phenotypes is becoming progressively fundamental to improve the understanding of these disorders pathogenesis and to develop promising therapies. Efforts to create a homozygous FKRP knockout mouse were not successful because the complete absence of FKRP protein gave rise to embryonic lethality before day 12 of embryogenesis [105].

a) LARGE^{myd}; LARGEmyd mice present an autosomal recessive neuromuscular phenotype. Grewal and colleagues showed that the mutated gene (LARGE) encodes a putative glycostyltransferase, with a dual role. LARGE has two separate Asp- Xaa- Asp motifs, and two coiled-coil regions flanking the glycosyltransferase family 8 domains, which are typical sites of protein-protein interaction. These mice carry the deletion of exons 5-7 of the LARGE gene, resulting in frameshift and a concomitant premature termination codon (PTC). LARGE^{myd} mice display a typical muscular dystrophy phenotype. Moreover, they present both cortical and cerebellar abnormalities, reduced lifespan, pronounced kyphosis, muscle atrophy and a characteristic hindlimb paralysis [118]. Even though the clinical phenotype resembles more closely the MDC1C disorder, this mouse model has been extensively exploited in the field of both MDC1C and LGMD2I research, because of the lack of other animal models.

b) P448L; P448L mice were firstly produced by the McColl-Lockwood Laboratory for Muscular Dystrophy Research. They show a homozygous missense mutation (c1343C>T, p. Pro448Leu) in the FKRP gene. FKRP^{P448L} mutant mice present a moderate dystrophic phenotype, characterized by myofiber regeneration and degeneration cycles, consistent fiber size variability, mononuclear cell infiltration, and fibrosis arising around 26 weeks of age. The decreased α-DG glycosylation in all skeletal muscles except in a small proportion of fibers, the revertant fibers, determines a diffused muscle weakness, witnessed by limb muscle retraction. These mice present elevated serum CK and ALT levels and a dystrophic pathology typically associated with LGMD phenotype, without clear defects of the CNS [106, 118].

c) L276I^{KO} ; L276I^{KO} animal model was firstly created by Vissing's group in 2015, in collaboration with Polygene AG (Rümlang, Switzerland). Mice were created as an FKRP L276I^{KI} model with a neomycin selection cassette,

flanked by frt domains and excised by mating mice to Flp1 recombinase expressing mice. FKRP is flanked by LoxP sites, leading to an $FKRP^{KO}$, if mated to a Cre-expressing mouse, or alternatively a hemizygous FKRP L276I, if mated to an FKRP $L276I^{KI}$ mouse. Vissing's group analysed the histopathology and the level of FKRP in the mouse model at various ages and found that homozygous FKRP L276I mice develop a mild phenotype with progressive increase of muscle regeneration and fibrosis, probably due to the growing hypoglycosylation of α-dystroglycan. The homozygous $FKRP^{KO}$ is embryonic lethal, but the hemizygous L276I model resembles the age-matched homozygous FKRP L276I model [119].

d) $L276I^{KI}$; $L276I^{KI}$ mice were generated by creating a knock in mutation, the human mutation (nucleotide C826 to A), into the coding sequence of FKRP gene, resulting in the aminoacidic replacement [120]. Mutated mice display a very late onset of muscular dystrophy pathology. The mouse model displays a normal level of physical activity, viability and fertility. At 6 months, mice biopsies histology of the EDL, tibialis anterior and quadriceps appear as normal, with no significant signs of myopathy; only at 12 months muscles start to show evidence of progressive fibrosis and ongoing regeneration. At 20 months, the progression of the pathology is more pronounced. Moreover, it has been demonstrated that this mutation principally affects proximal muscles (tibialis anterior and quadriceps), rather than distal muscles (EDL) and muscles with oxidative or mixed oxidative/glycolytic fiber type composition are more prone to degeneration/regeneration cycles than glycolytic fibers [119]. The homozygous $L276I^{KI}$ has reduced muscle functions, such as shorter treadmill running distance and lower in vitro isometric force production [120]. The mild progression in the homozygous FKRP L276I knock in model mirrors patients' phenotype associated to LGMD2I, who are homozygous for the same mutation [119]. If compared to the severe phenotype of P448L mutated mice, $L276I^{KI}$ show less fibrosis and

cellular infiltration in their muscles, often focal and not uniform in the same muscle groups. The most severely -affected muscle is the diaphragm; similarly heart tissue fibrosis has been observed, signifying the insurgence of cardiomyopathy [120]. Many other mouse models for FKRP- related muscular dystrophy were generated throughout the years, however most of them did not display visible muscle abnormalities since they died either prenatally or in the early post-natal age [106, 121].

1.5.4 Therapeutical approaches in α-Dystroglycanopathies

Despite all the efforts carried out for finding effective therapies for α-dystroglycanopathies, so far a cure has yet to come. However, some outstanding achievements and progresses have been recently achieved by researches, hopefully opening the way for new generation treatments of these disorders.

Exon skipping

This therapeutic technique is aimed at directly remove the molecular damage on the messenger RNA (mRNA) of the mutated gene, restoring the correct reading frame, and permitting a functional rescue of a part of the protein. The exon skipping strategy exploits the antisense olygonucleotides (AONs), which are short RNA fragments, or synthetic oligonucleotides such as morpholino (PMO, phosphorodiamidate morpholino oligo), matching to their complementary sequence and promoting the skipping.

In 2011, Tanigushi-Ikeda and his group experimented the exon-skipping strategy in a mouse model of FCMD. The introduction of AONs targeting the splicing modulating regions restored the normal FKTN mRNA expression and normal protein levels, with a recovery of alpha-DG glycosylation and binding to laminin. However, FCMD and most of other forms of alpha-dystroglycanopathies are characterized by symptoms arising in early infancy or even during the fetal phase and are determined by CNS complications.

Thus, since oligonucleotides are unable to cross the blood-brain barrier and blood-placental barrier [122], AONs could not be considered a resolving therapy [88]. Another deleterious limit of exon skipping –based therapy is the necessity to deal with a protein in which specific domains can be skipped without irreparably invalidating the protein function. To solve these limitations, an alternative therapeutic strategy could be represented by gene replacement, based on the injection of viral vectors (adeno-associated viruses, AAVs).

Adeno-associated viruses (AAVs)

Adeno-associated virus (AVV)-mediated gene therapy has been experimented for the treatment of various diseases. AAVs are not-pathogenic vectors, which are able to replicate and infect not-proliferating cells, such as muscle fibers and neurons and vehicle the wild-type cDNA, corresponding to a specific mutated protein. In the field of muscular dystrophies different groups focused on the application of this therapeutic strategy to obtain the rescue of a mini-dystrophin gene in both the mdx and the GRMD animal models of DMD, trying to partially recover dystrophin expression and function [123, 124]. This therapeutic approach was also investigated in the field of alpha-dystroglycanopathies. In 2004, Barresi and his group performed gene therapy exploiting the Large^{myd} mouse. Barresi showed that the expression of LARGE, mediated by the injection of adeno-associated viral vectors expressing the wild-type isoform of LARGE gene, ameliorated the dystrophic phenotype of Large^{myd} mice and induced the synthesis of glycan-enriched α-DG with high affinity for extracellular ligands [125]. In 2013, Kaganawa and his group also achieved systemic gene delivery: they injected Myf5-fukutin-cKO mice, resembling a distinct dystrophic phenotype with considerable muscle fibrosis and fat infiltration and consequent reduced muscle force. They obtained an unexpected amelioration of the mice phenotype and muscle function [126]. At the same

time, the group of Qilong Lu published interesting results regarding the possibility to restore the expression of FKRP functional protein by an adeno-associated virus serotype 9 vector (AAV9)-mediated gene therapy in a mutant mouse model characterized by a proline to leucine missense mutation (P448L) [127]. These observations suggest that even small quantities of exogenously delivered genes expressing normal enzymatic activity could be sufficient to restore the correct enzymatic function. However, the problem with this technology for CMDs treatment are developmental neurological symptoms associated with these pathologies, so that an *in utero* intervention should be performed. Although different clinical trials reported undesirable effects provoked by the systemic injection of AAVs, such as host immune reaction against the viral vector and the transgene products, AAVs still represent one of the most potentially promising therapies for many types of alpha-dystroglycanopathies [128].

Enzyme replacement

In 2002, Nguyen and his group demonstrated that the overexpression of GalNac transferase from cytotoxic T cells in skeletal muscle is able to ameliorate the symptoms of muscular dystrophy in the *mdx* mouse model. The enzyme favours the linkage of a terminal GalNac residue to cytotoxic T cells. This enzyme ectopic expression determines dystroglycan to abnormally express CT antigen and the altered glycosylation pattern of dystroglycan favours an amelioration of therapeutic benefit. According to these observations, the ectopic expression of various glycosyltransferases may be a successful strategy to treat CMDs associated to α-dystroglycan hypoglycosylation [129]. Among them, LARGE protein exerts an important role in the process of O-glycosylation of alpha-DG. In 2004, the group of Campbell demonstrated that the overexpression of LARGE gene determines a hyperglycosylation of α-DG, thus promoting an increased laminin-binding activity not only in the LARGE^{myd} animal model, but also in FKTN-mutated

cells, POMGnT1-mutated patients and even wild-type myogenic cells. Many groups of research investigated the effects of AAVs-based transfer of LARGE wild type gene into different animal models of alpha-dystroglycanopathies, always obtaining promising results [118] [105]. However, the in vivo therapeutic benefit of LARGE activity is controversial. In 2015, Toda and his group explored the contrasting effects of LARGE gene therapy in the LARGE-deficient and FKTN-deficient mouse models for MDC1D and FCMD, respectively. Even though LARGE expression via systemic adeno-associated viral gene transfer ameliorates the dystrophic pathology of Large-deficient mice, the same strategy fails to ameliorate the dystrophic phenotype of fukutin conditional KO mice [130]. Finally, it was also reported that an overexpression of LARGE may even results in the worsening of the dystrophic phenotype. For instance, they observed that $FKRP_{MD}$ mice (a mouse model generated with a knock-down mutation in FKRP limited to muscle tissue) overexpressing LARGE have a reduced lifespan, if compared to $FKRP_{MD}$ mice. Specifically, they displayed a more severe pathology with an increased variation in fiber size, centrally nucleated muscle fibers, fibroadipose tissue infiltration and inflammation [105].

Metabolite supplementation

An innovative attempt to treat α-dystroglycanopathies was made by Kanagawa in 2016. After the discovery of ISPD and its role as a CDP-ribitol synthase, his group was prompted to perform a supplementation of CDP-Rbo in a ISPD-deficient cell line. They showed that the addition of CDP-Rbo restores the functional glycosylation of a-DG in targeting cells, suggesting that metabolic components such as Rbo5P and CDP-Rbo in the Rbo5P glycosylation pathway can be exploited to develop a molecular supplementation therapy for a-dystroglycanopathy. This strategy was found to be successful, however further studies on animal models should be performed to verify the safety and feasibility of this approach [98]. Moreover,

since it has been proved that an hypoglycosylation of α-DG contributes to the worsening of cancer cells behaviour in terms of proliferation and invasive potential [131, 132] and the downregulation of ISPD favours renal carcinoma cells mortality [132], CDP-Rbo supplementation may be also experimented in cancer therapy.

Corticosteroids

The use of corticosteroids represents nowadays the standard therapy for DMD patients in many countries. Their beneficial effects have been clearly demonstrated. Steroids principally act by reducing muscle necrosis and inflammation, but also by favouring the proliferation of myogenic precursor stem cells and myoblasts, leading to an increased muscle regeneration and deceleration of the pathology progression [133]. Corticosteroids administration has been found to produce beneficial effects also in LGMD2I patients [134]. Of course, corticosteroids can't represent a radical therapy, but a first palliative treatment to decrease patients' physical pain.

Rapamycin

In 2016, Beedle and his colleagues firstly investigated signalling cascades in models of dystroglycanopathies. They showed that disruption of α-DG and laminin interactions may result in downstream signalling consequences. Specifically, a dysregulation of the serine/threonine kinase Akt may occur, causing an increased apoptosis in cultured myotubes. The activation of Akt leads to the activation of mTOR complex 1 (mTORC1), which stimulates muscle growth and hypertrophy by increasing proteins synthesis. By inhibiting mTOR, it is possible to decrease muscle necrosis and the infiltration of T cells in the *mdx* mouse model.

These findings underline the possible contribution of an abnormal regulation of cell growth to the development of the disease. The authors tested the therapeutic benefit of rapamycin (RAPA) treatment in a model of *FKTN*-deficient mice. They observed that RAPA treatment is capable of delaying

disease progression, but it is unable to reverse dystrophy. Furthermore, mice with a more severe muscle involvement at the beginning of the treatment, present a weaker response to the drug [135].

Stem Cell Therapy

Very recently, Lin's group firstly exploited induced pluripotent stem cells (iPSCs), generated from cortical neurons of a patient with a mutation in FKRP gene, to evaluate targeted gene correction using CRISPR/Cas9-mediated genome editing. They demonstrated that targeted gene correction of FKRP recovers α-DG physiological glycosylation and they proved the feasibility of using CRISPR/Cas9-engineered human iPSCs for modelling dystroglycanopathies. Even though they only performed in vitro experiments, this is the first evidence in the field of α-dystroglycanopathies of a stem cell-based approach, providing the basis for an in vivo application.

1.6 Glycosyltransferases

1.6.1 General introduction to glycosyltransferases

The process of proteins and lipids glycosylation has a wide range of biologic functions. Glycosylation is the most frequent protein modification in eukaryotic cells: between 0,5% and 1% of the genes in the human genome encode proteins involved in the synthesis, degradation and function of glyco-conjugates, which have a key role in enhancing other proteins stability, mediating ligand-receptor interactions and controlling the quality of secreted proteins [136].

There are many potential roles of glycosylation in peculiar physical properties, including folding, trafficking, packaging, stabilization, protease protection, quaternary structure and organization of water structure. Changes in sugar prints may lead to physiological changes and cause disorders, i.e. cancer, rheumatoid arthritis and the development of muscular disorders such as CMDs [137].

Glycosyltransferases (GTs) represent a wide family of enzymes that are responsible for the biosynthesis of oligosaccharides, polysaccharides, and glycoconjugates. 200 glycosyltransferases have been identified in nucleated cells. The glycosylation machinery is located in the endoplasmic reticulum (ER) and in the Golgi, throughout the so called ‘’secretory pathway’’. In eukaryotes most of the glycosylation reactions, giving rise to the variety of oligosaccharide motifs of eukaryotic cells, occur in the Golgi apparatus.
Golgi resident GTs are type-II transmembrane proteins characterized by a large C-terminal globular catalytic domain facing the luminal side. Two of the most abundant forms of glycosylation are N-linked (to asparagine) or mucin-type-O-linked glycosylation (to serine or threonine) [138].

1.6.2 O-Glycosylation

O-glycosylation process begins with the addition of a GalNAc sugar to the hydroxyl group of serine or threonine residues. These glycans are very rich of mucins, proteins characterized by domains rich in proline, threonine, and serine (PTS domains).
The wide O-glycosylation present within these repeating domains favours the extension of the protein backbone of mucins, transforming it from a globular structure to an extended rod-like structure. Moreover, O-glysosylated domains protect proteins from proteolysis. Mucin-type O-glycans can be also identified on many other cell membranes and secreted proteins, proving an active and functional recruitment to modulate recognition, adhesion, and communication between cells and their surrounding environment. Several studies in animal models have shown crucial roles for O-glycans in signalling pathways of embryonic development, organogenesis, and tissue homeostasis. These studies have further suggested that O-glycosylation may also be involved in perceiving and directly regulating the secretory apparatus [139].

1.6.3 Circulating Glycosyltransferases

Even though the canonical understanding of the glycosylation pathway identifies glycosyltransferases residing intracellular, many of these enzymes are also in the systemic circulation and are known as ‘’extrinsic-glycosyltransferases’’. Originally, the physiologic function of these blood glycan-modifying enzymes was enigmatic, principally due to the absence of circulating sugar-donor substrates. However, the clinical association of these blood-residing GTs with a wide range of pathological disorders, such as liver diseases, atherosclerosis, diabetes and leukemia, prompted researchers to investigate their origin and role. Recently, it has been discovered that while many of these glycosyltransferases are freely circulating in the plasma, platelets may be the carriers for others, such as ST3Gal-1 and β4GalT released upon platelet activation [140]. These results highlighted the ability of plasma and activated platelets to supply active glycosyltransferases with the potential to remodel functionally key glycan motifs on the surface of target cells [141]. Platelets (PLTs) are megakaryocyte subfragments that participate in haemostatic and host defence reactions and deliver pro- and antiangiogenetic factors throughout the vascular system. PLTs have a life span of only 8 to 10 days in the circulation [142]. Glycosyltransferase activities in platelets are proposed to mediate different aspects of platelets functions; these findings were surprising because platelets lack an organized glycosylation apparatus. In 2012, Wandall and his group investigated the mechanisms of platelets glycosyltransferases. They showed that human platelets express three functionally distinct classes of genes encoding for glycosyltransferases: GalNac-Ts, Gal-Ts and syal-Ts. Moreover, since glycosyltransferases are predominately packaged inside platelets, they elucidated the role of platelets as a *reservoir* of glycosyltransferases that are released during platelets activation. Platelets activation due to PAR-1 release, mediate the activation

of about 50% of total GalNac-T, Gal-T ad sialyl-T GTs. As previously mentioned, a variety of carbohydrate moieties are exposed on the membrane of mammalian cells. Such carbohydrates are generally linked to specific biomolecules to create the so-called glyco-conjugates [143]. This glyco-conjugate expression changes, depending on the stage of development, differentiation, cell activation, and apoptosis. Thus, the variability in certain protein glycosylation of tissues, cells and cell-released microvesicles (MVs) may be considered as a promising biomarker of health or disease. To date, only a few published studies have connected MVs directly or indirectly with glycoproteins and glycosyltransferases. For example, recent findings show that urine-derived EVs contain a complex and biologically important glycome. As in certain kidney-associated diseases the physiological process of glycosylation is abnormal, EV-associated glycans analysis may lead to the identification of a pathological process ongoing. In 2012, Larsen and his group isolated and characterized MVs membrane proteins released by a pancreatic β-cell line (NHI 6F Tu28), before and after cytokine stimulation. The proteomic analysis revealed the presence of several sialyltransferases and glycosyltransferases in MVs, changing in abundance as a consequence of cytokine treatment [144].

1.7 Extracellular Microvesicles (EVs) and Exosomes

1.7.1 General introduction to Extracellular Vesicles (EVs)

Both prokaryotic and eukaryotic cells physiologically release vesicles: spherical microparticles delimited by a phospholipid bilayer [145]. These particles dimensions range from 30 nm to 5 μm. Their peculiar role in the intercellular communication among different cell populations throughout the whole body immediately inspired researchers from all over the world, and the interest in these microvesicles is still continuously increasing. Specifically, there is a growing curiosity about their potential in clinical applications, as it

has been recently discovered that they may represent an outstanding therapeutic approach for various disorders, with a key role in their prognosis. Moreover, they have also been identified as biomarkers of disease. EV subpopulations differ in their distinct biogenesis, nature, feature and proposed function.

They have been classified in three main categories: exosomes, microvesicles (MVs) and apoptotic bodies. However, in 2009, Théry and her group proposed the existence of another subgroup of EVs, called ectosome, exosome-like vesicles and membrane particles. These particles could be distinguished on the basis of their physical-chemical characteristics, including size dimensions, appearance in microscopy, sedimentation, lipid composition and protein markers. However, there is still insufficient evidence to support their real existence.

MVs are generally referred to as 50-1000 nm vesicles, originating from the outward budding of cell membranes and released from the plasma membrane during cell stress.

Apoptotic bodies are PS-exposing vesicles, released by cells undergoing apoptosis with dimensions ranging between 1 to 5 μm. Finally, exosomes are specialized nano-sized vesicles, derived from the endocytic compartment. Morphologically, they can be considered as the smallest vesicles released by cells [146].

1.7.2 Exosomes: Biogenesis, Composition and Physiological Function

Exosomes were firstly described in the 1980s as small microvesicles of 30-100 nm, released by reticulocytes [147]. Originally, they were identified as a mechanism for elimination of unfolded proteins or other undesirable molecules from the cell [148].

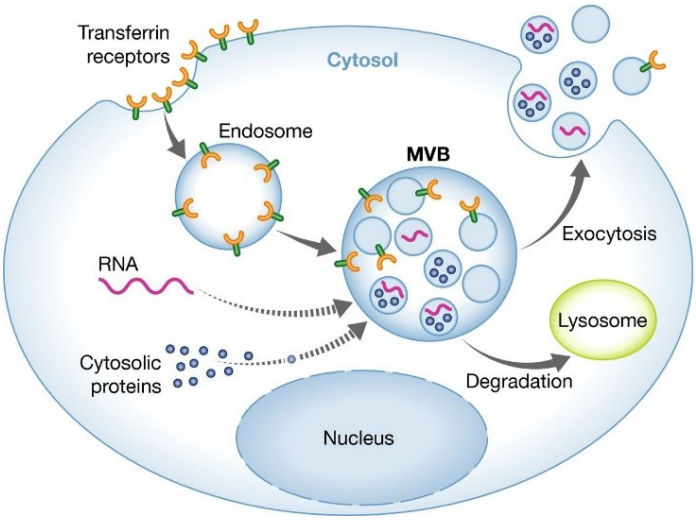

FIGURE 8. *Exosomes biogenesis and release mechanisms (J.S. Schorey et al.; EMBO Reports, 2014)[11].*

In the last decade, the exosome role as mediators of intercellular communication has emerged. So far, exosomes have been isolated from various body fluids, including blood, plasma, serum, urine, saliva, breast milk, amniotic fluid, ascites, bile, semen and cerebrospinal fluid. Exosomes carry out a wide range of functions and sometimes they exert opposing effects on targeting cells, depending on their tissue of origin and molecular content. Their morphology has been reported as cup-shaped after visualization by transmission electron microscopy (TEM) [146].The pathway of exosomes biogenesis is extremely dynamic.

Early endosomes develop into late endosomes, accumulating intra-luminal vesicles (ILVs). ILVs generate by the inward budding of late endosomes. These structures are known as multi-vesicular bodies (MVBs).

MVBs undergo two possible faiths: the fusion with lysosomes or the fusion with the plasma membrane (PM), with the consequent release of the so called ‘exosomes’ [3]. However, an alternative pathway has also been described, based on the direct gemmation of exosomes from the PM. Once

released, exosomes are captured by receiving cells following three main routes.

They may activate cell signalling by physical ligand/receptor interactions or by fusing with their target cells and transferring their contents. They may also be endocytosed by target cells or they may directly release their contents into the extracellular space. In 2007, Valadi and his group discovered that exosomes carry nucleic acids, principally mRNA and miRNA. It has been demonstrated that these mRNAs may be translated in target cells, thus cooperating with miRNA in the influence of recipient cells gene expression [149]. Recent studies also suggest that mRNA and miRNA are not randomly included into exosomes, but the process is strictly regulated through the recognition of export sequences. However, this mechanism has not been deeply investigated yet. Some research has also reported the presence of mtDNA in different EVs preparations. Proteomic studies have shown that exosomes display a wide range of proteins: some of them mirror their secreting cells, while others seem to be expressed regardless of cell type.

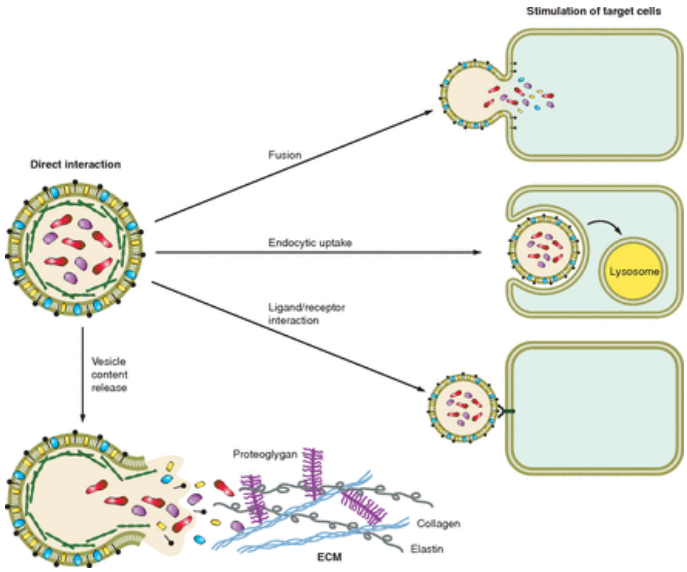

FIGURE 9. *Exosomes mechanisms of fusion to target cells (G.Turturici et al.; The American Journal of Physiology, 2014) [4].*

Exosome proteins principally derive from the PM and the cytosol, whereas those originating in the nuclear, mitochondrial, and reticular compartments are almost absent.

Various protein complexes cooperate to determine exosome biogenesis and fusion to PM. Proteins belonging to these complexes are ubiquitously expressed.

The tetraspanins CD63, CD9 and CD81 are the most enriched proteins in microvesicles, so that they are generally considered as exosome key markers in biochemical analysis. Finally, as concerns lipid composition, this group of EVs shows enrichment in sphingomyelin, PS, cholesterol, ganglioside M3 and ceramide, thus suggesting the inclusion of PM lipid rafts in their phospholipidic bilayer [3].

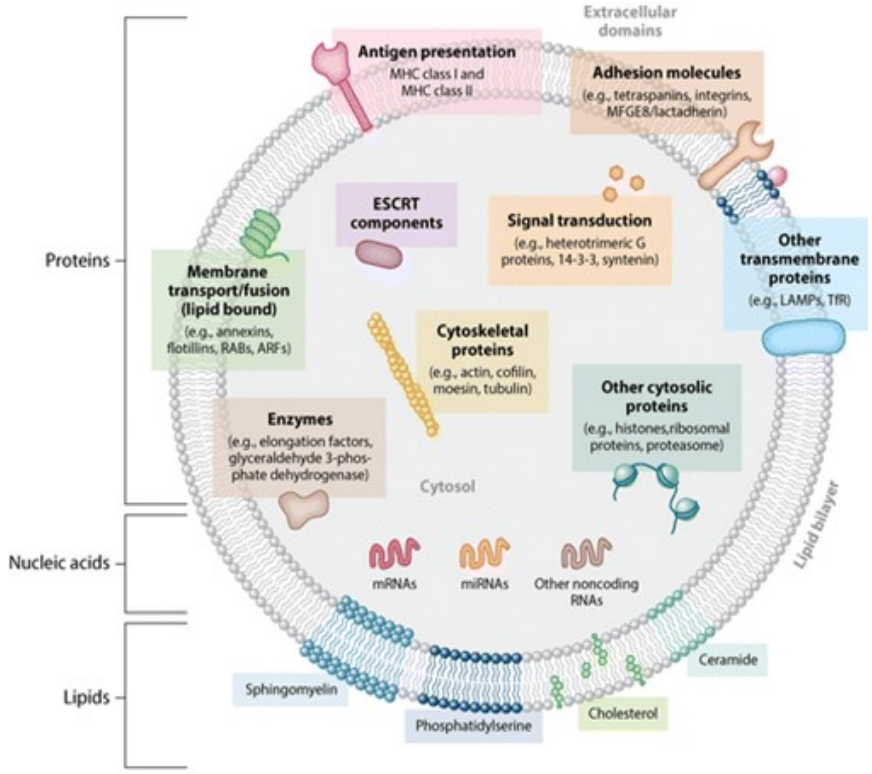

FIGURE 10. *Exosomes composition (Colombo M. et al; Annual Review of Cell and Developmental Biology, 2014)[3].*

1.7.3 Exosomes isolation techniques

To date, various procedures have been experimented to isolate exosomes. Both biochemical and biophysical characteristics can be employed to isolate exosomes, including their solubility, charge, dimensions, mass density and antigen expression. Briefly, the most performed procedures are:

- Differential ultracentrifugation
- Size Exclusion Chromatography
- Immuno-capture
- Density gradient centrifugation
- Ultrafiltration
- Commercial kits

Of note, each technique presents its own advantages and limitations [150] [151].

A) Differential ultracentrifugation (UC) has been the most popular procedure so far. Basically, it isolates exosomes according to their dimensions by progressively augmenting the centrifugal force. However, UC usually suffers from contamination of other EVs, since the distance to pellet is extremely similar among the different EVs subpopulation and since culture medium affects EVs shape and density. Moreover, it is well- known that very high-speed centrifugations create protein aggregates which co- precipitate with the exosome pellet. Furthermore, this method is extremely time-consuming and low throughput [150]. Some authors have combined UC to Density Gradient Centrifugation (DCG), based on a sucrose or iodinaxol gradients. DCG isolates exosomes according to their size and mass density. However, this method is unable to overcome contamination issue as it has been reported that HDL lipoproteins density is comparable to the one of exosomes and LDL are able to interact with EVs. Moreover, as well as DC, DCG is a very laborious method.

B) Size Exclusion Chromatography (SEC) favours size-based exosomes isolation. SEC excludes 99% of soluble plasma proteins and lipoproteins; it avoids the formation of protein aggregates and allows to recover very rapidly and efficiently (40% to 90%) exosomes, without affecting their biological properties. In comparison with DC and DCG, SEC-isolated exosomes are biophysically intact although at the expense of dilution, causing a very low final concentration.

C) Immuno-capture assay exploits monoclonal antibodies to capture exosomes, thanks to their binding to specific ligands expressed on their surface. Although the assay is rather time-consuming, it is recognized as a clinically suitable approach. It may capture exosomes of a unique cell origin and discriminate among subpopulations of exosomes with specific exosomal tags. This method provides the yield of very pure despite a very low dose of recovered exosomes.

D) Density gradient centrifugation favours the achievement of exosome isolation on the basis of their mass, size and density. When the sample is subjected to a centrifugal force in a centrifuge tube with a decreased density from bottom to top, particles move to individual zones through the density gradient, according to their sedimentation rate. This technique allows to overcome the limits related to other exosome contamination associated to differential ultracentrifugation. Unfortunately, this procedure is extremely expensive and time-consuming.

E) Ultrafiltration (UF) is based on particles separation according to their size and molecular weight. UF determines exosome separation by applying a filter in an ultracentrifuge and exerting a specific pressure. Membrane filters possess a specific cut-off to select a unique population of interest. UF guarantees a very high efficiency in exosome recovery (up to 80%) and it is very time effective. Unfortunately, it suffers from clogging and

vesicle trapping since exosomes can easily attach onto filters and samples become unavailable for downstream analysis.

F) Finally, various commercial kits have been produced. Kits are usually based on the use of polyethylene glycol, which is a water-soluble and volume-excluding polymer. The buffer co-precipitates both exosomes and non-EVs components, although exosomes recovery can be very high (around 90%). Commercial kits are not too much expensive and the procedure is extremely fast and simple [150, 151].

1.7.4 Exosomes physiological and clinical relevance

Exosomes participate in the preservation of normal physiology, such as stem cell maintenance and tissue repair. Exosomes have been recognized as morphogen carriers during development and differentiation. Moreover, they have been implicated in stem cells maintenance and plasticity, indicating their key role in tissue regeneration after injury. In the contest of pathological tissues, exosomes may determine an increased cell survival and may activate endogenous mechanisms of tissue repair and regeneration in a paracrine way. Moreover, they may exert an autocrine effect on the cell itself. Exosome release is regulated in a calcium-dependent manner; an increase in the intra-cytoplasmic influx of Ca2+ favours the EVs efflux. Moreover, some pathogenic conditions considerably influence the amount of exosome release. For example cancer cells, which are exposed to a hypoxic environment, are known to produce a higher number of MVs. During hypoxia, exosomes are secreted by tumor cells, causing an increase in angiogenic factors and metastatic potential. This observation suggests that tumor cells are able to adapt to a hypoxic microenvironment by the secretion of exosomes to promote angiogenesis and facilitate metastasis to a more appropriate microenvironment [152].

In the field of regenerative medicine, the most investigated cells are mesenchymal stem cells (MSCs). Adult stem cells, including MSCs, isolated

from different sources, confer a regenerative effect in animal models of injury and disease and they are in the phase I or II of clinical trials for limb ischemia, heart failure and myocardial infarction. Firstly, it was supposed that transplanted stem cells integrate in the damaged tissue end differentiate to substitute damaged cells. However, it was demonstrated that the systemic transplantation of cells, resulted in a very low efficiency of cells homing in the target tissue (1%). Cells probably followed other routes, and localized in the lungs, spleen, liver and kidney. Accumulating evidence suggested that the predominant, immunosuppressive therapeutic effects of adult stem cells was exerted by secreting molecules, such as growth factors, cytokines, chemokines and extracellular MVs into the surrounding environment via a paracrine mechanism. This concept has been summarized as the so called ‘’*paracrine-autocrine hypothesis”.* EVs are now considered as a prominent and universal form of cell –to-cell communication. Fundamentally, all cells in the organism release EVs that are taken up by cells at distance. Thus, EVs mediate autocrine, paracrine and endocrine effects that can be exploited therapeutically. MSCs and other progenitor cells normally used in cell therapy studies, mediate cytoprotective, angiogenic and regenerative effects, which can be explained by exosome release [153]. This observation introduces the concept of ‘’cell therapy without the cells’’.

Exosomes as biomarkers of disease. As previously cited, exosomes released in the peripheral blood and in other body fluids mirror their deriving cells, thus showing a specific content. Healthy subjects’ and patients’ exosomes display a different pattern of protein and RNA expression. So, they may be measured as potential diagnostic biomarkers [154]. For example, tumor-released exosomes are enriched in specific miRNAs, usually considered as tumor biomarkers. In 2008, Skog and his group investigated circulating exosomes of patients suffering from glioblastoma and found increased level of EGFRVIII mRNA; this observation suggested the idea of replacing the classical invasive tissue biopsy with a liquid biopsy [155].

Similarly, in 2015 Melo and his group detected proteoglycan glypican-1 (GP1)-positive exosomes in the serum of patients suffering from pancreatic cancer. The levels of GP-1 positive exosomes were strictly correlated to the tumor burden and survival of pre- and post- surgical patients, thus suggesting a prognostic relevance of this marker [156]. EVs were also evaluated as indicators of disease of multiple organs, including the CNS, the liver, kidney and lung.

Therapeutic potential of naturally secreted EVs. It was proved that EVs physiologically secreted by certain cell types retain their therapeutic potential. For example, MSC-derived exosomes possess the same immunomodulatory and cyto-protective characteristics of their parental cells; exosomes isolated from bone marrow (BM) derived MSCs guarantee protection in the contest of myocardial ischemia or reperfusion injury, hypoxia-induced pulmonary hypertension and brain injury. It was recently reported that human adult cardiac-resident progenitor cells secrete exosomes with a cardio-protective and pro-angiogenic potential [157]. In 2014, Barile and his group performed an intra-myocardial injection of these exosomes and they observed an improved cardiac function after myocardial infarction in rats [158]. Differentiating neuronal cells- secreted microvesicles were shown to stimulate neuronal differentiation in human MSCs [154]. The finding that EVs released by B-cells carry MHC-II, co-stimulatory and adhesion molecules, suggested that such vesicles could directly stimulate CD8 T-cells clones. This idea was further supported by the demonstration that vaccination of mice with tumor peptide-pulsed DC- derived exosomes primes specific CTLs and suppresses tumor growth in a T-cell dependent manner. The capacity of EVs to stimulate T cells, including T naïve, can be enhanced by the interaction of vesicles with DCs. AVs harbour ligands that participate in binding to target cells or extracellular matrix proteins. Once internalized by DCs, exosomes can be degraded and used as a source of peptides to interact directly with T cells. Exosomes also transfer native

antigens to APCs: tumor -deriving exosomes carrying tumor specific Ags can be efficiently taken up by DCs for antigens processing and presentation to tumoral CTLS [159]. Mice vaccination with tumor- derived exosomes produced a massive CD8 T cell-mediated anti- tumoral effect. Finally, EVs released by immune cells may induce either an immune stimulation or inhibition under different conditions [159]. In 2010, Viaud's group showed dendritic cells (DCs)- released exosomes capability to present antigens to the immune system and introduced the concept of an exosome-based vaccine against cancer and infection [160]. Tumor-derived exosomes have been reported either to stimulate or suppress tumor specific and non-specific immune response. As exosomes mirror the protein composition of their parent cells, tumor-derived exosomes are enriched in tumor antigens. Therefore, these EVs have been used as a source of tumor antigens to stimulate an anti tumoral response. As well as carriers of protein Ags, exosomes favour the intercellular passage of genetic information, principally RNAs, thus suggesting their potential role in gene therapy.

Therapeutical potential of loaded and targeted exosomes. Exosomes may be loaded with therapeutic cargo molecules. There are two alternative approaches for exosome loading: an *ex vivo* extracellular strategy and an *in vitro* intracellular approach, exploiting the mechanisms of physiological EVs biogenesis [154]. Exosomes may be loaded with therapeutic miRNA, mimic or antagonists, by co-transfecting producing cells with two plasmids, one encoding the precursor miRNA and the other one the fusion targeting peptide. Otherwise, electroporation may be used to produce transient pores in the membrane, thus supporting small RNAs crossing of the phospholipidic bilayer. Electroporation was also employed to load EVs with small-molecule drugs. A lot of exosome-based drug delivery systems have been already developed. Among them, curcumin encapsulated exosomes have been systemically injected to target the central nervous system across the blood brain barrier (BBB) and different chemotherapeutic agents, such as

Doxorubicin and Paclitaxel, have been loaded into exosomes and systemically injected to arrest the tumor growth [161]. One of the main limits related to exosome-based therapy is represented by these vesicles biodistribution profile after an in vivo injection. Secreted EVs with no modifications to their natural composition prohibit their systemic administration due to their limited tropism to a specific cell type. Just a few cell types release vesicles exhibiting an own target selection; DCs-EVs interact with activated T-cells through ICAM-1 transmembrane protein [162]. Targeting strategy may be accomplished by engineering the parent cells using fusion constructs between a targeting ligand and a EV transmembrane protein [163]. The released-EVs will bear the ligand/homing peptide on their surface. Alternatively, EVs surface may be coated with antibody fragments, recognizing antigens expressed on the target-cell surface. Finally, peptides facilitating the EVs uptake, such as vesicular stomatitis virus-G (VSV-G) protein can be displayed on EVs. These engineered vesicles achieve improved cargo delivery and therapeutic immune response to exosomal vesicles [164].

1.7.5 Exosomes-based therapy advantages and disadvantages

Immune tolerance

Physiologically secreted exosomes express immune-recognition molecules, including functional MHC-I and/or MHC-II depending on their cell origin. Experimental evidence suggests that allogenic exosomes may be hypo-immunogenic and well- tolerated.A recent study investigated the immunogenicity of xenogeneic (human) or allogeneic cardiosphere-derived exosomes [165]. A continuous subcutaneous injection of human cells-secreted exosomes induced a gradual humoral and cell-mediated immune response, although at lower levels compared to the injection of parental cells. Allogeneic EVs did not induce significant immune response after repeated

doses. These findings suggest that allogeneic EVs may be suitable for clinical applications [165].

Biocompatibility and safety

Biocompatibility is ensured by EVs endogenous origin; neither the insurgence of tumorigenesis, nor rejection episodes have been observed by monitoring exosomes-transplanted mice. Nanometric dimensions allow these vesicles escape from the uptake of the endothelial reticulum system, thus favouring the crossing of endothelium barrier. Moreover, the already mentioned recovery of glyoblastome- released MVs in the circulating blood, witnesses their skill to traverse the blood brain barrier (BBB) [167-169].

Methods of exosomes isolation

One of the major limits related to the field of EVs is represented by the absence of a standardized method of isolation. Nowadays the gold standards are considered: differential ultracentrifugation, density gradients, size exclusion chromatography and commercial kits. However, each technique has its advantages and disadvantages and the absence of other MVs co-precipitation with exosomes has not been excluded yet [151] [150].

Tumorigenesis

It has been demonstrated that tumoral cells release a high amount of vesicles, however these vesicles express specific factors and proteases, which are able to promote the tumor progression and digest the extracellular matrix, thus determining the insurgence of metastasis [170, 171].

Exosomes half-life

Exosomes lifetime after in vivo injection has not been well elucidated yet. Researchers report antithetic observations about MVs half-life and biodistribution in vivo. Someone observed a very brief survival, which would not be consistent with the development of an efficient clinical therapy. In 2013, Takahashi Y. et al., isolated exosomes from B16-Bl6 melanome cell-

line. Exosomes were labelled with gLuc-lactadherin and intravenously injected in a murine model to analyse their biodistribution. The kinetic study of exosomes concentration in injected mice peripheral blood (two minutes after exosomes injection) highlighted a lifespan of about two minutes. A residual luciferase activity was detected in the liver and in the lungs serum 4 hours post injection, suggesting a very fast clearance by these organs [172].

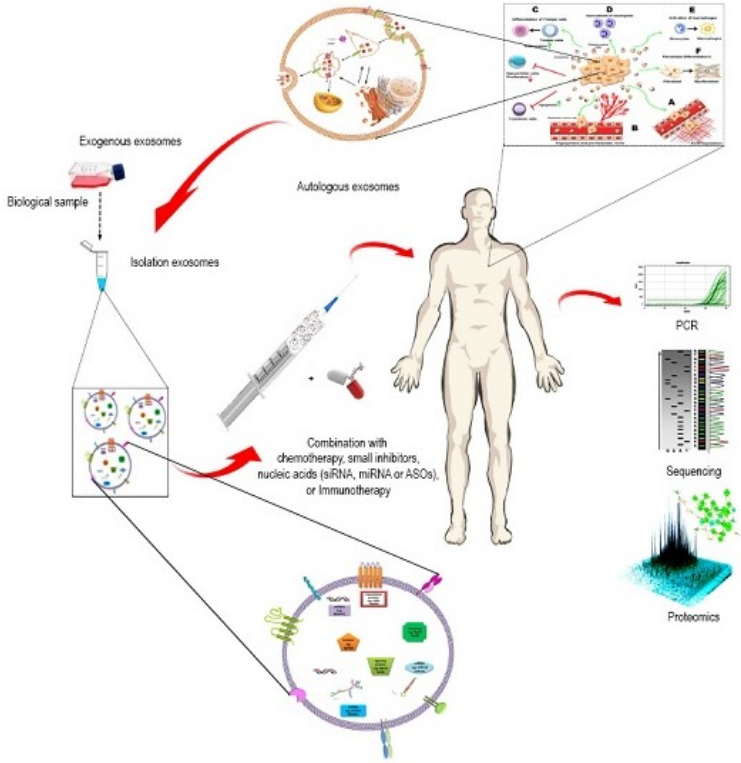

FIGURE 11. *Exosome-based diagnostics and therapeutics (M.H Rached; International Journal of Molecular Sciences, 2017).*

In 2015, Wiklander O.P.B and his group described the progressive biodistribution of exosomes at different time-points after injection. The localization profile of MVs remained unchanged within the first 24 hours after injection (heart, gastrointestinal tract, kidneys), whereas after 48 hours a decrease in these districts and an increased exosome concentration in

pancreas were observed. Authors correlated these changeable distribution profiles to the presence of marker artefacts, due to an aspecific staining. Moreover, markers half-life was found to be longer than the one of exosomes themselves, thus constituting one of the major issues for their detection. In order to perform an exosome-based transplantation, the precise knowledge of exosomes lifespan should be essential to establish the right doses and intervals of administration and the potential effects in terms of toxicity [173].

2 AIM

To date, there are no resolving therapies for α-dystroglycanopathies. Even if some approaches, such as AAV-based gene therapy, have shown promising results when applied in vivo into mouse models, they still present many limits preventing their applicability in clinical trials.

Based on successful results previously obtained by our group in the *mdx* mouse model, resembling the Duchenne muscular dystrophy phenotype [57], we aimed to test for the first time the combination of stem cell and gene therapy in the field of α-dystroglycanopathies.

1) We isolated CD133+ stem cells from a MDC1C patient's peripheral blood and we engineered cells with a lentiviral vector expressing the wild-type isoform of FKRP mutated gene with the aim to evaluate the recovery of fukutin related protein expression. We tested the best performing infection condition, in terms of cytotoxicity lack and proper rescue of functional FKRP protein. Both of them represent essential requirements for a prospective clinical translation of this approach.
2) In order to test the effectiveness of this strategy in conceived animal models, and given the lack of immunodeficient mice, we engineered satellite cells derived from L276I^{KI} mice, resembling the LGMD2I dystrophic phenotype, for intramuscular autologous transplantation. We examined the best performing MOI of infection, the LV dose- associated cytotoxic outcomes, as well as the FKRP expression/functional recovery. Since the recovery of functional FKRP expression would determine a proper a-DG glycosylation, we have also tested the minimum level of FKRP expression that guarantees a physiological glycosylation of α-DG.
3) Since recently published works underlined cell capacity to release FKRP in their culture medium, we sought for an exosome involvement in glycosyltransferase trafficking. To this end, we firstly determined the secretion of exosomes from engineered stem cells, and we investigated the presence of exogenous FKRP as cargo of released exosomes.

4) Once proved exosome-mediated FKRP secretion in vitro, we performed an intramuscular transplantation of engineered cells to evaluate the in vivo release of FKRP+ exosomes, and to investigate their capacity to prompt FKRP expression and functionality in both the site of injection and distal tissues. Moreover, we aimed to deepen our knowledge in exosomes kinetics and biodistribution by reproducing their trafficking in vitro exploiting a microfluidic bioreactor.

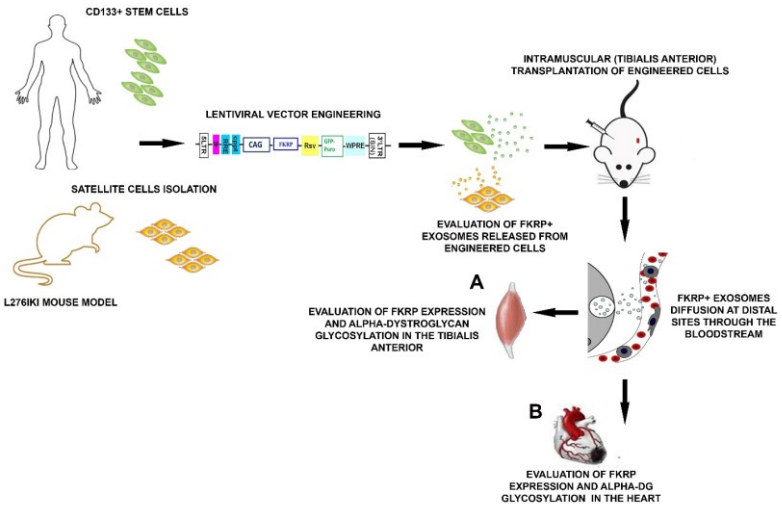

FIGURE 12. *Schematic representation of our experimental plan*

An exosome-based approach would further sustain and boost the therapeutical effect of a combined gene and cell therapy. Above all, its applicability could be interesting in the field of metabolic myopathies and all muscular dystrophies presenting an enzymatic defect, such as α-dystroglycanopaties. For instance, while structural proteins necessitate to be re-expressed on targeted membranes, we hypothesize that exosome-mediated enzyme transfer would allow to obtain a fast response in targeted tissues. Engineered cells continuous release of FKRP+ exosomes would permit a long-lasting maintenance of the enzymatic levels required to supply its deficiency.

3 MATERIALS AND METHODS

3.1 In vitro analysis of CD133+ blood-derived stem cells

3.1.1 Isolation of MDC1C blood-derived CD133+ stem cells

CD133+ stem cells were purified from the blood of a patient affected by Muscular Congenital Dystrophy Type 1C (MDC1C). The patient presented two mutations in heterozygosity in the FKRP gene: C518T>G and C1087G>C. CD133+ stem cells were sorted with a MACS magnetic column (Miltenyi Biotech; Bergisch Gladbach, Germany). Blood was firstly diluted 1:3 in Iscove's modified Dulbecco's medium (IMDM) (Gibco, Thermo Fisher Scientific; Waltham, Massachusetts, USA). Following mononuclear cells centrifugation, (Ficoll-Hypaque; Pharmacia Biotech, Uppsala, Sweden) cells were incubated with a CD133+ cells isolation kit, consisting in CD133 monoclonal antibody, linked to paramagnetic MicroBeads (Miltenyi Biotech; Bergisch Gladbach, Germany). Cells were washed and processed exploiting the MACS magnetic separation column (Miltenyi Biotech; Bergisch Gladbach, Germany). Thus, a CD133+ cell population was finally isolated.

3.1.2 Characterization of human blood-derived CD133+ cells for FACS analysis

To perform flow cytometry, $1x10^5$ cells were incubated with CD34–APC (allophycocyanin), CD133/2–PE (phycoerythrin) (Miltenyi Biotech; Bergisch Gladbach, Germany), and CD45–FITC (Becton Dickinson, Immunocytometry Systems; San Diego, California, USA). For all moAbs, a proper isotype-corresponding mouse Ig was exploited as control. Each staining was carried out by incubating cells for 20 minutes at 4 °C, than cells were washed in PBS with 1% inactivated foetal calf serum (FCS) (Gibco, Thermo Fisher Scientific; Waltham, Massachusetts, USA) and 0.1% sodium azide. The analysis was executed with a FC500 cytomics flow cytometer (Beckman Coulter; Brea, California, USA) and 2.1 CXP software. Each

analysis involved not less than 15000–30000 events. A light-scatter gate was settled to exclude cell debris. The percentage of CD133+ cells in the sample was calculated after the adjustment for the percentage of cells reacting with the control.

3.1.3 Blood-derived CD133+ stem cell culture conditions

Blood-derived CD133+ cells were seeded in six-well tissue culture plates (Falcon Labware; Oxnard, California, USA). 10^5 cells were plated per well and cultured in DMEM/F-12 (1:1) and 20% FBS (Gibco, Thermo Fisher Scientific; Waltham, Massachusetts, USA), in the presence of HEPES buffer (5mM), glucose (0.6%), sodium bicarbonate (3 mM), and glutamine (2mM). Some cytokines were addiced to the medium: vascular endothelial growth factor (VEGF), 50 ng/ml (Tebu-Bio; Frankfurt, Germany), stem cell factor (SCF), 100 ng/ml, and leukemia inhibiting factor, 20 ng/ml (R&D Systems Inc; Minneapolis, Minnesota, USA). Cells were passed weekly and incubated in a fully humidified atmosphere of 5% CO 95% air at 37 °C.

3.2 FKRP L276I^{KI} mouse model

Mice were gently provided by Qilong Lu's group (McColl-Lockwood Laboratory for Muscular Dystrophy Research, Neuromuscular/ALS Center, Carolinas Medical Center, Charlotte, North Carolina, USA). The FKRP L276I^{KI} mouse model was generated by introducing a knock in mutation in the human FKRP gene (a missense mutation leading to nucleotide replacement C826 to A) into the coding sequence of the corresponding murine gene, causing an amino acid substitution: leucine to isoleucine (L276I). As reported by Lu's group, the neomycin resistant (Neo^r) cassette was introduced into intron 2, around 140 bp upstream from the coding exon 3. Heterozygous and homozygous mutated mice were genotyped using the following PCR primers: FKRP-WT-F: TTC TTG CCT CGG ATT GTG TAT G; FKRP-WT-R: TCA CTC TCC AAG GGC CTA CAG C; Neo-F-FKRP: AAC

AAG ATG GAT TGC ACG CAG G; Neo-R-FKRP: TGG TCG AAT GGG CAG GTA G [120]. Animals were maintained in Charles River Laboratories (Calco; Italy) and supplied with limitless water and food.

3.3 Satellite Cells isolation and characterization

3.3.1 Isolation of satellite cells from FKRP L276I^{KI} muscles

Satellite cells (SCs) were dissociated from FKRP L276I^{KI} new born hind limbs mice muscles as already reported [174]. Firstlly, biopsies were cleaned in PBS: 8g/l NaCl, 0,2g/l KCl, 1,44g/l Na2HPO4, 0,24g/l KH2PO4 in distilled water; pH 7.4) to wash off blood residuals. Muscles were resuspended in Dulbecco's modified Eagle's medium (DMEM) (Gibco, Thermo Fisher Scientific; Waltham, Massachusetts, USA) with penicillin/streptomycin (100µL/10ml) and fungizone (120µL/10ml): connective and adipose tissues, blood vessels and nerves were manually discarded using a dissection microscope. Then, sample was mechanically homogenized and subsequently digested at 37 °C for 30 min with an enzymatic solution made of collagenase V (Sigma-Aldrich, St. Louis, USA) 0,11 mg/ml, dispase (Gibco, Thermo Fisher Scientific; Waltham, Massachusetts, USA) 0,45 mg/ml, DNase (Roche; Basilea, Switzerland) 0,01 mg/ml in 12 ml of Hank's balance salt solution (HBSS) (Gibco, TechnologiesThermo Fisher Scientific; Waltham, Massachusetts, USA). A 70-µm cell strainer was used to filter the previously dissociated muscular tissue. After a 15-minutes incubation, cells were centrifuged at 458g for 20 minutes at room temperature. Subsequently, the pellet was resuspended in DMEM at 20% of FBS with antibiotics, 1% embryonic extract chicken (CEE) (Gibco, Thermo Fisher Scientific; Waltham, Massachusetts, USA) and 2% horse serum (HS) (Gibco, Thermo Fisher Scientific; Waltham, Massachusetts, USA) and plated cells were incubated at 37 °C, 5% CO_2. The supernatant was harvested and centrifuged at 458g for 20 minutes. Trypan Blue Assay was performed (Sigma-Aldrich; St. Louis,

USA) and cells were seeded at a density of 380 cells/cm^2 in culture dishes, previously incubated overnight with collagen. After 24 hours, fresh medium was replaced.

3.3.2 FKRP L276I^{KI} SCs FACS analysis

SCs were phenotypically analysed by FACS analysis. Cells were incubated with Pax7 (Hybridoma Bank; Lowa, USA) and CD29-FITC (Miltenyi Biotech; Bergisch Gladbach, Germany). For Pax7 detection, cells were firstly fixed with 1,5% paraformaldehyde, then incubated overnight with the primary antibody at 4 C° (1:10) and with monoclonal goat anti-mouse 488 Alexa Fluor secondary antibody (Molecular Probe; Thermo Fisher Scientific; Waltham, Massachusetts, USA) (dilution 1:100). CD29 staining was performed by incubating cells for 20 minutes at 4°C. Anti-7-alpha-actin-mycin D (7-AAD) (Becton Dickinson, Immunocytometry Systems; San Diego, California, USA) was exploited to determine cells vitality. After the incubation step for 20 minutes at 4 °C, cells were washed in PBS1X, containing 1% heat inactivated FBS and 0,1% sodium azide. The analysis was performed using FC500 cytomics flow cytometer (Beckman Coulter; Brea, California, USA) and 2.1 CXP software. Each test comprehended not less than 15000-30000 events.

3.3.3 FKRP L276I^{KI} SCs Immunofluorescent Analysis

Satellite cells immunofluorescence staining (IF) was executed to evaluate dystrophic satellite cells myogenic differentiation potential. When cells reached confluence of about 80-90%, the growing medium was substituted with differentiation medium, composed of DMEM addictioned with 2% HS .Firstly, cells were fixed in formaldehyde 4% for 10 minutes at RT, and then incubated in blocking solution (5% of FBS, 2% of HS, 0,3% TRITON in PBS1X) for 30 minutes. SCs incubation with Pax7 antibody (dilution 1:20) was performed overnight (Hybridoma bank; Lowa, USA) at 4°C. After that, cells were stained with the α-mouse biotinilated (dilution 1:100) for 30

minutes and with Cy3-streptavidin-conjugated secondary antibody (Sigma-Aldrich, St. Louis, USA) for 1 hour. Afterwards, the sample was incubated with desmin antibody (diluted 1:50) (Abcam; Camdridge, UK) for 1 hour and visualized with anti-rabbit Alexa Fluor 488 antibody (Molecular Probe; Becton Dickinson, Immunocytometry Systems; San Diego, California, USA) (diluted 1:100). DAPI was used for nuclear staining (4′, 6-Diamidino-2-phenylindole dihydrochloride) (Sigma-Aldrich; St. Louis, USA). Satellite cells were stained at three different time points: at T0, before culturing cells in serum starvation medium, at T7 and at T14, after one week and two weeks in differentiation conditions. Images were taken with Leica TCS SP2 confocal microscope.

3.4 MDC1C CD133+ blood-derived stem cells and L276I^{KI} FKRP SCs transduction

3.4.1 Lentiviral vector (LV) design and titer of viral preparation

The LV was created by AMS Biotechnology (AMSBIO; Abingdon, UK) company, as previously published [175]. Human FKRP gene (NM_001039885.2) was recovered from a gene bank and it was inserted into the lentiviral vector. Human FKRP gene was placed under the cytomegalovirus early enhancer/chicken β-actin [7] promoter. Green fluorescent protein and puromycin were exploited to positively select lentiviral-infected cells and they were both expressed under a Rous sarcoma virus promoter. Consequently, FKRP and the GFP genes were autonomously transcripted. The Lentiviral vector was obtained from the human immunodeficiency virus (HIV-1). Lentivector sequence verified expression was co-transfected with lentiviral packaging plasmids. The re-engineered lentiviral packaging plasmid contained the coordinated, optimized expression of gag /pol, rev and VSVG and generated high titers of lentivirus in 293T packaging cell line as described by manufacturing instruction. The packaging plasmid was engineered to minimize the likelihood of recombination between expression vector and packaging

components for enhanced safety and high yield virus production. After co-transfection with the third generation lentiviral expression vector, it generated only replication incompetent lentivirus. Lentivirus was then concentrated via ultracentrifugation and resuspended in PBS solution. A LV expressing only GFP and puromycin selection without the target gene was also produced and used as control.

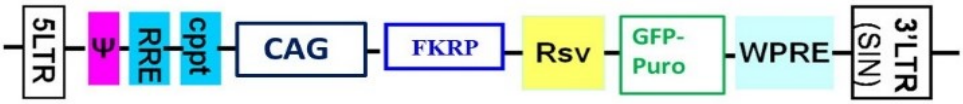

***FIGURE 13**. The lentiviral backbone structure. Human wild-type FKRP gene was expressed under the CMV early enhancer/chicken b-actin [7] promoter. GFP-Puromycin reporter gene was expressed under a Rous sarcoma virus [Rsv] promoter.*

To determine the proper MOI of infection, 10^5 CD133+ dystrophic cells were infected with 5 x 10^5 ip, 10^6 ip, 2 x 10^6 ip (MOI of 5, 10, 20) in a 96-wells plate, soon after the isolation procedure. LV infection was conducted in 100 µl of DMEM supplemented with 10% FCS overnight. Then, fresh medium was added and cells were maintained at 37°C and 5% CO2. Each MOI was tested in three experimental settings. The immunophenotypical analysis and the evaluation of the % of GFP+ cells in the 488 nm emission wavelengths and by GFP+ cells count (Fiji Analyze Particles function, Image J program) were performed after 6 days, to evaluate the transduction efficiency. MOI 20-transduced cells viability was monitored to detect potential impairments due to an unexpected virus cytotoxic effects. Dystrophic CD133+ cells infected with MOI 20 and the not-infected corresponding cells proliferation were estimated exploiting the Trypan Blue Exclusion assay every 5 days for 30 days. FKRP L276I^{KI} dissociated SCs were cultured in 48 wells (10000/well) and infected with increasing lentiviral MOI: 10, 20, and 40. Different MOI outcomes on FKRP L276I^{KI} SCs were also evaluated. As previously reported for human CD133+ dystrophic stem cells, transduced and not-transduced

satellite cells proliferation was calculated at 5-days intervals for 25 days, performing Trypan Blue Exclusion assay. We also monitored the outputs of the lentiviral vector expressing only the GFP protein, to exclude the prospect of GFP LV-induced toxicity. Trypan Blue Exclusion Assay was carried on FKRP L276I^{KI} SCs infected with 10, 20, and 40 MOI of the empty vector. Cells deriving from each condition (including cells infected with different MOIs with the empty lentiviral vector) were cultured in serum starvation to induce myogenic differentiation and eventually detect unexpected MOI-related deleterious outcomes. After a week in serum starvation, we evaluated the Fusion Index (FI)(number of myotubes nuclei/total number of nuclei). To determine the IF, differentiated satellite cells were cleaned with PBS and fixed in 4% paraformaldehyde for 10 minutes. Afterwards, SCs were incubated with desmin antibody (1:50) (Abcam; Cambridge, USA) for 1 hour and stained with DAPI, thus allowing to visualize myotubes nuclei. FI was finally calculated using the NIH ImageJ software. If muscle cells were found to contain 3 or more nuclei, they were considered myotubes, as previously reported [176].

3.4.2 Evaluation of wild-type FKRP expression in human MDC1C CD133+ blood-derived and murine dystrophic L276I^{KI} satellite infected cells

Infected human MDC1C CD133+ blood-derived stem cells and infected murine dystrophic L276I^{KI} SCs were lysed in NP40 lysis buffer (20mM Tris-HCl (pH 7.8), 140mM NaCl, 1mM EDTA, and 0.5% NP40, 1mM phenylmethylsulfonil fluoride) and addictioned with a cocktail of protease and phosphatase enzymes inhibitors (Complete and PhoSTOP) (Roche Diagnostics; Basilea, Switzerland). Cell lysates were incubated at 4°C for 30 min, and centrifuged at 15682g for 15 min at 4°C. The protein concentration was measured performing Lowry's assay. Following protein concentration analysis, 30 µg of samples were loaded on a polyacrylamide gel (10%) for

WT FKRP detection; 8% polyacrylamide gels were used to detect α-DG glycosylation levels. Subsequently, proteins were transferred to supported nitrocellulose membranes (Bio-Rad Laboratories; Hercules, CA, USA). A blocking solution (10 mM Tris (pH 7.4), 154 mM NaCl, 1% BSA, 10% horse serum, and 0.075% Tween-20) was exploited to saturate nitrocellulose membranes. FKRP detection was performed exploiting the FKRP-5643 (FKRP-STEM) antibody, which was kindly provided by Dr Qilong Lu and his group (McColl Lockwood Laboratory for Muscular Dystrophy Research, Neuromuscular/ALS Center Carolinas Medical Center, Charlotte, North Carolina, USA). FKRP-STEM is a rabbit polyclonal antibody recognizing the stem region (amino acids 29–130) of the murine FKRP protein. The antibody only recognizes the wild type isoform of FKRP protein, and it is unable to stain mutated isoforms. Therefore, WB positive bands are necessarly related to lentiviral-mediated exogenous FKRP recovery. The secondary antibody (rabbit anti-FKRP antibody, diluted 1:600) was incubated overnight at 4°C. Mouse anti-α-DG (IIH6-C4-5, dilution 1:50) (Hybridoma Bank; Lowa, USA) was exploited to detect the level of α-DG-glycosylation. Anti-β-actin (1:600) (Sigma Aldrich; St. Louis, USA) was used as housekeeping protein. There are two commercially available antibodies to detect α-DG-glycosylation: VLA4 and IIH6. Both of them recognize epitopes of the entirely glycosylated form of α-DG. In both in vivo and in vitro experiments, the immunoreactivity of these two antibodies has been correlated to laminin binding activity. However, only IIH6 inhibits this linkage. These observations underline how the two antibodies identify different, glycan-dependent sites and highlight the strict connection between these epitopes and the laminin binding site (Hewitt, 2009). As IIH6 principally interacts with the laminin-binding site of DG, the observed decreased staining underlines an abnormal laminin binding in patients with this clinical phenotype. Visualization was accomplished with horseradish peroxidase (HRP)-conjugated antibodies (Dako; Glostrup, Denmark) 90 minutes at RT and by enhanced chemiluminescence (ECL)

development (GE Healthcare; Little Chalfont, UK). Pre-stained molecular weight markers (Bio-Rad Laboratories; Hercules, CA, USA) were loaded on each gel. Visualization was performed using Amersham Hyperfilm™ (GE Healthcare; Little Chalfont, UK). CanoScan LiDE60 Scanner (Canon) and the Canon ScanGear Software were used to obtain images of bands. Densitometric analysis was conducted using ImageJ software (http://rsbweb.nih.gov/ij/). Not-infected CD133+ stem cells and not-infected L276I FKRP^{KI} SCs were loaded as controls. Immunofluorescent staining was performed on FKRP L276I^{KI} satellite cells infected with MOI 20, to identify both GFP fluorescent protein and human exogenous FKRP expression. After SCs fixation with 4% paraformaldehyde for 5 minutes, the membrane was incubated in blocking solution (1% BSA, 0, 05% Tween, 5% FBS in PBS1X) for 30 minutes and then for 2 hours with rabbit anti FKRP-STEM (dilution 1:50) and mouse anti-GFP (dilution 1:500) (Abcam; Cambridge, UK) antibodies in the same solution. Secondary monoclonal antibodies (anti-rabbit 594 and monoclonal anti-mouse 488) (Molecular Probe, Thermo Fisher Scientific; Waltham, Massachusetts, USA) were used at a dilution of 1:100 in PBS for 1 hour. Nuclei were stained with DAPI (Sigma-Aldrich; St. Louis, USA). Images were captured with Leica TCS SP2 confocal microscope (Leica, Germany).

3.5 Isolation and characterization of human MDC1C CD133+ blood-derived stem cells and murine dystrophic L276IKI satellite cells-derived exosomes

3.5.1 Purification of exosomes by Differential Ultracentrifugation

The most widely applied method for concentrating and purifying exosomes consists of differential ultracentrifugation. This isolation procedure is based on serial cycles of centrifugation at increasing centrifugal force, to pellet smaller and smaller particles. Exosomes are separated from other culture medium particles according to their differences in terms of density and size.

Cell debris are immediately removed from culture medium (CM) through a centrifugation at 2000g for 30 minutes. Subsequently, CM is centrifuged at 10000g for 45 min to pellet apoptotic bodies and other big particles. Supernatants (SN) are then filtered (pore size 0.2μm) to remove remaining large particles. Filtered SN are ultracentrifuged at 130000g for 2 hours. The obtained pellet is washed with PBS and pelleted again at 130000g for 2h to remove protein contamination. The final pellet is resuspended in filtered PBS or NP40 Lysis Buffer, according to the predicted following analysis. All samples are ultracentrifuged in polyallomer 36 ml centrifuge tubes, using a Beckman Coulter ultracentrifuge (Beckman Coulter Optima L-90K ultracentrifuge), with a fixed angle rotor type 50.2Ti.

Recovered exosome protein concentration was measured with the microBCA kit assay (Thermo Fisher Scientific; Waltham, Massachusetts, USA). This assay allows for the evaluation of very low doses of recovered proteins.

3.5.2 Purification of exosomes by Size Exclusion Chromatography (SEC)

The fundamental of SEC analysis is the separation of particles according to their dimensions or molecular weight. This method can be applied to isolate vesicles from both body fluids and cell culture medium. Collected culture medium was centrifuged at 2000g to discard floating cells and cell debris and subjected to concentration in 10K molecular weight cut-off (MWCO) (Merck Millipore; Darmstadt, Germania) filter units. A maximum of 15 ml supernatant was centrifuged at 4000g for 20 min at RT in a swinging-bucket rotor, to obtain a final volume of about 500 μl. Subsequently, chromatography was performed taking advantage of the qEV Size Exclusion Columns (qIZON; Schaefer, South East Europe). In brief, 500 μl of concentrated culture medium were loaded on one column. PBS filtered buffer was exploited as appropriate eluent buffer. 500 μL fractions were collected. According to the

manufacturer's instructions, the first six fractions (3 mL) represent the void volume, whereas exosomes are predominantly eluted in fractions 7, 8 and 9. According to datasheet instructions, SEC columns rescue particles bigger than 50000 KDa, thus eliminating bulk proteins in solution. MicroBCA assay revealed that the exosome most-abundant fraction was fraction 7, followed by fraction 8. A very low amount of exosomes was found also in fraction 9.

3.5.3 Purification of exosomes by Commercial Kits

To test the efficiency of exosomes enrichment by using commercial kits we exploited the Total Exosome Isolation Reagent from Cell Culture Medium (Thermo Fisher Scientific; Waltham, Massachusetts, USA). According to the manufacturer's suggestions by tyning up water molecules, the reagent forces less-soluble components such as vesicles out of solution and allows collection by a short low-speed centrifugation. Briefly, collected medium was mixed 1:2 with the reagent and incubated ON at 4°C. Isolated exosomes are recovered by standard centrifugation at 10000g for 60 minutes.

3.5.4 Setting of cell seeding conditions for culture medium collection

To further analyse the process of exosome release, we focused on the possibility to set the proper culture conditions for recovering the most homogeneous population of vesicles. C2C12 myoblast cell line was exploited to perform these experiments. Cells were seeded in 10-cm dishes at 40000 cells/cm^2 density. Cell proliferation and exosome secretion were observed at three specific time points: T1 (24h of culture), T2 (48h of culture) and T3 (72h of culture). Prior to use, FBS was ultracentrifuged at 130000g overnight to remove the possible contaminant vesicles. For T1 condition, cells were directly cultured in DMEM with exosome-depleted FBS after seeding. As for T2 and T3, complete medium was replaced with exosome-depleted medium 24 hours before the collection. Cell proliferation was evaluated performing an MTT assay.

3.5.5 Purification of exosomes from cell culture medium of cells growing in suspension

According to the isolation procedure previously published by Clothilde Théry and her group in 2006, cells were firstly centrifuged 10 minutes at 300g. Then, the supernatant was poured off and cells were resuspended in medium addictioned with exosome-depleted FBS. Conditioned medium was collected only after 24 hours in culture [146]. For instance, most lineages of cells growing in suspension have a very fast proliferation rate and may reach over confluence, starting to die within 48 hours. Once collected, the CM was centrifuged at 300 g for 10 minutes: the supernatant was transferred into new tubes, while pelleted cells (and other large dead cells and debris) were plated again. After CM collection, exosomes were isolated exploiting size exclusion chromatography (SEC).

3.5.6 Exosome detection methods

Transmission Electron Microscopy (TEM) Exosome samples used for electron microscopy were resuspended in filtered PBS and 5µl were immediately loaded onto formvarcarbon-coated grids. Samples were then examined in an electron microscope. Vesicles dimensions were analysed exploiting ImageJ software.

Nanoparticles Tracking Analysis (NTA) The analysis of the absolute size distribution of EXOs was executed using Nano Sight LM10 (Malvern, UK).
With NTA, particles are automatically tracked and sized based on Brownian motion and the diffusion coefficient (laser 532 nm). After isolation, exososomes were diluted in 1ml of filtered PBS. Control medium and filtered PBS were used as controls in this technique and NTA measurement settings were set as follows: temperature 23.75±0.5°C; viscosity 0.91±0.03 cP, frames per second 25, measurement time 60s. Three recordings/sample were performed.

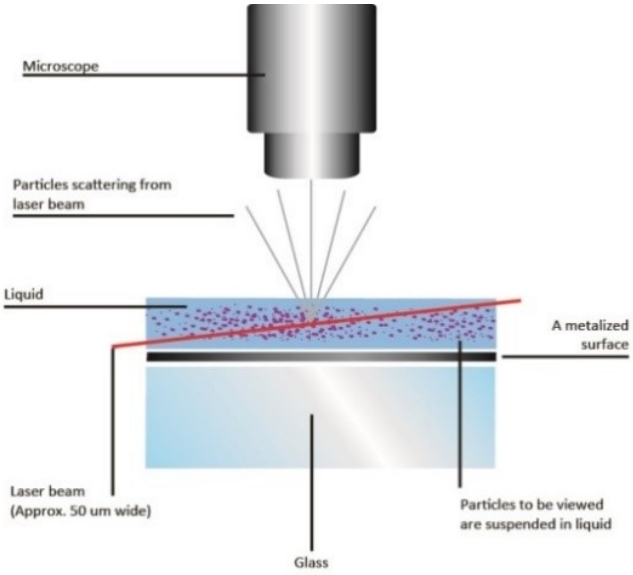

FIGURE 14. *NanoSight LM10 structure. NTA technique is used in conjunction with an ultramicroscope and a laser illumination unit that together allow small particles in liquid suspension to be visualized moving under Brownian motion.*

Exosomes labelling To obtain fluorescent exosomes, samples were labelled with the red fluorescent cell dye PKH26 (Sigma-Aldrich; St. Louis, USA). PKH26 Fluorescent Cell Linker dye stably incorporates with long aliphatic tails into the lipid regions of the cell membrane. Briefly, a 2X mix was prepared by adding 1 ml Diluent C to the exosome pellet (if the isolation was performed by differential ultracentrifugation), or to the concentrated culture medium (if exosomes were isolated by SEC). Diluent C is an aqueous solution provided in the kit, which ensures the maintenance of cells viability, maximizing dye solubility and staining efficiency. A 2X Dye solution was prepared by adding 4 µl of the fluorescent dye to 1 ml of Diluent C. Then, the 2X exosome suspension/concentrated CM was mixed with the 2X dye solution and incubated 5 minutes. The reaction was stopped by adding to the mix an equal volume of exosome-free FBS for 1 minute. For exosomes isolated exploiting differential centrifugation, an extra centrifugation at 130000g of 2 hours was sufficient to discard the excess of unbound PKH26

marker. As for concentrated CM, SEC protocol allows the exclusion of the unbound marker directly during the process of MVs isolation. Moreover, it is possible to obtain PKH26+ exosomes directly labelling their releasing cells, according to the manufacturer's instructions.

FACS analysis For cytofluorimetric analysis, 2 µg of exosomes were stained with CD63-PE-vio770 (Miltenyi Biotech; Bergisch Gladbach, Germany) and CD81-PE (Beckman Coulter; Brea, California, USA) antibodies for 20 minutes at 4°C. Afterwards, 10 µl of magnetic CD63-coniugated beads were added to the mix (ThermoFisher Scientific; Waltham, Massachusetts, USA) and incubated overnight at 4°C under moderate agitation. Then, the sample was vortexed to guarantee the optimal beads recovery and it was washed with PBS1X and BSA 1% exploiting a magnet (Ademtech; Pessac, France) to avoid the loss of the beads during the washing step. FACS analysis was performed on a FACS Cytomic FC 500. The analysis was conducted using CXP 2.1 software.

3.5.7 Evaluation of FKRP expression in human CD133+ blood-derived and murine L276I^{KI} SCs infected cells-derived exosomes

For WB exosomes analysis, particles were isolated from cell culture medium by SEC; 5 µg of fraction 7-enriched exosomes were directly mixed with Laemmli sample buffer (62.5 mM Tris-HCl pH 6.8; 2% SDS; 5% 2-mercaptoethanol, glycerol 10%, Bromophenol Blue 0.004%) and boiled at 65 °C for 10 minutes. Boiling temperature was maintained below standard values (95 °C) to avoid particles clustering. Samples were loaded on a 10% polyacrylamide gel and then transferred to a supported nitrocellulose membrane. Then, filters were saturated in blocking solution (10 mM Tris pH 7.4, 154 mM NaCl, 1% BSA, 10% horse serum, and 0.075% Tween-20). The monoclonal primary antibodies: the mouse anti-TSG (1:200) (Abcam; Cambridge, UK), the mouse anti-Ago2 (1:200) (Proteintech; Europe, Manchester, UK) and the rabbit anti-FKRP-STEM (1:600) antibodies were

incubated at 4°C in the blocking solution O/N or, alternatively, using the Signal-boost Immunoreaction Enhancer Kit (Calbiochem; Inalco, Italy), when the enhancement of the signal was necessary due to very low levels of the protein expression in the samples. Enhanced chemiluminescence (ECL) development (GE Healthcare; Little Chalfont, UK) was performed to detect the positive signal after incubation with (HRP)-conjugated secondary antibodies. Pre-stained molecular weight markers were loaded on each gel. Bands were detected by autoradiography using Amersham Hyperfilm™ (GE Healthcare; Little Chalfont, UK) and captured taking advantage of the CanoScan LiDE60 Scanner and the Canon ScanGear Software. ImageJ software (http://rsbweb.nih.gov/ij/) was exploited to perform the densitometric analysis.

3.6 In vivo transplantation of LV-FKRP L276I^{KI} satellite cells into FKRP L276I^{KI} mouse model

12 months-old FKRP L276I^{KI} mice were anesthetized with 2% avertin (0.015 mL/kg) and intramuscularly transplanted in the tibialis anterior (TA) with 3 increasing doses of FKRP L276I^{KI} SCs engineered cells: 35x10^3 (N= 4), 75x10^3 (N=5), and 100x10^3 (N=4); N=6 mice were not injected and used as controls.Cells engineering was performed with the LV expressing the wild-type isoform of human FKRP; for in vivo transplantation, cells were infected with MOI 20. Briefly, SCs were resuspended in 100 µl of PBS, using a 33G Hamilton syringe (Hamilton company; Reno, Nevada, USA). 15 days after cells transplantation, mice were sacrificed by cervical dislocation.

3.6.1 Evaluation of human wild-type FKRP expression and α-Dystroglycan glycosylation in injected TAs and heart muscles

- Immunofluorescent Analysis

IF was performed on muscle samples which were snap-frozen in liquid nitrogen and stored at -80°C soon after the mice sacrifice. The staining was

performed on FKRP L276I^{KI} transplanted tibialis anterior (TAs); not-transplanted FKRP L276I^{KI} TAs were exploited as negative control and C57BL TAs as positive control. 12 μm- thickness serial tissue sections were cut by cryostat (Leica CM1850), and monitored for the exogenous FKRP isoform expression with rabbit anti-FKRP-STEM antibody, kindly provided by Dr. Qilong Lu (1:50), and mouse anti-GFP (dilution 1:500) (Abcam, Cambridge, UK). anti- α-DG IIH6-C4-5 (dilution 1:50) (Hybridoma Bank, Lowa, USA), an anti-mouse monoclonal antibody detecting the N-terminus α-DG (the laminin-binding glycan epitope) staining was also performed on the same tissue sections. moAb anti-rabbit 594, moAb anti-mouse 594 and moAb anti-mouse 488 (Molecular Probe Invitrogen, Carlsbad, CA, USA) were used at a dilution of 1:100 for 1 hour. Nuclei were counterstained with DAPI (Sigma-Aldrich, Milan, Italy). Finally, images were taken with Leica TCS SP2 confocal microscope, equipped with a 63X/1.40-0.60 objective (Leica, Germany).

-Western Blot biochemical analysis

Transplanted TAs, contralateral TAs and hearts (HTs) were harvested from all injected and not -injected L276I^{KI} FKRP and C57BL mice, immediately after sacrifice by cervical dislocation. The WB analysis of contralateral TAs muscles and hearts was performed to determine the systemic circulation of exogenous WT FKRP protein and its rescued functionality. According to this perspective, muscles were directly homogenized in NP40 lysis buffer with a POTTER S Homogenizer (B.Braun Biotech International-Sartorius group, Melsungen, Germany) and incubated for 30 min at 4°C. Finally, they were centrifuged at 15682g for 15 min at 4 °C and the recovered total protein concentration was determined by Lowry's assay. The biochemical analysis was conducted as already described for cell lysates. Briefly, samples (30 μg) were loaded on polyacrylamide gel (10%) and incubated with FKRP-STEM antibody, (1:600) for exogenous FKRP detection and on 8% polyacrylamide

gel to detect α-DG glycosylation (IIH6-C4-5 antibody) (1:50) (Hybridoma Bank, Iowa, USA), and than transferred to nitrocellulose membranes (Bio-Rad Laboratories). Anti-α-actin (1:600) staining was performed for normalization. TAs and HTs removed from C57BL mice were exploited as positive controls, not-injected mice (NI) as negative controls.

3.6.2 Histopathological Analysis

L276I^{KI} injected and not-injected mice TAs previously frozen in liquid nitrogen, were cut in serial tissue sections of 12 μm thickness by cryostat (Leica CM1850). Hematoxylin and eosin staining was performed to examine histoarchitectural changes.

3.6.3 In vitro modelling of dynamic FKRP-carrying exosome trafficking

To imite FKRP flux within exosomes, a microfluidic, miniaturized bioreactor was used and installed as previously reported with little adjustments [177]. The dynamic technique is optically transparent and made of three independent chambers. Each one hosts a unique polystyrene scaffold for cells seeding (dimensions 6 × 3 × 0.4 mm, 3D Biotek; Hillsborough, NJ, USA). Each scaffold has four layers of fibers (100 μm in diameter, with 300μm pore size, 150μm reciprocally separated) (Fig 4A). Three single microfluidic channels connect the chambers. Firstly, the scaffolds were pre-conditioned in sterility with DMEM, as previously reported [177]. Then, 10^6 FKRP L276I^{KI} SCs infected with LV-MOI 20 were marked with PKH26; this way, cells were able to release PKH26+ exosomes. These cells were resuspended ed in 400 μl of medium and seeded on one scaffold. Similarly, not labelled 10^6 FKRP L276I^{KI} SCs were cultured on the other scaffold. The scaffolds were incubated at 37 °C ON to let cells attach. Subsequently, they were inserted into two independent bioreactor chambers, covered by magnetic bottoms. DMEM 10% FCS was pushed with an unidirectional flow rate of 5 μl/min in to the first chamber, were infected FKRP L276I^{KI} SCs were

previously seeded, taking advantage of a multi-channel programmable syringe pump (PHDULTRA; Harvard Apparatus, Holliston, MA, USA) in a gas permeable tubing system (0.03″ ID × 0.065″ OD, Silastic Tubing, Cole-Parmer, Vernon Hills, IL, USA). The outward supernatant enriched with PKH26+ exosomes, secreted by PKH26+ infected FKRP L276I^{KI} SCs, penetrated the second chamber were not-infected FKRP L276I^{KI} SCs were plated. Afterwards it was accumulated in a reservoir. The experiment was run for 8 hours, subsequently the scaffolds were recovered and stained by IF to detect exosome induced-FKRP expression. Scaffolds holding FKRP L276I^{KI} SCs were fixed with 4% paraformaldehyde for 30 minutes, incubated with blocking solution (1% BSA, 0,05% Tween, 5% FBS in PBS1X) for 1 hour and incubated overnight at 4°C with rabbit anti FKRP-STEM antibody in blocking solution (diluted 1: 50). Monoclonal anti-rabbit 488 (Molecular Probe; Thermo Fisher Scientific; Waltham, Massachusetts, USA) was used at a dilution of 1:100 in PBS for 1 hour. Nuclei were counterstained with DAPI (Sigma-Aldrich; St. Louis, USA) and images were taken with Leica TCS SP2 confocal microscope.

3.6.4 Muscle Functional Analysis

All the injected mice (N=4 35x10^3 cells, N=5 75x10^3 cells, N=4 100x10^3 cells) were examined by Treadmill and Rotarod tests, to measure their performances. Not-transplanted mice (N= 6) and age-matched C57BL mice (N=5) were exploited as controls. Animals were tested a week before cells transplantation, the day of cells injection (T0), 7 and 14 days (T7 and T14) after transplantation. After in vivo functional measures, they were finally sacrificed. Treadmill was performed as a simple motor exercise. Briefly, mice were placed on a motorized treadmill (Harvard Apparatus) to run with an upward angle of 15° at a rate of 15m/minute. In order to determine the high variability among mice belonging to the same group, running distance results from transplanted and not-transplanted mice at T14 were normalized to the

corresponding pre-transplantation outcome (-T7). Data obtained at T-17 were considered as ''baseline level''. Results are expressed as the % of averaged variations in running distance, evaluated as [(Activity at T14/Activity 7 days before the injections) x 100] - 100. Treadmill experiments were interrupted when the mice stayed 5 seconds standing on the shock grid. Rotarod is a moderately complex motor training exercise, which investigates coordination and balance features of motor performance. Mice were positioned on the instrument and then acceleration from 5 to 45 rotations/ minute within 15 seconds was set. When a mouse ran for up to 500 seconds without fallings the rod was stopped. Mice undergoing fallings within 500 seconds were allowed to perform the experiment two more times. The best performance was held in consideration for the analysis.

3.7 Blood analysis

3.7.1 Plasma collection, Isolation of plasma-exosomes and evaluation of FKRP expression

Immediately before sacrifice, blood was collected into EDTA-coated tubes from the submandibular vein of the $35x10^3$, $75x10^3$, and $100x10^3$ LV-FKRP infected SCs transplanted FKRP $L276I^{KI}$ mice (~300 µl/mouse). Subsequently, blood was centrifuged at 1200g for 10 minutes at 4°C to obtain plasma samples. Plasma was placed in a new 1.5 ml tube and frozen at - 80 °C. Plasma-exosomes were isolated performing SEC chromatography (qEV IZON Science; Scheafer, Souh East Europe). In accordance with the manufacturer's suggestions, plasma was diluted 1:2 in filtered PBS1X. Plasma-exosomes characterization was performed as already described by Nanosight Tracking Analysis, to measure microvesicles dimensions, and by Transmission Electron Microscopy, to define their morphology. Subsequently, biochemical analysis was conducted to evaluate the presence of exogenous wild- type FKRP in the plasma, exploiting anti FKRP-STEM

antibody. The analysis was performed as already reported for CD133+ stem cells and FKRP L276I^{KI} satellite cells culture medium- derived exosomes.

3.8 Statistical Analysis

Prism 5.0 (Graphpad) was used to perform statistical analysis. Comparisons were based on Student's t-test or analysis of variance (ANOVA) with Tukey post-hoc test for pairwise comparisons. A confidence level of 95% was assumed as significant, as well as P-values < 0.05.

4 RESULTS

4.1 MDC1C CD133+ blood-derived stem cell in vitro characterization and transduction

4.1.1 Characterization of MDC1C blood-derived CD133+ stem cells

CD133+ cells were isolated from control and dystrophic MDC1C patient's peripheral blood. The patient was a three-years-old boy presenting two mutations in heterozygosis in the fukutin related protein gene: C518T>G and c1087G>C. Freshly purified CD133+ blood-derived stem cells were immediately cultured in vitro and their morphology was daily monitored. Images were captured by optical microscopy immediately post isolation and after 14 days to demonstrate that cell culture conditions did not affect their morphology: cells maintained their original round shape and unvaried dimensions both soon after the isolation procedure (Fig. 15A) and after 15 days in culture (Fig. 15B). Blood-derived CD133+ stem cells were characterized through flow cytometry analysis. Fig. 15C represents the scatter plot. 92,3% of magnetically isolated cell population was CD133+ (Fig. 15 C'); 98% of CD133+ cells were also positive for CD45 marker (Fig. 15 C'') and 90,1% of isolated cells proved to be positive for CD34 marker (Fig. 15C'''). Cells exhibited a viability range between 70-90% throughout the culture period (30 days).

4.1.2 Lentiviral infection of CD133+ stem cells isolated from a MDC1C patient's peripheral blood

Immediately after cells isolation, CD133+ blood-derived stem cells were exposed to lentiviral particles delivering constructs encoding for the human wild-type isoform of FKRP protein (pLenti-CAG (hFKRP)-Rsv (GFP-Puro)). Multiple MOI of infection (MOI 5, 10, 20) were tested to evaluate the most performing transduction condition. Transduction efficiency was assayed by

both cytofluorimetric analysis (FACS) and fluorescent microscopy by evaluating green fluorescent protein (GFP) expression.

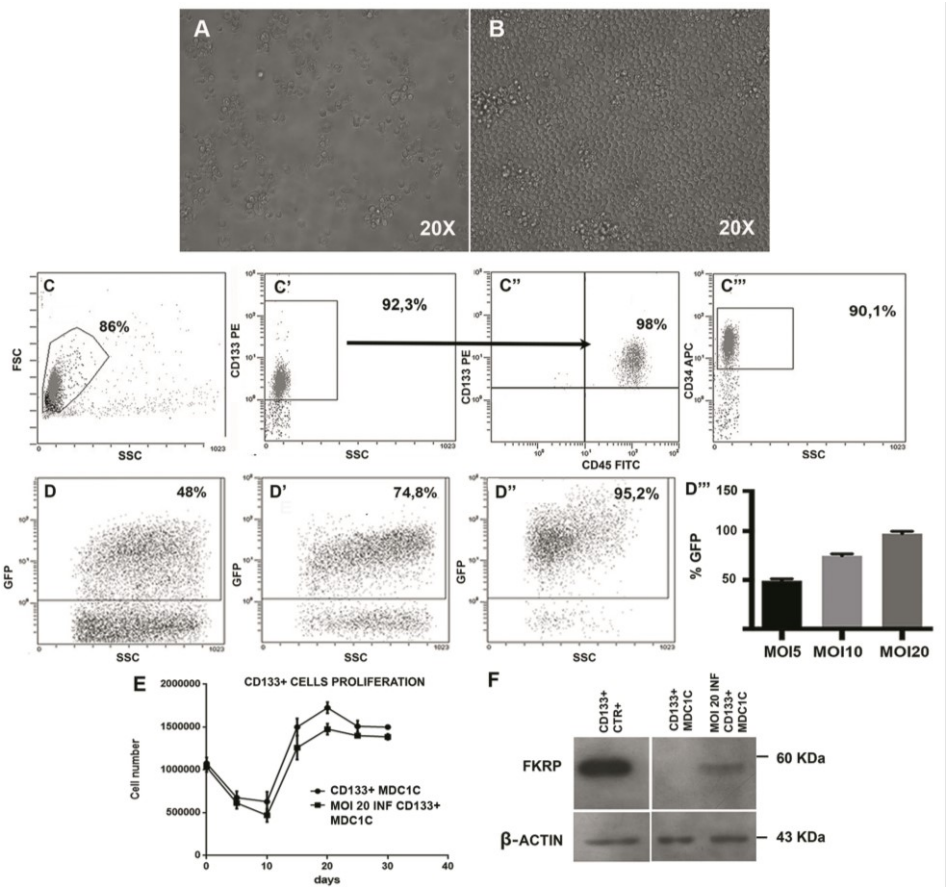

FIGURE 15. *Characterization of CD133+ stem cells isolated from a MDC1C patient's peripheral blood. Cells morphology was observed by bright field microscopy soon after cells isolation procedure (A) and after 14 days in proliferation medium (B). Images were captured at 20X magnification. FACS analysis of CD133+ stem cells. Each study involved not less than15000–30000 events. The scatter plot is shown (C). CD133+ stem cells median purity was around 92,3% (C'); 98% of CD133+ cells were also positive for CD45 marker (C'') and 90,1 % of CD133+ cells were also CD34+ (C'''). Immunophenotyping analysis of CD133+ stem cells infected with the LV (pLenti-CAG (hFKRP)-Rsv (GFP-Puro)).The reported % of GFP+ cells was 48% for MOI 5 (D), 74.8% for MOI 10 (D') and 95.2% for MOI 20 (D''). Histogram summarizing CD133+ cells infection efficiency at MOI 5, 10 ad 20 (D'''). Values are represented as means ± SD. MDC1C CD133+ infected with MOI 20 and corresponding not infected cells proliferation curve. Proliferation was calculated in triplicate at 5- days intervals for 30 days, performing Trypan Blue Exclusion Assay (E). Values are reported as means ± SD. WB confirmed FKRP rescue in MDC1C CD133+ stem cells infected with MOI 20 (lane MOI 20 INF MDC1C CD133+). Not infected cells and healthy donor's CD133+ cells were respectively loaded as negative (lane MDC1C CD133+) and positive (lane CD133+ CTR+) controls. β-actin was used as house-keeping protein (F).*

FACS analysis disclosed enhanced transduction efficacy as the MOI increased: 48%, 74.8%, and up to 95.2% respectively for MOI 5, 10 and 20 (Fig. 15D, 15D', 15D'').

The histogram graph in figure 15 D''' is representative of the percentage of GFP+ cells observed by fluorescent microscopy analysis. These data overall suggested that MOI 20 presented the best outputs in terms of transduction efficiency, thus we decided to infect MDC1C blood-derived CD133+ stem cells with lentiviral vector MOI 20. Trypan blue exclusion assay was performed on MOI 20- infected CD133+ MDC1C stem cells and not-infected MDC1C CD133+ cells at 5-days intervals for 30 days. MOI 20- transduced FKRP CD133+ stem cells did not display deleterious outcomes in their proliferation curve. For all the experimental time- points the proliferation curve was comparable to the distinctive trend of not-infected CD133+ stem cells, characterized by a starting decrease of cells viability and a peak between 15 and 20 days (Fig. 15E).

To test whether the lentiviral transduction could restore the expression of wild- type fukutin related protein in MDC1C CD133+ blood-derived stem cells, we performed a biochemical analysis 7 days after the lentiviral infection. WB analysis confirmed the presence of a positive signal at approximately 60 KDa, corresponding to lentivirus-mediated FKRP exogenous protein restoration in MOI 20- infected MDC1C CD133+ blood-derived stem cells (lane MOI 20 INF CD133+ MDC1C), compared to the absence of a positive signal in not-transduced cells (lane CD133+ MDC1C). CD133+ blood-derived stem cells isolated from a healthy patient were exploited as positive control (lane CD133+ CTR) (Fig 15F). These results were in agreement with the specificity of FKRP-STEM antibody for the wild-type isoform of FKRP glycosyltransferase. The signal intensity of FKRP expression within cells was quantified by NIH image J densitometric analysis using α-actin as housekeeping protein.

4.2 FKRP L276I^{KI} satellite cell in vitro characterization and transduction

4.2.1 FKRP L276I^{KI} Satellite Cells characterization

Satellite cells (SCs) were dissociated from FKRP L276I^{KI} new born mice muscles. Freshly isolated SCs were cultured in 48-wells tissue plates in proliferation medium. FACS analysis showed that 97.6% of isolated cells was Pax7 positive (Fig. 16A) and 80.3% of Pax7+ cells were also positive for CD29 (Fig. 16A'). Both satellite cells morphology and the presence of myogenic markers were investigated before the supplementation of serum starvation medium (T0) and after culturing cells in myogenic differentiation medium, at two different time-points: 7 days (T7) and 14 days (T14). As expected, at T0 SCs still showed the expression of Pax7 satellite cell marker (in red) and desmin+ (in green) (Fig. 16B, E). At T7, SCs had already begun to differentiate, progressively appearing as small Pax7-desmin+ myotubes (Fig. 16C, F). After 14 days (T14), the number and size of SCs-derived Pax7-desmin+ myotubes was evidently increased (Fig. 16D, G).

4.2.2 Lentiviral transduction of isolated FKRP L276I^{KI} Satellite Cells

FKRP L276I^{KI} satellite cells LV-hFKRP lentiviral vector transduction was performed with three different increasing MOI (10, 20, 40); cells proliferation and fusion index were evaluated and compared to not- infected FKRP L276I^{KI} SCs. Trypan Blue Exclusion assay proved that FKRP L276I^{KI} SCs infected with lentiviral MOI of 10 and 20 did not exhibit detrimental consequences on cells viability in comparison with not infected corresponding cells. Similarly, FKRP L276I^{KI} SCs infected with higher MOI 40, displayed a trend towards a decrease in cell proliferation rate, which was probably due to 5% of cell mortality (Fig. 16H). Interestingly, the evaluation of LV-EMPTY (pLenti-Rsv (GFP-Puro)) infected FKRP L276I^{KI} SCs did not show any statistical difference among the three distinct MOI of infection (Fig. 16I). Once again,

only MOI 40- infected SCs proliferation displayed a not significant trend towards a proliferation rate delay beginning at day 15 and presumably produced by the occurrence of 3.5% cell mortality. Thus, we defined the absence of a lentiviral-vector induced toxicity, whether (pLenti-CAG (hFKRP)-Rsv (GFP-Puro)), or (pLenti-Rsv (GFP-Puro)), even throughout 25 days in culture. Furthermore, dystrophic SCs fusion index (FI) was calculated for each MOI of infection. Overall, we found similar results among cells infected with MOI 10, 20 and 40 (Fig. 16L).

Observed values were compared to FKRP L276I^{KI} SCs infected with LV-empty (pLenti-Rsv (GFP-Puro)) outcomes (data not shown), but no differences were evidenced. MOI 10, 20 and 40 LV-empty infected SCs conserved a rate analogous to not-infected FKRP L276I^{KI} SCs (30% myotubes nuclei/total nuclei). The not-statistically different FI observed for MOI 40- infected L276I^{KI} SCs could be explained by a slight decrease in cell number rather than a decreased differentiation capacity. The biochemical analysis performed on FKRP L276I^{KI} infected satellite cells highlighted an increased FKRP protein expression between MOI of 10 and 20, whereas MOI 40- infected cells looked like a steady point causing a plateau in the glycosyltransferase expression level (Fig 16M).

Afterwards, the biochemical analysis of α-DG glycosylation was performed to evaluate FKRP restored function. Interestingly, the blot revealed no MOI-dependent differences in all the three analysed settings. The previously observed FKRP expression plateau at MOI 40 produced a constant level of α-DG glycosylation, in comparison with MOI 10 and 20. Not-infected FKRP L276I^{KI} satellite cells were loaded as control (lane NOT INF) (Fig. 16M). Fig 2N displays the immunofluorescence staining (IF) of MOI 20- LV-FKRP L276I^{KI} SCs. Cells were analysed for the expression of GFP and FKRP proteins, exploiting anti-GFP and anti-FKRP-STEM antibodies. The staining confirmed the diffused localization of GFP (in green) within the cell cytoplasm, while exogenous FKRP (in red) was detected in the same cell

compartment, but the positive signal was more evident in the perinuclear region (Fig. 16N).

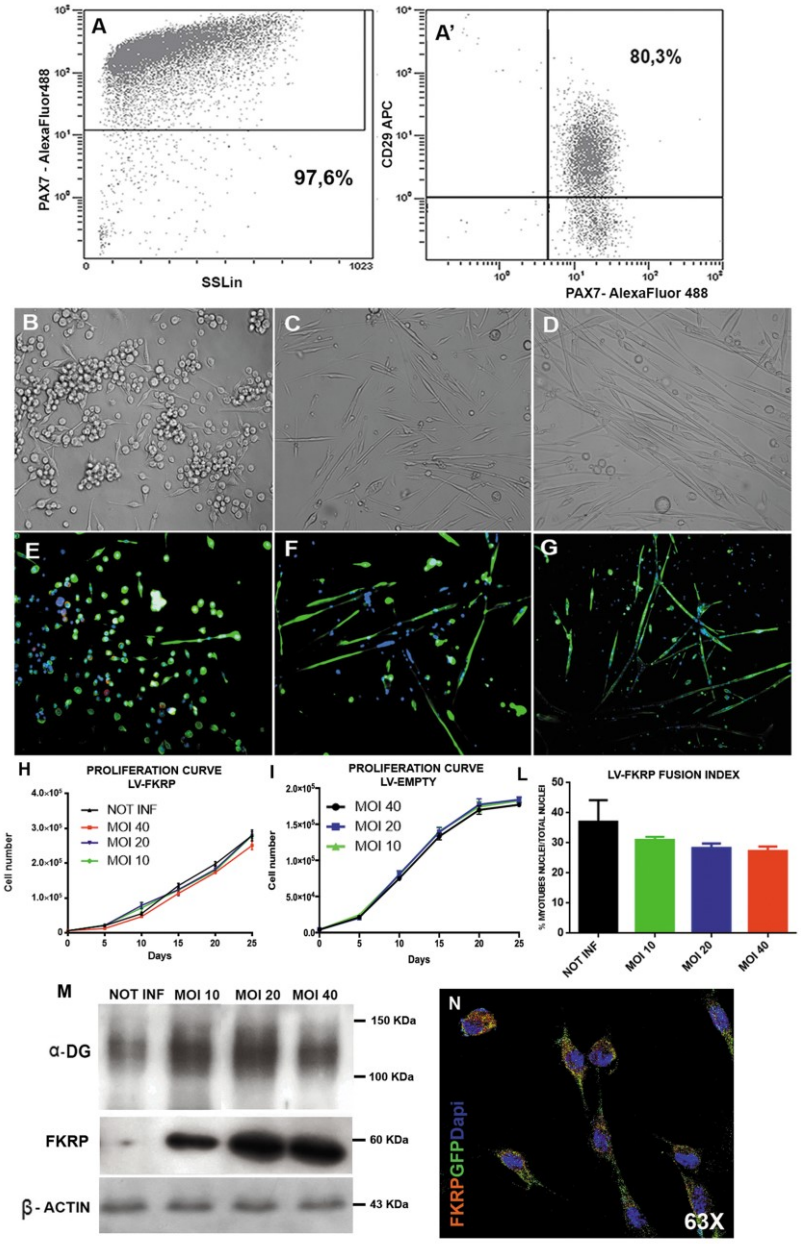

FIGURE 16. *Characterization of FKRP L276I^{KI} SCs. FACS analysis of isolated FKRP L276I^{KI} SCs. Each study included not less than 15000–30000 events. 97.6% cells expressed*

PAX7 myogenic marker (A); 80.3% of PAX7+ cells were also positive for CD29 (A'). SCs morphology was visualized by bright field microscopy at various time-points: soon after SCs seeding (T0)(B), one week (T7)(C) and two weeks (T14) later (D) in serum starvation medium. IF analysis was executed to determine specific myogenic satellite markers positivity. The day of transplantation (T0), satellite clones expressed α-desmin (in green) and Pax7 (in red) (E). At T7 cells were negative for early myogenic marker Pax7 expression, and were still positive for α- desmin; α- desmin staining underlined the presence of some myotubes in culture (F). After two weeks (T14), cells still expressed α-desmin and were definitively fused in myotubes (G). Images were taken at 20X magnification. Infected and not infected FKRP L276I^{KI} SCs proliferation curve (H) and LV-EMPTY infected and not-infected SCs proliferation curve (I). SCs proliferation was calculated for 25 days at 5-days intervals performing Trypan Blue Exclusion Assay. Values are represented as means ± SD. Evaluation of LV-FKRP infected (MOI 10, 20 and 40) and not infected (NOT INF) FKRP L276I^{KI} SCs fusion index, representative of the percentage of myotubes nuclei/ total nuclei, after a week in serum starvation (L). Values are expressed as means ± SD. WB showed α-DG protein glycosylation (smeared band around 150 KDa) and FKRP rescue (60 KDa) in infected SCs. α-DG glycosylation was higher in transduced cells, rather than not transduced SCs (NOT INF, lane 1), but without any difference between the three increasing MOI of infection (MOI 10, lane 2, MOI 20, lane 3, MOI 40, lane 4). FKRP protein expression increased from MOI 10 to 20, but reached a plateau with MOI 40. β-actin (43 KDa) was used as house-keeping (M). IF analysis of SCs infected with MOI 20, demonstrating both cytoplasmic and perinuclear protein expression (in red) and cytoplasmic GFP (in green) staining. Nuclei were counterstained with Dapi (in blu). Images were captured with a confocal microscope (63X magnification)(N).

4.3 Optimization of exosomes isolation and characterization procedures

4.3.1 Exosomes isolation Techniques

To optimize the exosome isolation protocol, we compared three main techniques:

- Differential ultracentrifugation (UC)
- Commercial kits
- Size-exclusion chromatography (SEC)

Protocols were set up exploiting supernatant in contact with C2C12 murine myoblast cell line. We chose a cell line with a good proliferative capacity to obtain a high amount of conditioned cell culture medium, and a reliable source.

Differential Ultracentrifugation

Cell supernatant was collected and exosomes were isolated as previously described (Materials and Methods section) (Fig. 17A). Once isolated,

exosomes were resuspended either in PBS1X buffer or NP40 lysis buffer and analysed.

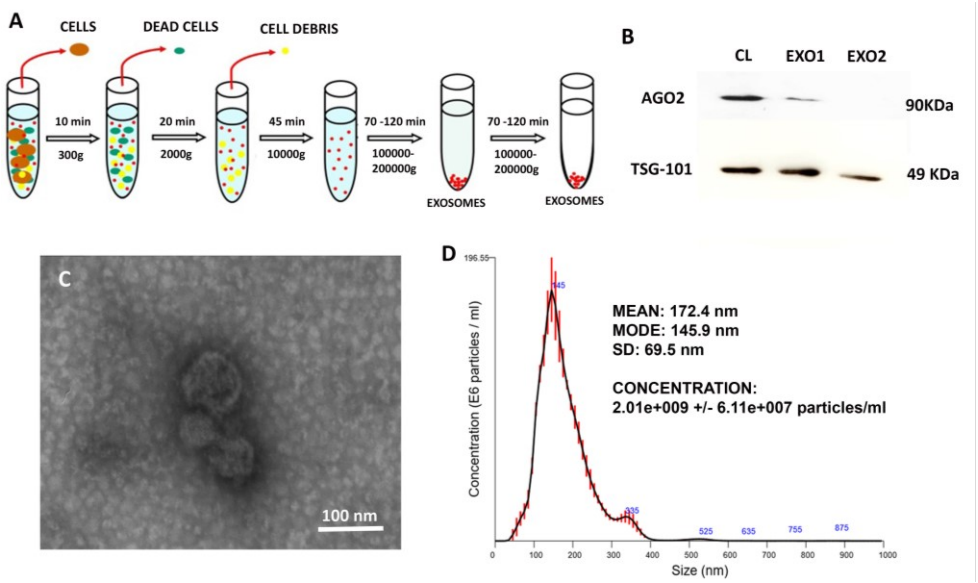

FIGURE 17. *Optimization of exosomes isolation by differential ultracentrifugation. C2C12 culture medium was subjected to a serial cycles of centrifugations to obtain the final pellet (A). Isolated exosomes were biochemically analysed by WB for the expression of TSG-101 and Ago2 proteins (B) Exosomes morphology was evaluated by transmission electron microscopy (TEM) (C) and their dimensions/concentration was analysed by Nanosight Tracking Analysis (NTA) (D).*

The experimental procedure was repeated several times to prove its reproducibility. Unless microBCA assay showed a high protein concentration in the exosome- enriched samples, the Poinceau staining performed on the nitrocellulose revealed very low amount of loaded proteins. The presence of a major band at ~ 60 KDa suggested that culture medium- derived bovine serum albumin (BSA) could represent the main enriched protein in exosome samples. NP40-resuspended exosomes were biochemically analysed for the expression of TSG-101 exosomal biomarker. As expected, TSG-101 signal was found to be positive in both the cell lysate (CL, lane 1) and exosomes isolated in two different experiments (EXOs, lanes 2, 3), confirming the exosomal origin of isolated particles (Fig. 17B). However, a weak band representative of AGO2 protein was observed in both cell lysate and one

exosome sample, highlighting the occurrence of protein contamination (Fig. 17B). To evaluate UF-isolated exosome morphology, size and concentration we exploited PBS-resuspended particles. TEM analysis revealed the presence of cup-shaped vesicles of ~100 nm (Fig. 17C). However, NTA analysis recorded a mean size value of 172.4 nm and a mode size value of 145.9 nm, thus showing more heterogeneity in the analysed sample than we expected and confirming WB data (Fig. 17D). According to our results and recently published data [178], even though differential ultracentrifugation still represents one of the most performed isolation procedures, it presents many limits such as protein contamination and exosomes low recovery.

Precipitation by Commercial Kits

We performed exosomes isolation exploiting the Life Technologies Total Exosome Isolation Kit from Cell Culture Medium (Fig. 18A).

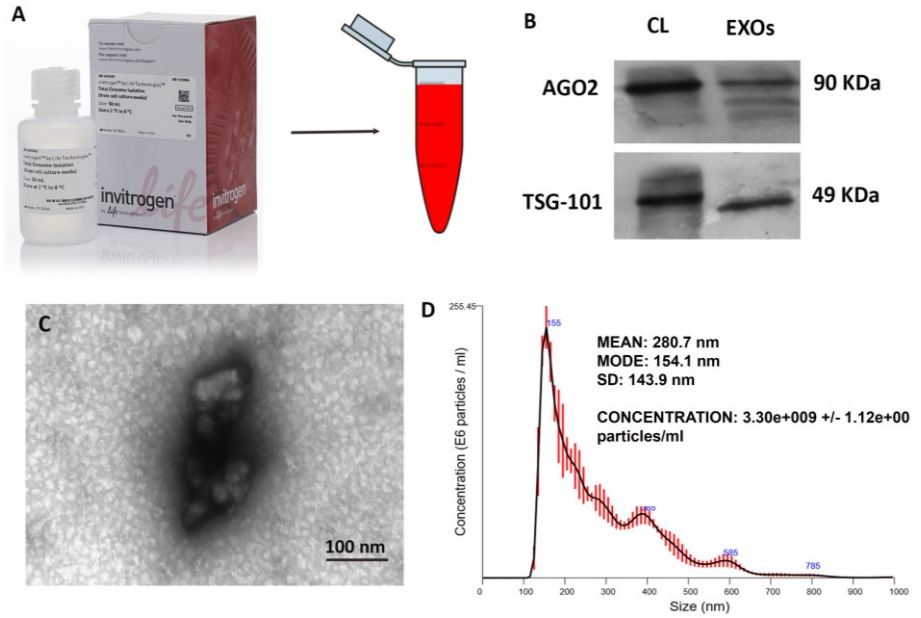

FIGURE 18. *Optimization of exosomes isolation by commercial kits (A). Isolated exosomes were biochemically analysed by WB for the expression of TSG-101 and Ago2 proteins (B) MVs morphology was evaluated by transmission electron microscopy (TEM) (C) and their dimensions/concentration was analysed by Nanosight Tracking Analysis (NTA) (D).*

The WB analysis of these isolated exosomes outlined the expression of both AGO2 and TSG-101 (Fig 18B).

The Poinceau staining pointed out a marked co-precipitation of BSA together with the particles of interest (data not shown), thus highlighting a clear protein contamination of the pellet. Also the morphological analysis produced an unclear outcome: TEM analysis showed big particle aggregates, preventing the possibility to distinguish the precise isolated-particles morphology (Fig. 18C). NTA displayed the presence of a heterogeneous population, with a mean size value of 280.7 nm and a mode size value of 154.1 nm. Calculated particle concentration was around 3.3 x 10^9 particles/ml (Fig. 18D). Even though NTA data could suggest a more efficient recovery of exosomes if compared to ultracentrifugation procedure, the high level of contamination revealed by biochemical, NTA and TEM analysis, stressed out the unknown nature of these isolated particles.

Size Exclusion Chromatography (SEC)

Nowadays, one of the most emerging techniques for exosomes isolation is size-exclusion chromatography (SEC) (Fig. 19A). After the isolation step, we executed the biochemical characterization of exosome- enriched fractions. WB analysis revealed the expression of TSG-101 marker in fractions 7, 8 and 9 (lanes F7, F8, F9), as expected, as well as in the cell lysate (lane CL). No signal was detected in the void volume, represented by fractions 10 to 12 sample (lane F10-12). On the contrary, AGO2 expression was positive in the cell lysate sample and the F10-12, while it was absent in F7, F8 and F9, suggesting the lack of contaminants in exosomes-enriched fractions (Fig. 19B). Moreover, the Poinceau staining excluded bulk proteins contamination in F7, F8 and F9: the BSA band at ~ 60 KDa was not detected in SEC samples (data not shown). However, the microBCA analysis highlighted the presence of a very low amount of proteins for each exosome-enriched fraction, with a slight decrease from fraction 7 to fraction 9. As it was observed for UF-isolated exosomes, also SEC-enriched vesicles presented a cup-shaped

morphology when analysed by TEM, and dimensions ranging around 100 nm (Fig. 19C). NTA and TEM analysis performed on F7, F8, and F9 did not show any differences between the three exosomes-enriched fractions.

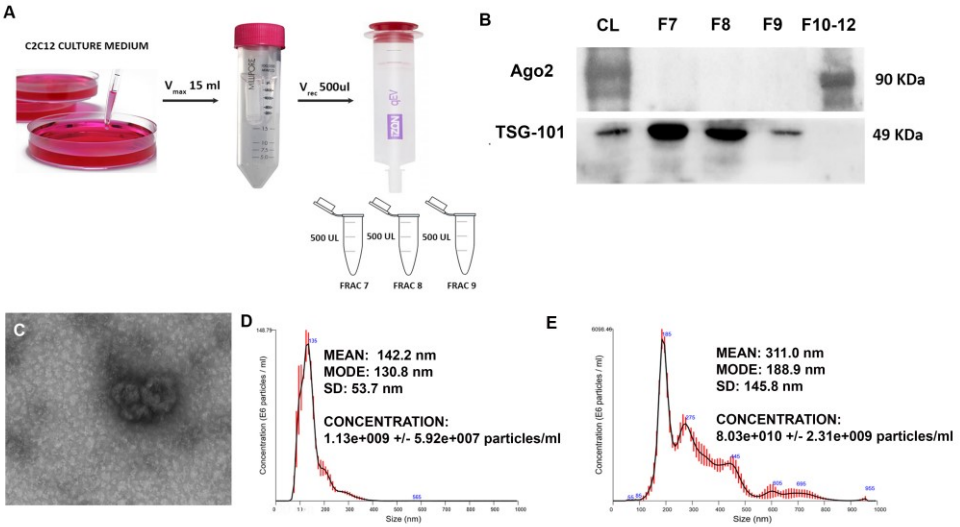

FIGURE 19. *Optimization of exosomes isolation by size exclusion chromatography (SEC)(A). Isolated exosomes were biochemically analysed by WB for the expression of TSG-101 and Ago2 proteins (B) Fraction 7- enriched exosomes morphology was determined by TEM analysis (C) and their dimensions/concentration were analysed by Nanosight Tracking Analysis (NTA)(D). NTA analysis was performed also for Fraction 10-12 (E).*

As regards NTA recording, we observed more homogeneous dimensions in comparison to previous observations, with a reported mean size value of 142.2 nm and a mode size value of 130.8 nm. As regards particles recovery, NTA showed an amount of particles of about 1.19 x 10^9 particles/ml (Fig. 19D). Finally, we tracked by NTA the F10-12 sample; as expected the produced graphic showed a very scattered trend demonstrating the presence of a heterogeneous population, probably represented by endosomes, apoptotic bodies and culture medium- derived bulk proteins, which are eluted by qIZON columns immediately after exosomes (Fig. 19E). Finally, SEC was proved as the most efficient method to isolate specific MVs. Comparing SEC results with those obtained by ultracentrifugation and particles precipitation with commercial kits, SEC produced the best recovery of exosomes and the

lowest level of protein and other microvesicles contamination. Thus, we decided to perform SEC to isolate exosomes from our cells of interest.

Setting of the proper culture conditions to recover exosomes

Following C2C12 myoblast seeding, cells were cultured for 72 hours. Cell supernatants were harvested at three different time points: 24, 48 and 72 hours. Simultaneously, an MTT assay was performed to evaluate cells proliferation throughout the different time points (Fig. 20A). Images representative of cell confluence were captured with an optical microscope at 10X magnification. After 24 hours cells showed a confluence of 30-40% (Fig. 20B), after 48 hours of 50-60% (Fig. 20C) and after 72 hours the confluence was around 80-90% (Fig. 20D).

We hypothesized that seeding density (number of cells/cm^2), and consequently the physical distance between cells, may directly influence both the amount and features of released exosomes. To this end, for each time-point, we isolated exosomes from supernatant collected at different time points by SEC. We then evaluated the exosomal concentration and size distribution by performing NTA analysis. Recorded graphics showed a more homogeneous dispersion of particle dimensions associated to the increase of their confluence in vitro.

At T1 (after 24 hours), exosomes distribution showed a mean value of about 209.9 nm with a standard deviation (SD) of about 83.9 nm (Fig. 20B'); at T2 (after 48 hours), the mean value was 158.1 nm and mode value was 141 nm, with a SD of about 52.5 nm (Fig. 20C'). NTA data relative to T3 (after 72 hours) displayed the maximum homogeneity: at this time point microvesicles showed homogeneity in size and shape (mean size 150 nm, mode value 145 nm, SD 12.3 nm)(Fig. 20D'), further ruling out the possibility of other microvesicles contamination.

Therefore, we established this latter condition as the most appropriate to recover culture media for exosome isolation.

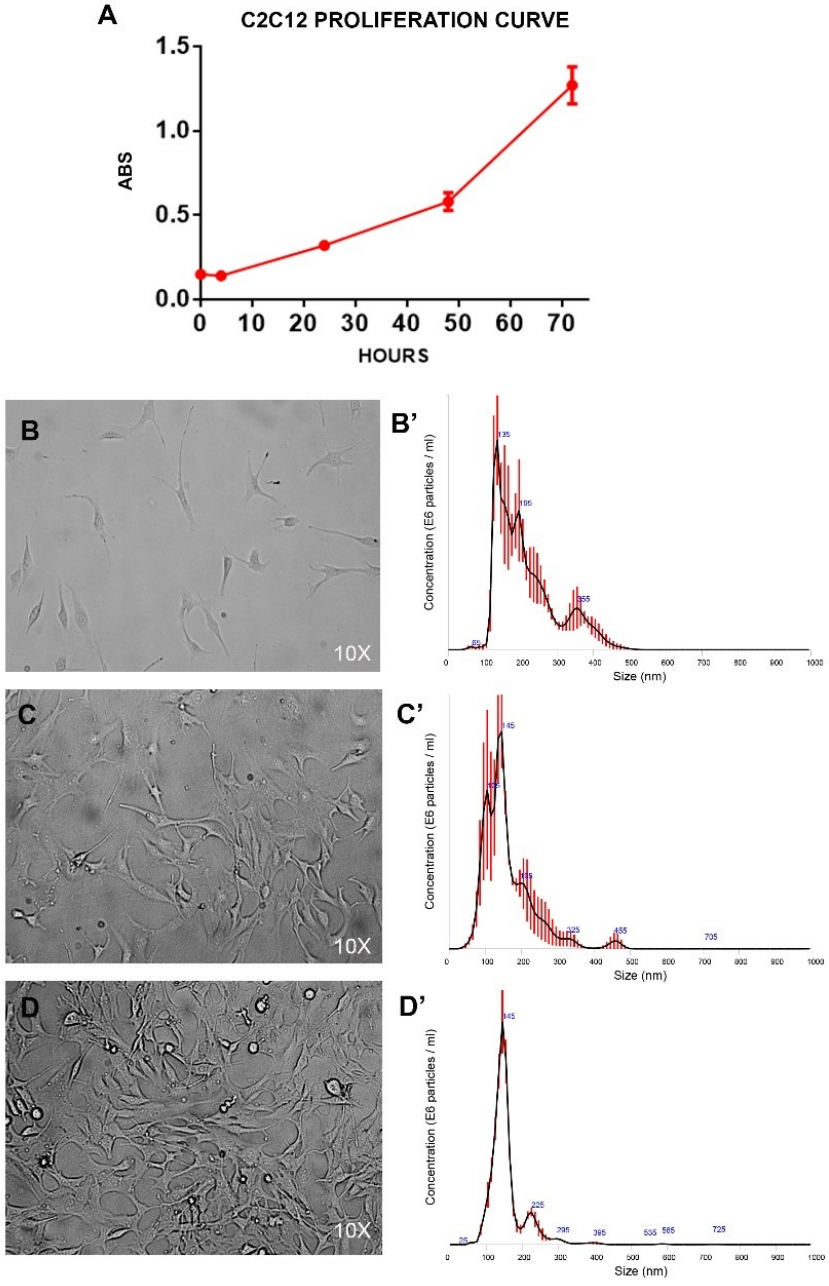

FIGURE 20. *C2C12 murine myoblast cell line proliferation curve (A). Cells were seeded at 40000 cellule/cm2 density. Images, representative of cells proliferation, were captured at 10X magnification at 3 time-points: 24, 48, 72 hours after cells seeding. (B, C, D). For each time-point, NTA analysis of exosomes isolated by SEC was performed (B', C', D').*

4.3.2 Optimization of exosome isolation from cells growing in suspension

Once investigated the most efficient isolation procedure and the proper cell culture conditions to obtain exosomes from adherent cell cultures, we focused on particles recovery from cells growing in suspension. These preliminary analyses were performed on RPMI 8226 cell line (multiple myeloma- deriving lymphocytes).

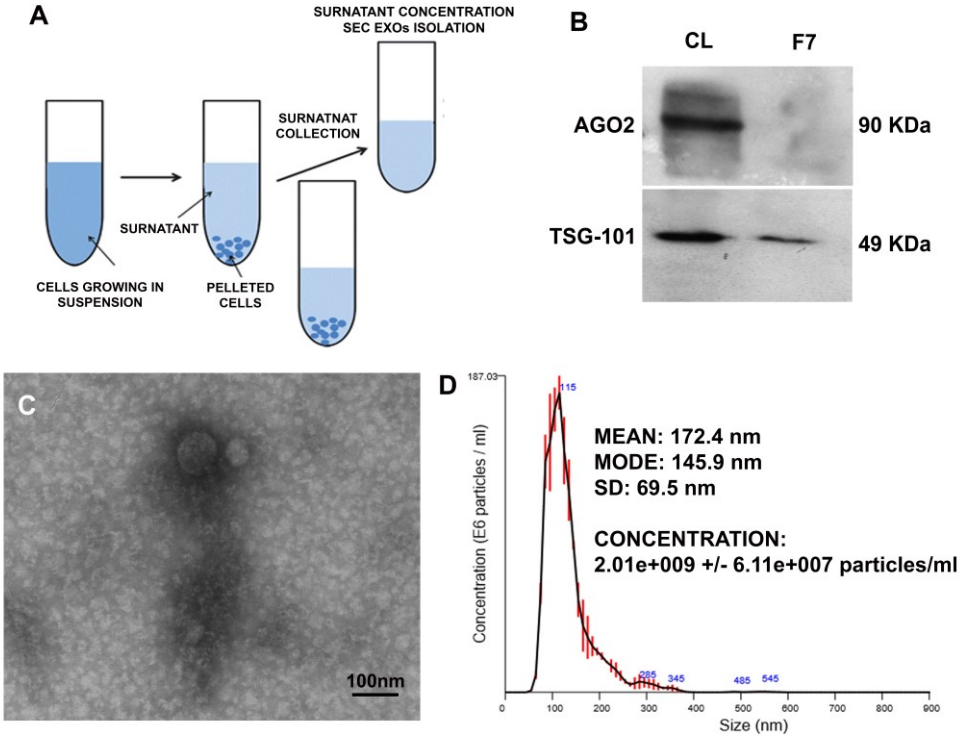

FIGURE 21. *Optimization of exosomes isolation from culture medium harvested from cells growing in suspension. Cells were pelleted by centrifugation and the surnatant was collected (A). Isolated exosomes were biochemically analysed by WB for the expression of TSG-101 and Ago2 proteins (B) MVs morphology was evaluated by transmission electron microscopy (TEM) (C) and their dimensions/concentration was analysed by Nanosight Tracking Analysis (NTA) (D).*

Once again, following the isolation procedure (Fig. 21A), exosomes were analysed by biochemical analysis, NTA and TEM (Fig. 21B, C, D). WB revealed a positive band corresponding to TSG-101 protein expression both

in RPMI 8226 cell lysate and exosomes isolated by SEC collected in fraction 7. The negative signal for the expression of Ago2 confirmed the absence of exosome contamination (Fig. 21B). Images captured with transmission electron microscopy exhibited the presence of particles very similar to those previously showed in Figure 19C. Finally, NTA graph recorded a concentration of 1,36 x 10^9 vesicles/ml, a mean size value of 127,5 nm and a mode size value of 112,3 nm (Fig. 21D).

4.4 Isolation and characterization of exosomes from infected MDC1C CD133+ blood-derived stem cells and FKRP L276I^{KI} satellite cells culture medium

According to previous observations, demonstrating that FKRP glycosyltransferase can be released in vitro by cultured cells, we have speculated that FKRP positive expression detected in conditioned medium could underline the protein internalization within exosomes, subsequently released in vitro from transduced cells.

Firstly, we established the proper conditions to collect medium from MOI 20-infected FKRP L276I^{KI} satellite cells culture: medium was harvested when cells reached a confluence of ~ 80%, after 72 hours in DMEM with exosome-depleted FBS. Isolation was performed by SEC chromatography, as previously described. Figure 22 summarizes data obtained by the characterization of infected LV-FKRP L276I^{KI} SCs and CD133+ stem cells-derived exosomes. NTA graphs show exosomes dimensions and concentration, confirming the presence of exosome similar particles. MOI 20 infected MDC1C CD133+ blood-derived exosomes displayed a mean size value of 154.1 nm and a mode size value of 128.2 nm (SD 64.4 nm) (Fig. 22A), with a particle concentration of about 1.17 x 10^9 particles/ml), whereas MOI 20- infected FKRP L276I^{KI} SCs- isolated exosomes exhibited a mean size value of 166.6 nm and a mode size value of 139.9 nm (SD = 71.5). The particle concentration was about 1.79 x 10^9 particles/ml (Fig. 22B). FACS

analysis confirmed the exosomal nature of isolated particles. The immunophenotyping analysis underlined the positivity of CD63 and CD81 tetraspanins in both MOI 20- infected MDC1C CD133+ - secreted exosomes (92,2% exosomes were positive for CD63, 82,5% for CD81) (Fig. 22C), and in MOI 20- infected FKRP L276I^{KI} SCs- derived vesicles (88% exosomes positive for CD63, 89% for CD81) (Fig. 22D).

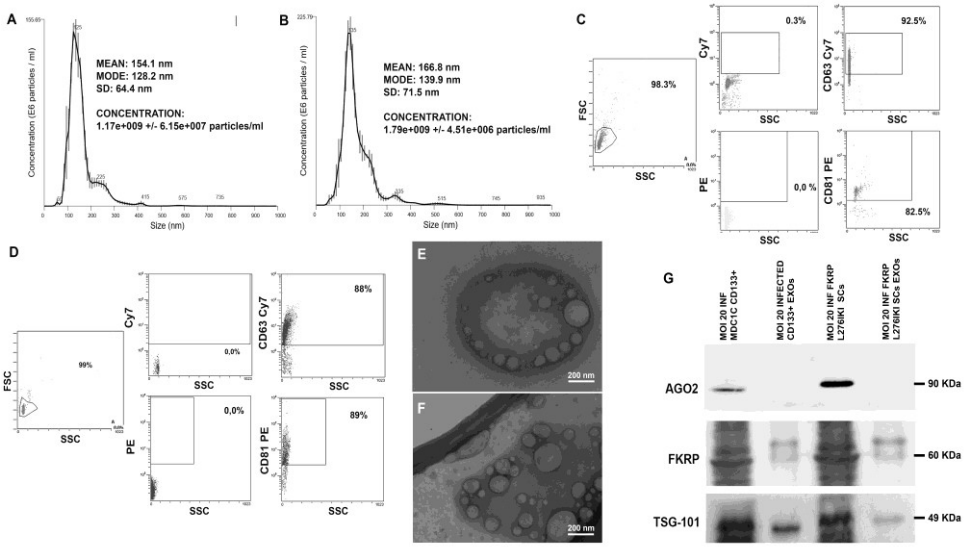

FIGURE 22. *Nanosight Tracking Analysis (NTA) of MOI 20 infected MDC1C CD133+ stem cells- secreted exosomes (A) and FKRP L276I^{KI} SCs (B). Plots show the mean value of 3 recordings run for each sample. FACS analysis of MDC1C CD133+ stem cells- (C) and transduced FKRP L276I^{KI} SCs MOI 20-secreted vesicles (D). Each study included not less than 100000 events. 92,2% of CD133+-secreted exosomes were positive for CD63 tetraspanin, 82,5% for CD81; 88% of SCs- derived exosomes were positive for CD63 and 89% for CD81+. Magnified image of TEM micrograph of MOI 20- infected MDC1C CD133+ stem cells- secreted exosomes (mean value 92,7 nm ± 39,5 nm SD) (E) and FKRP L276I^{KI} satellite cells (mean value 109 nm ± 46,3 nm SD)(F). NIH ImageJ software was exploited to measure exosome diameters. Scale bar, 200 nm. WB analysis of FKRP, AGO2 and FKRP proteins expression in MOI 20 infected MDC1C CD133+ stem cells- (MOI 20 INF MDC1C CD133+ EXOs, lane 2) and MOI 20 FKRP L276I^{KI} SCs- (MOI 20 INF L276I^{KI} SCs EXOs, lane 4) secreted exosomes. MOI 20 infected CD133+ blood-derived cell lysate (MOI 20 INF MDC1C CD133+, lane 1) and MOI 20 infected SCs lysate (MOI 20 INF L276I^{KI} FKRP, lane 3) were loaded as positive controls.*

Transmission electron microscopy (TEM) images reported the presence of particles exhibiting a cup-shaped morphology (Fig 22E, F). Overall, both exosome populations displayed similar size and morphology (MOI 20-

infected MDC1C CD133+ stem cells exosomes: 92, 7 nm ± 39,5 nm SD; MOI 20- infected FKRP L276I^{KI} SCs- secreted exosomes: 109 nm ± 46,3 nm SD). WB analysis was performed on both MOI 20- infected MDC1C CD133+ and FKRP L276I^{KI} satellite cell lysates (MOI 20 INF CD133+ MDC1C cells and MOI 20 INF L276I^{KI} FKRP SCs, respectively lane 1, 3) and corresponding secreted exosomes (MOI 20 INF CD133+ MDC1C EXOs and MOI 20 INF L276I^{KI} FKRP SCs EXOs: lanes 2, 4 respectively).

A positive signal at ~60 KDa was observed, demonstrating exogenous FKRP wild-type expression in both infected cell population lysates and released exosomes.Ago2 positive staining (90KDa) in cell lysates and negative expression in exosome samples prompted us to exclude the presence of contaminants during the isolation procedure. On the contrary, TSG-101 positive expression (49 KDa), authenticates the specificity of FKRP as an exosome cargo (Fig 22G) (13).

4.5 In vivo engineered satellite cells transplantation

According to previous results, we transplanted MOI-20 engineered satellite cells into the right TAs of 1-year-old FKRP L276I^{KI} mice. Firstly, we aimed at defining if engineered satellite cells autologous transplantation could allow transplanted cells fusion to the host muscle tissue and to prove the recovery of wild-type exogenous FKRP protein and the consequent α-dystroglycan glycosylation.

Moreover, we aimed at observing an amelioration of the dystrophic phenotype by evaluating transplanted mice endurance. Finally, we focused on the investigation of an exosome-mediated FKRP systemic effect, to determine an overall rescue of the glycosyltransferase protein and its function in α-DG glycosylation at distant sites. 12 months- old FKRP L276I^{KI} mice were divided into three groups and injected with an increasing number of LV-hFKRP engineered cells ($35x10^3$, $75x10^3$ and $100x10^3$ cells). Not-

transplanted FKRP L276I^{KI} mice were exploited as negative controls for the following analysis.

4.5.1 Immunobiochemical and Immunofluorescent analysis of injected muscles

Figure 23 A, B, C show a positive signal at ~ 60 KDa, representative of exogenous FKRP expression in all injected right TAs (lanes +), but highlighting an increasing trend of protein rescue on the strength of the number of injected cells. 35x10^3 engineered satellite cells- L276I^{KI} transplanted mice (N= 4 mice) showed a weak FKRP positive signal (Fig 23A, lanes #1, #2, #3, #4), while the transplantation of 75x10^3 engineered satellite cells (N= 5 mice) outlined a stronger signal (Fig. 23B, lanes #5, #6, #7, #8, #9), which was found to be comparable to the one obtained with 100x10^3 engineered cells injection (N= 4 mice) (Fig. 23C, lanes #10, #11, #12, #13).

Meanwhile, we checked the exosome-mediated systemic effect of transplantation by performing WB analysis in injected mice contralateral TAs (lanes -). FKRP signal was found to be increased between 35 and 75x10^3 cell doses and comparable between 75 and 100x10^3 injected mice groups. Not-injected FKRP L276I^{KI} TAs (lane NI) and C57BL TAs (lane CTR+) were exploited as negative and positive controls.

Since FKRP-STEM antibody is unable to detect the endogenous mutated FKRP protein [120], there was no FKRP signal in not transplanted FKRP L276I^{KI} TA analysed muscles, whereas the wild-type form of C57BL mouse was distinctly distinguishable. Interestingly, the FKRP-STEM antibody revealed a faint positive signal representative of exogenous FKRP in the

contralateral TAs muscles, thus sustaining the first proof of a systemic exosome-mediated FKRP protein distribution (Fig. 23A, B, C).

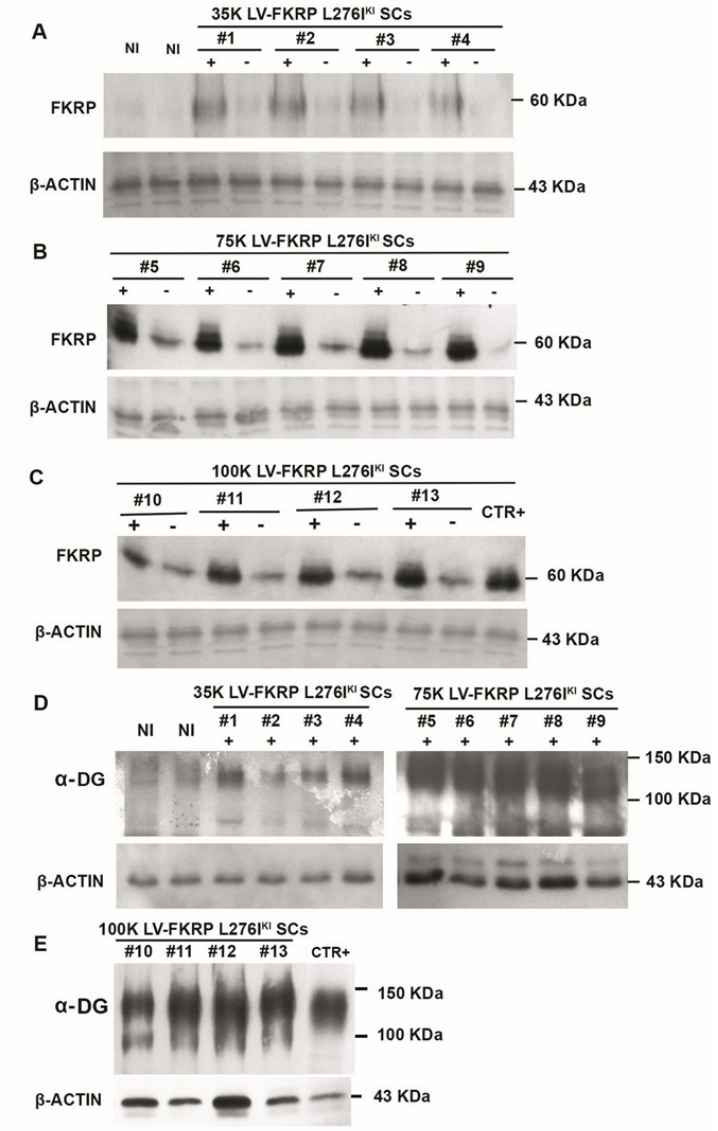

FIGURE 23. *WB analysis of 1-year-old FKRP L276I^{KI} mice transplanted muscles. Mice were transplanted with 35x10^3 (N=4, lanes #1, #2, #3, #4), 75x10^3 (N=5, lanes #5, #6, #7, #8, #9) and 100x10^3 (N=4, lanes #10, #11, #12, #13) FKRP L276I^{KI} SCs cells infected with MOI 20. Either transplanted (+ lanes) and contralateral (- lanes) TAs were evaluated for FKRP protein positivity (A, B, C). Immunophenotyping analysis of α-DG glycosylation was investigated in transplanted TA (lanes +) (C, D). N=2 not transplanted FKRP L276I^{KI} TAs (lanes NI) were considered as negative controls (A). C57BL TA (lane CTR+) was loaded as positive control (C).*

Transplanted TAs were also biochemically evaluated for α-DG glycosylation rescue. As previously mentioned, α-DG is a heavily glycosylated protein: even though its expected molecular weight (MW) is around 72 KDa, it looks like a broad smear on western blot bands, with an apparent MW of 156 KDa in skeletal muscle. α-DG glycosylation is represented by the smear height. 35 x 10^3 engineered SCs transplantation didn't produce a noticeable difference in α-DG glycosylation in comparison to not transplanted dystrophic muscles (Fig. 23D; lanes #1, #2, #3, #4, NI). On the contrary, 75x10^3 and 100x10^3 cells injection, by determining a significant rescue of FKRP function, were able to elicit an appreciable increase in α-DG glycosylation, as shown by the more extended smeared band on the blot. (Fig. 23D, E; lanes #5, #6, #7, #8, #9, #10, #11, #12, #13).

Immunofluorescence staining (IF) showed the recovered expression of FKRP in all engineered SCs –injected FKRP L276I^{KI} mice. The 35x10^3 injected mouse group exhibited irregular sarcolemmal positive signal of wild-type FKRP, limited to a few myofibers, whereas 75x10^3 and 100x10^3 doses revealed a more regular and diffused sarcolemmal fluorescent staining (Fig 23B, C, D). A patchy positive staining of a perinuclear FKRP expression was also detected in some muscle fibers (Fig. 24C and D enclosures, white arrows). As the lentiviral vector was produced with two distinctive promoters for the expression of the wild type FKRP insert and GFP-Puro dual marker, FKRP and GFP were not transduced into a single peptide but produced two independent transcripts.

As expected, GFP signal was identified as diffused in myofibers cytoplasm with a more intense staining in muscles transplanted with 75 and 100x10^3 cells (Fig. 24B', C', D'), rather than in 35x10^3 cell dose. Interestingly, both some GFP+ and some GFP- muscle fibers presented with FKRP sarcolemmal positive expression. As IF was performed exploiting FKRP-STEM antibody, not-injected FKRP L276I^{KI} mice were used as negative controls and did not show any positive staining (Fig. 24A). Afterwards, we

also performed an IF staining of α-DG. As expected, untreated FKRP L276I^{KI} mice TAs exhibited a moderate and variable positive signal of alpha-DG glycosylation, (Fig 24A''). On the other hand, transplanted muscles showed a more intense positive signal, proportional to the cell dose increase (Fig 24B'', C'', D''). These observations confirmed that FKRP recovered expression is strictly linked to the level of functionally glycosylated α-DG in the injected FKRP L276I^{KI} mice.

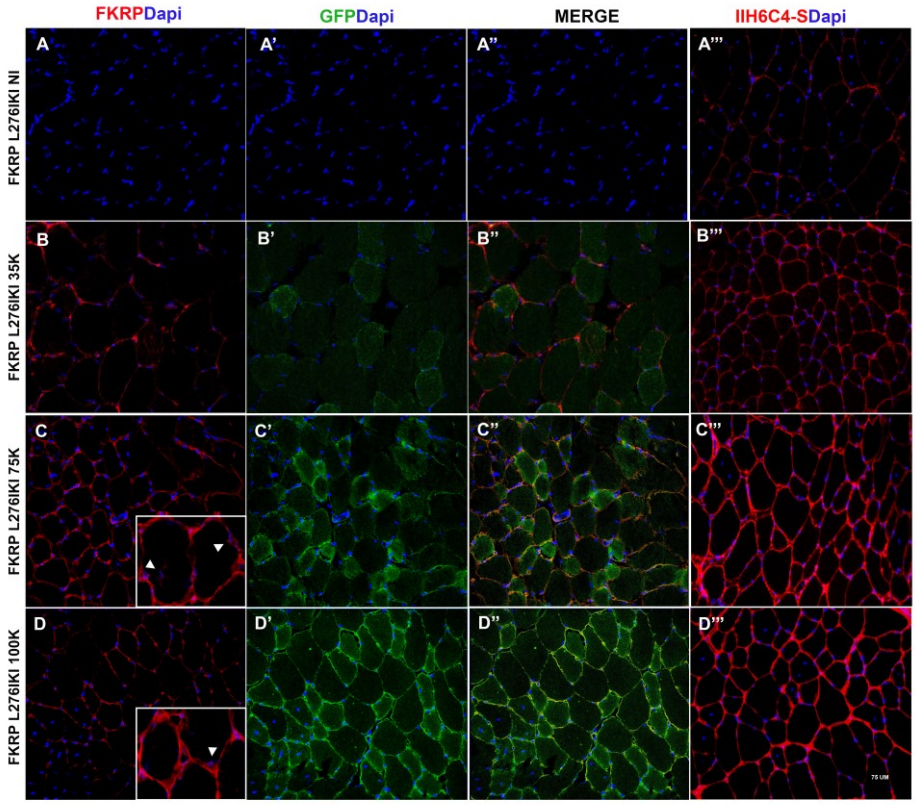

FIGURE 24. *Immunofluorescent analysis of serial sections of FKRP L276I^{KI} not injected (FKRP L276I^{KI} NI) and FKRP L276I^{KI} TAs injected with 35x10^3 , 75x10^3 , 100x10^3 engineered satellite cells (FKRP L276I^{KI} 35K, 75K, 100K). Exogenous FKRP staining (in red) (A, B, C, D) was performed on tissue sections. Fig. C and D inserts display a magnification of exogenous FKRP perinuclear staining. GFP protein expression (in green) (A', B', C', D') was evaluated to identify the protein expression and localization. Merge of FKRP and GFP is also shown (A'', B'', C'', D''). The staining of α-DG glycosylation was also performed (in red) (A''', B''', C''', D'''). Nuclei were counterstained with Dapi. Images were captured at 40X magnification. Scale bar = 75 μm*

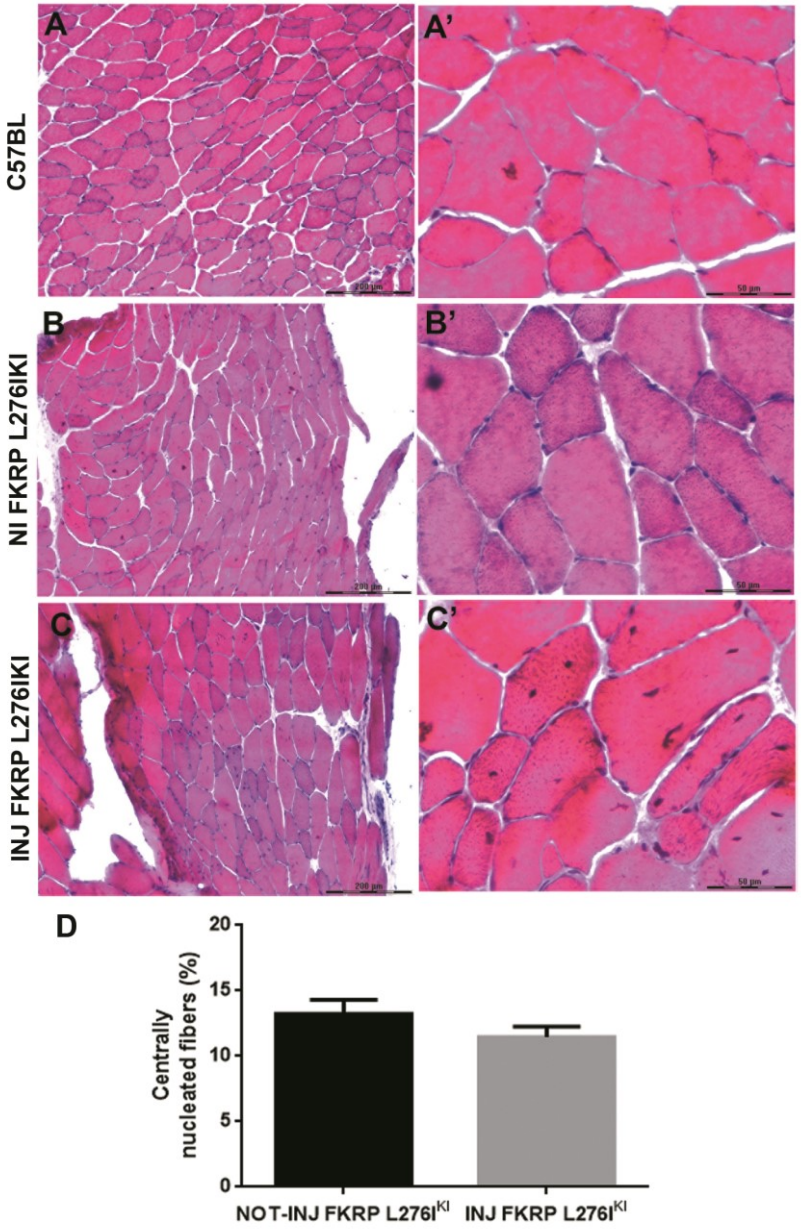

FIGURE 25. *Hematoxylin and eosin staining of transplanted FKRP L276I^{KI} TAs. Tissue sections from TA of positive control C57Bl mouse (A, A'), not transplanted (B, B') and transplanted FKRP L276I^{KI} mutant mice (C, C'). Scale bar = 200 µm (A, B and C), 50 µm (A', B', and C'). C and C' show TA muscles from FKRP L276I^{KI} mice transplanted with 75x10^3 LV-FKRP L276I^{KI} satellite cells. Quantification of centrally nucleated myofibers. The percentile of centrally nucleated fibers was defined as the percentage of centrally nucleated fibers versus the total counted myofibers (D).*

It is well known from literature that the FKRP L276I^{KI} mouse model exhibits a mild dystrophic phenotype, resembling the LGMD2I dystrophy. Of note, dystrophic muscles present with myofiber cycles of degeneration and regeneration, fiber size variability and adipose/ fibrotic infiltrates in the later stages of the disease progression.

The analysis of muscle morphology was performed by hematoxylin and eosin (H&E) staining (Fig. 25). Our outcomes confirm FKRP L276I^{KI} mild dystrophic phenotype, with a comparable pathological morphology between not transplanted TA (Fig. 25B, B') and transplanted TA muscles (Fig. 25C, C'), showing just a slight decrease, not statistically significant, of the percentage of centrally nucleated myofibers in injected mice (Fig. 25D).

4.5.2 Exosome-mediated systemic distribution of FKRP protein

To further reinforce the evidence that FKRP+ exosome release by infected SCs produces therapeutic effects at distal compartments, we aimed at demonstrating these exosomes trafficking in the bloodstream.

Exosomes were isolated from plasma samples of all the injected mice by SEC chromatography and biochemically analysed for the presence of exogenous FKRP.

At first, we characterized FKRP protein expression in the unprocessed total plasma, SEC exosomes-enriched elution fractions and exosomes-depleted plasma. A 60KDa band corresponding to FKRP was detected in total plasma and exosome elution fractions, whereas no signal was observed in exosome-depleted plasma (Fig. 26).

Indeed, it is likely that the systemic trafficking of exogenous FKRP is only mediated by release of exosomes, that act as carriers in the bloodstream.

Following this preliminary analysis, all FKRP L276I^{KI} isolated plasma exosomes were analysed for the glycosyltransferase expression in order to compare the protein expression level in the three groups of injection.

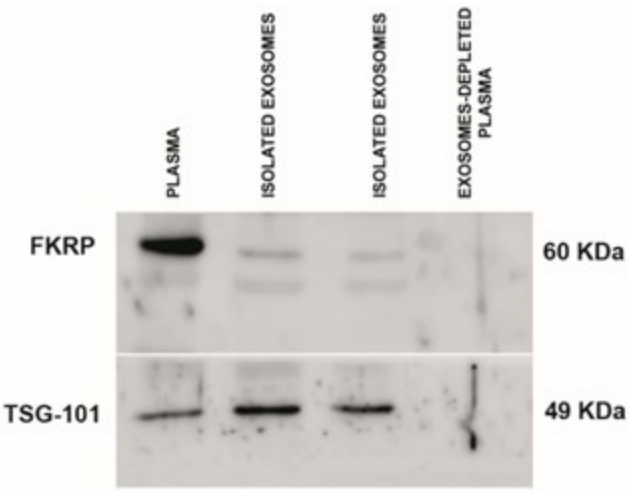

FIGURE 26. *Western blot images of plasma and plasma isolated exosomes from injected FKRP L276I^{KI} mice. Representative WB analysis of FKRP L276I^{KI} mice injected with 75K transduced FKRP L276I^{KI} SCs: total plasma (unprocessed), plasma-derived exosomes isolated by SEC (7 and 8 exosome elution fractions), and exosome-depleted plasma were evaluated for the expression of FKRP protein and TSG-101 exosomal marker expression.*

Loaded samples (lanes 35K, 75K, 100K) exhibited a positive signal at approximately 60 KDa, which appeared more intense as the number of transplanted cells increased. As expected by previous results, FKRP-STEM antibody didn't detect any signal in not-injected FKRP L276I^{KI} plasma exosome sample (lane NI). TSG-101 protein (49 KDa) was found to be positive in all the loaded samples (Fig. 27A), highlighting the efficiency of SEC in isolating exosomes from plasma. Plasma-derived exosomes were examined by transmission electron microscopy (TEM); TEM images showed cup-shaped particles characterized by a mean size value of 90 nm ± 36,6 nm SD (Fig. 27B); NTA revealed a mean size value of 142,2 nm, a mode size value of 130,8 nm and a concentration of 1,13x10^{9} particles/ml (Fig. 27C).

We evaluated the exosome-mediated systemic effect of engineered satellite cells intramuscular transplantation in the hearts of all transplanted mice, since it represents one of the most compromised muscle in the FKRP L276I^{KI} animal model [120]. Firstly, we measured the exogenous wild-type expression of FKRP, than we evaluated the consequent restoration of α-DG

physiological glycosylation levels. As observed in contralateral TAs samples, all transplanted mice hearts were positive for wild-type exogenous FKRP expression and displayed a positive band at 60 KDa, directly proportional to the increased cell dose. A plateau between $75x10^3$ and $100x10^3$ injected mice (Fig 27D) is still clearly visible in line with what observed for TAs. The specificity of the FKRP-STEM antibody produced a positive band in C57BL mouse heart, showing an undoubted wild-type expression of FKRP (lane CTR+), whereas the not-injected (lane NI) mouse heart didn't exhibit any detectable signal. No differences were evidenced among the three cell doses concerning alpha- DG glycosylation. However, a significant glycosylation increase, detectable by the higher smeared band, was noticeable between the not injected mice and C57BL mouse heart (Fig. 27D, E).

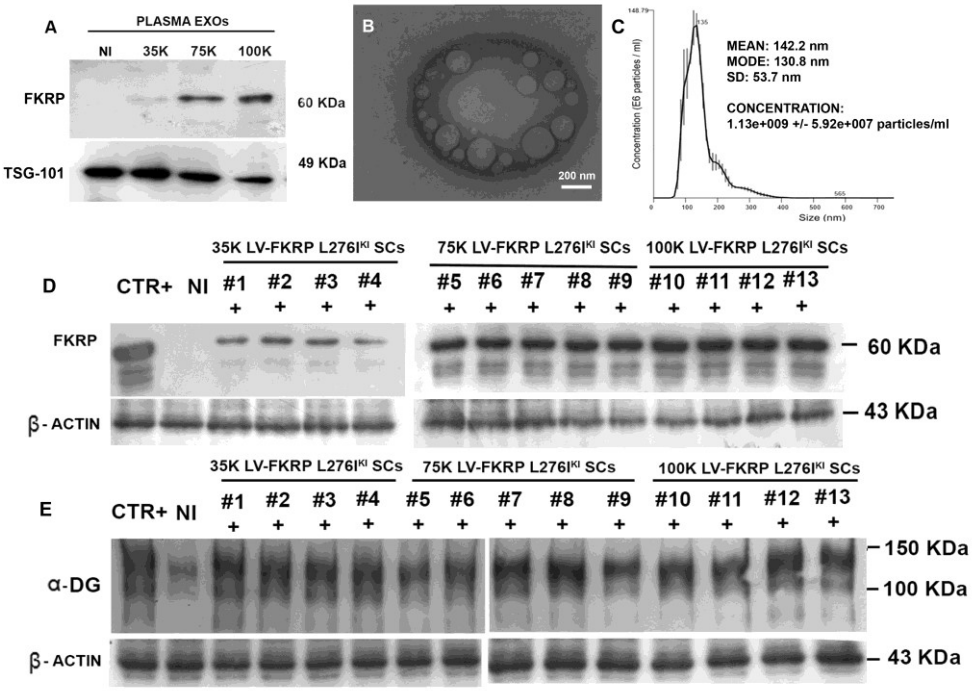

FIGURE 27. *WB analysis of exosomes isolated from plasma. Vesicles were sedimented from the plasma of 1-year old FKRP L276I^{KI} mice transplanted with 35, 75, and $100x10^3$ engineered FKRP L276I^{KI} SCs and not-transplanted FKRP L276I^{KI} mice. Exosomes were characterized for the expression of FKRP and TSG-101 proteins (A). TEM image representing plasma-derived exosomes morphology (mean size 90 nm ± 36.6 nm SD).Scale*

bar: 200nm (B). NTA graph representing plasma- exosomes concentration and dimensions (C). WB analysis of FKRP L276I^{KI} engineered SCs-transplanted mice hearts. FKRP (D) and α-DG glycosylation (E) positive signals were evaluated considering N=4 mice transplanted with 35x10^3 (#1, #2, #3, #4), N=5 with 75x10^3 (lanes #5, #6, #7, #8, #9), and N=4 with 100x10^3(lanes #10, #11, #12, #13) engineered SCs. Not injected FKRP L276I^{KI} and C57BL heart muscle were loaded as negative and positive controls (lane NI, CTR+)(D, E).

4.5.3 In vitro modelling of dynamic FKRP-carrying exosomes tracking

We exploited a miniaturized bioreactor to show in vitro exosome flow and to mimic the in vivo exosome kinetics, trafficking dynamic, timing of distribution and fusion to targeted tissues. Exosomes, released by PKH26+ FKRP L276I^{KI} SCs infected with MOI 20, travelled along a microfluidic channel to reach target- FKRP L276I^{KI} SCs cells. Fig. 28B showed a diffused GFP signal in cell cytoplasm, which confirmed the correct infection by lentiviral MOI of 20.

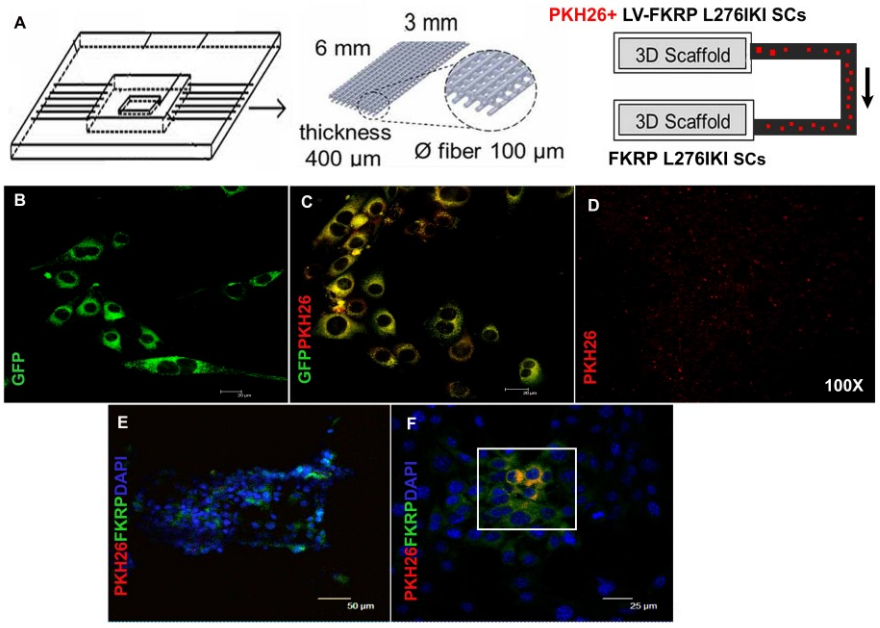

***FIGURE 28**. Schematic representation of the bioreactor. The bioreactor is composed of three scaffolds (6x3 mm, 400µm thickness, 0,6 µm fiber pore size), connected by microfluidic channels. PKH26+ FKRP L276I^{KI} satellite cells were seeded on the first scaffold and secreted PKH26+ exosomes, able to reach not-infected SCs seeded on the second scaffold, running through a microfluidic channel connecting the two chambers (A). IF analysis of infected FKRP L276I^{KI} SCs; GFP signal was detected in the cell cytoplasm (B).*

PKH26- labelled FKRP L276I^{KI} SCs cells (C). PKH26- exosomes secreted by PKH26-labelled FKRP L276IKI SCs cells (D). Images were taken at 100X magnification. Immunofluorescent analysis of not-infected SCs seeded on the second scaffold. PKH26+ exosomes- (in red) targeted SCs recovered the expression of wild-type FKRP (in green). Nuclei were stained with Dapi (E, F).

Similarly, Fig 28C proved the optimal FKRP L276I^{KI} SCs membrane staining by PKH26 marker, guaranteeing PKH26+ exosome secretion. PKH26+ exosomes were followed for 8 hours within the microfluidic channels by confocal fluorescent microscopy at 100X magnification (Fig. 28D). FKRP L276I^{KI} SCs- released exosomes were able to reach the not infected cell population, where they fused, transferring exogenous FKRP protein and favouring its expression in mutant receiving cells. In order to verify the occurrence of exosome-mediated FKRP convey, IF analysis was performed on the not infected FKRP L276I^{KI} SCs. The staining showed an exogenous FKRP positive signal (in green) (Fig. 28E, F), mainly restricted to those cells in which exosome fusion had occurred (in red) (Fig. 28E, F).

4.5.4 Functional Analysis

To define if the local and the systemic rescue of exogenous wild-type FKRP protein expression in engineered SCs-transplanted FKRP L276I^{KI} would determine an increased skeletal muscle force and cardiac muscle functionality, we evaluated the animals performance with two functional tests: treadmill and rotarod. Treadmill outcomes demonstrated that untreated dystrophic mice found very hard to achieve the conclusion of the experimental sets. FKRP L276I^{KI} mice appeared to adapt to the exercise after the starting training sitting (-T7), becoming familiar with the treadmill. They were able to run for the first week (T7), despite they constantly ran below 400 meters with a running time of about 1000 seconds. After two weeks (T14), untreated mice became incapable to maintain previous performances, exhibiting acute fatigue. Conversely, engineered SCs- transplanted mice performance was dependent on the number of injected LV-FKRP satellite

cells. Overall, FKRP L276I^{KI} injected mice displayed an increase in running distance outputs compared both to the pre-injection measured performance and to not transplanted animal outcomes. Of note, all injected mice rapidly displayed the positive effects of cell transplantation, demonstrating an increased tendency, produced immediately after the cells transplantation, although the 75K group showed a more pronounced and remarkable amelioration. 75K group seemed to produce a long-lasting increase of both the distance and time of running, presenting a leap from 403 meters (averaged running distance) at T0 to 698.7 meters at T7, and up to 724 meters a T14. The tendency of the 75x10^3 engineered cells transplanted mice running time went through a rapid increase in the first week after transplantation (T0 averaged running time 779.2 seconds vs. T7 average running time 2827 seconds), settling after two weeks (T14) at ~2411 seconds. 100K- transplanted mice group treadmill test outputs exhibited a more moderate increasing tendency, reaching the maximum distance and time at T7, followed by a plateau level at T14 (averaged running distance: 547 meters; averaged running time: 1898 seconds) (Fig. 29A, B). 35K cells-treated FKRP L276I^{KI} mice demonstrated instead more pronounced inter individual differences with a slow diminution of the endurance results. Although a reported trend towards an increased running distance and time within T7, at T14 the 35K group degenerated and produced performances comparable to those recorded pre-injection (averaged running time: 1315 seconds; averaged running distance: 301 meters). The averaged coefficients of variations at T14, were -86% for not transplanted FKRP L276I^{KI} mice, -18% for FKRP L276I^{KI} injected with 35x10^3 cells, and +95% and +62% respectively for FKRP L276I^{KI} transplanted with 75x10^3 and 100x10^3 LV-FKRP infected L276I^{KI} SCs.

Rotarod functional results confirmed the poor outcomes of not transplanted mice, as well as the cell dose-dependent functional amelioration of the transplanted FKRP L276I^{KI} mice. On the rotarod, untreated FKRP L276I^{KI}

mice rarely run for 300 seconds. Even though the running distance was comparable between –T7 and T7 time-points, it began to decrease significantly within T7 and T14. $35x10^3$ injected group showed a remarkable amelioration within T7, after which the running time was maintained almost unchanged throughout the experimental settings (averaged running time at T14: 377 seconds). Likewise, 75K and 100K groups underwent amelioration in running time throughout the first week after the injection (averaged running time at T7: 418 seconds and 398 seconds, respectively) (Fig. 29C). For both groups, although there were further improvements of the endurance reported after two weeks from the transplantation (T14) ($75x10^3$ transplanted mice, averaged running time: 429 seconds; $100x10^3$ transplanted mice, averaged running time: 411 seconds) the positive tendency decreased, reaching a steady point.

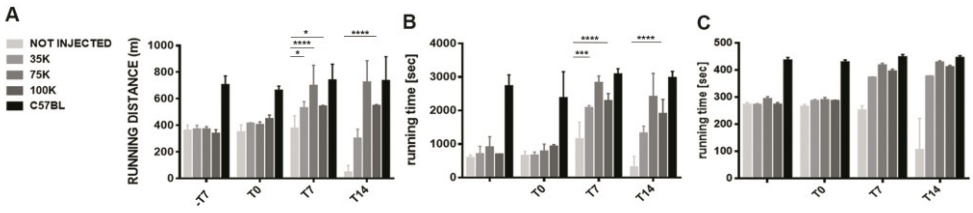

FIGURE 29. *Mice endurance was determined by Treadmill (A, B) and Rotarod tests (C). N=5 C57BL mice, N=6 not transplanted, N=4 $35x10^4$, N=5 $75x10^4$, and N=4 $100x10^4$ MOI 20- infected FKRP L276I^{KI} satellite cells- transplanted mice have been evaluated at different time-points: a week before the cell transplantation (7 days pre-INJ), the day of cells injection (T0), and one and two weeks (T7, T14), before the mice sacrifice. Values are means ± SD. ***, p value <0.05 was considered statistically significant.*

For both Treadmill and Rotarod tests, transplanted and not transplanted FKRP L276I^{KI} mice outcomes were compared to the performances of C57Bl control mice (N=5; treadmill averaged running distance and time: 710 meters and 2788 seconds; rotarod averaged running time: 437 seconds). Only the 75K group was able to exhibit an improved performance comparable to the one of C57Bl mice at T7 and T14 (Fig. 29A, B, C).

5 DISCUSSION

α-Dystroglycanopathies are a group of inherited disorders, which arise from mutations occurring in various genes encoding for glycosyltransferase enzymes. α-DG is a glycoprotein localized on muscle peripheral membranes [87] [179] that undergoes post-translational modifications: N-glycosylation, mucin-type O-glycosylation, O-mannosylation, and the addition of an identified phosphorylated O-mannosyl glycan. Mutations occurring in glycosyltransferases involved in O-linked glycosylation usually lead to α-DG hypoglycosylation and a consequent disruption of the protein binding with laminin, neurexin, and agrin. α- dystroglycanopathies present a wide range of phenotypes, ranging from severe forms of congenital muscular dystrophies (CMDs), with brain and eye involvement, to the milder limb girdle muscular dystrophies (LGMD) [99]. Among all the genes found mutated in α-dystroglycanopathies, we have narrowed down our attention on fukutin related protein (FKRP) that acts in tandem with Fukutin as a transferase of ribitol 5-phosphate (Rbo5P) [117]. Mutations in FKRP gene, encoding for the glycosyltransferase fukutin-related protein, determine the occurrence of untreatable limb-girdle muscular dystrophy 2I and MDC1C. To date, no resolving therapies have been found for these disorders. Only the approach based on adeno-associated Virus 9 (AVV9)-FKRP treatment represents a promising cure for all the pathologies caused by a single-gene disruption, but it is limited by risks associated to viral toxicity [180], and it does not sustain muscle regeneration. Therefore, we have successfully evaluated the possibility to transplant gene- corrected stem cells, possessing both myogenic differentiation abilities and the capability to restore functional α-DG glycosylation by expressing wild type isoform of FKRP, for overcoming gene-therapy related limits. Moreover, starting from recent literatures employing viral or non-viral methods to engineer the parental cells to secrete modified exosomes, we have demonstrated that LV-FKRP engineered stem cells were able to release exosomes carrying the FKRP glycosyltransferase. The

widespread in vivo deployment of exosomes carrying FKRP, continuously released from intramuscularly transplanted engineered stem cells, determined a general and boosted therapeutic effect in FKRP L267I^{KI} animal model.

5.1 In vitro engineering of MDC1C CD133+ blood-derived stem cells

We have previously demonstrated that human blood-derived progenitors expressing the CD133+ marker possess in vivo myogenic potential [181]. Starting from successful and feasible results previously carried out from our group, we infected CD133+ blood-derived stem cells isolated from a MDC1C patient with a lentiviral vector carrying the wild-type isoform of human FKRP gene. This way, the expression of the wild-type FKRP was recovered in vitro without dose- related lentiviral-induced toxicity. In fact, none of the tested MOI of infection (MOI 5, 10, 20) produced a deleterious outcome in CD133+ proliferation curve. Overall, the lack of cytotoxic effects on MDC1C patient's cells, even at high LV-MOI, confirmed the reliability and feasibility of this strategy towards clinical relevant applications

5.2 In vitro engineering of L276I^{KI} satellite cells

We aimed to carry out in vivo experiments to definitively prove the efficiency of stem cell and gene combined approaches in restoring a LGMD2I phenotype. Thus, we performed an autologous transplantation of engineered myogenic cells into the TAs muscles of FKRP L267I^{KI} mice, resembling LGMD2I muscular dystrophy. The requirement of an autologous transplantation was due to the absence of an immunodeficient FKRP mutated animal model. For this purpose, we isolated satellite cells from new born FKRP L276I^{KI} mice and we infected them with the lentiviral vector. To avoid concerns related to LV- mediated cytotoxicity and myogenic capacity impairment, we have tested MOI of infection: 10, 20 and 40. For each

condition, no statistically significant differences were observed in terms of cell proliferation and fusion index in comparison to not-infected dystrophic satellite cells.

These results took distance from recent finding suggesting a dose-dependent toxicity of rAAV-FKRP vector, characterized by a decrease of α-dystroglycan glycosylation directly proportional to the AAV dose of injection [182]. Similarly, we wanted to exclude the chance to induce a detrimental α-DG hyperglycosylation that has been demonstrated to worsen the dystrophic phenotype in $FKRP_{MD}$ animal model [105].

Throughout WB experiments, we showed that LV- induced FKRP expression displayed an increasing trend between MOI 10 and 20, while MOI 40 seemed to represent a steady point, leading to FKRP expression plateau; also the amount of α-DG glycosylation was similar between MOI 20 and 40, thus ruling out the risk of an induced α-DG hyperglycosylation. These evidences suggested that infection with MOI 20 was able to restore the FKRP level necessary to saturate glycosylation sites of alpha-DG and to recover its physiological function and led us to choose MOI 20 for the infection of both the two cell populations.

For all the WBs and immunofluorescence analysed, we have utilized the FKRP-STEM antibody to specifically identify the exogenous wild-type protein from the endogenous mutated one [120].

Even though the mutation occurring in the $L276I^{KI}$ FKRP mouse model is a missense mutation, leading to an amino acidic change without any consequence on the protein expression, the amino acidic change alone compromises the protein recognition [120]. It is likely that the antibodies binding sites on the endogenous FKRP may be at least partially masked, possibly by other proteins, in a complex essential for the glycosyltransferase activity [183]. FKRP-STEM antibody allowed the detection of only the exogenous FKRP, thus undoubtedly demonstrating the successful LV-mediated rescue of the glycosyltransferase.

5.3 Engineered SCs-derived FKRP-carrying exosomes allow a systemic distribution of the glycosyltransferase after cells intramuscular transplantation

The attention on FKRP role as a glycosyltransferase and the recent evidence of circulating glycosyltransferases exerting their functional role at distant compartments [141], prompted us to investigate the hypothesis of a cell-mediated secretion of FKRP both in vitro, in cell culture medium, and in vivo in the bloodstream [115]. Previous studies had shown that fukutin protein (FKTN) and FKRP might be released in vitro by cells [115, 184]. However, they did not explained whether these glycosyltransferases were released either in a free form or enclosed within vesicles. Exosomes are a homogeneous population of extracellular microvesicles well- known for their capability to convey genetic material (mainly protein and miRNA cargos) to target cells, even at distant compartments by circulating in the bloodstream. Beyond genetic information [185], exosomes can also vehicle enzymes: kinases, phosphatases, and glycosyltransferases. Given that, we considered that cell- related FKRP release could be mediated by exosomes [114]. To prove this evidence, we aimed at optimizing the process of exosome isolation from engineered cells, both MDC1C CD133+ blood derived stem cells and LGMD2I- derived satellite cells. We compared three common exosomal isolation procedures: differential ultracentrifugation (UC), commercial kits and size exclusion chromatography (SEC). To examine the quality of isolated particles we biochemically evaluated the expression of TSG-101. Moreover, we investigated particles morphology, size and concentration by TEM microscopy and NTA analysis. Even though it is well- known from literature that exosomes dimensions usually range between 30 and 100 nm, all the analysed samples presented slightly bigger dimensions. We suggest that particles may aggregate during the isolation procedure, thus NTA recognizes an aggregate as a single particle during the recording step. Moreover, it calculates particles dimension taking in account their hydrodynamic radius.

This evidence may also explain the difference between TEM and NTA results. In line with exosomal isolation procedure literature, we found out that differential ultracentrifugation, beyond being highly time-consuming [186], allowed to isolate heterogeneous exosomes with significant overlapped dimensions and extracellular microparticles contamination.

Commercial kits, on the contrary, were extremely less time-consuming and they were able to recover high amounts of vesicles starting from a little amount of material. However, even this procedure was affected by both proteins and other MVs contamination.

Overall, we considered SEC as the most performing technique, determining an efficient and homogeneous exosome recovery without extracellular vesicle contamination. We have also found out that collecting supernatants that have been in contact with 70-80% confluent cells for 72 hours could be considered the optimal condition for achieving high exosomal number and size- homogeneity. Even though the underlying reasons have to be further investigated, the homogeneity of exosome subpopulations is likely related to their secretion from cell cycle-synchronized cells. Once defined the most performing isolation procedure and cell culture condition, we proceeded to isolate exosomes from MOI 20- infected MDC1C CD133+ cells and FKRP L276I^{KI} satellite cells. WB analyses confirmed for both cells the presence of exosomes expressing TSG-101 typical marker and FKRP [114], suggesting that in vivo exosomes might equally traffic and deliver glycosyltransferase to receiving cells. To investigate the in vitro cell- to cell transmission of systemic exosome FKRP, mimicking exosomes kinetics and timing of distribution, we took advantage of a miniaturized microfluidic bioreactor. This system allows to seed two cell populations in two independent chambers, connected by a microfluidic channel. The presence of an optical transparent tube connecting the chambers guaranteed the observation of FKRP- enriched exosomes flux from engineered FKRP L276I^{KI} SCs on one side (exosomal source), to not infected FKRP L276I^{KI} cells on the other side (target cells). The selective

uptake of exosomes was ensured by a unidirectional medium flow, mimicking the bloodstream directing exosomes release from injected TAs to distal body tissues. By exploiting this miniaturized microfluidic system, we confirmed that exogenous wild-type FKRP can be continuously delivered by exosomes towards receiving cells, where they randomly fuse and induce a fast expression of functional wild-type exogenous FKRP protein.

To highlight the in vivo function of FKRP-carrying exosomes and define the potential clinical application of a combined gene- and cell- based therapy, we carried out in vivo experiments. Firstly, we intramuscularly transplanted FKRP L276I^{KI} mice with three increasing doses of LV-FKRP engineered L276I^{KI} satellite cells. WB analysis performed on injected TAs proved the successful recovery of exogenous wild-type FKRP protein expression. Moreover, the observed increase in α-dystroglycan glycosylation confirmed FKRP recovered glycosyltransferasic function. Both FKRP and α-DG showed a cell-dose dependent effect in the injected FKRP L267I^{KI} TAs: 35x10^3 engineered FKRP SCs determined a weak FKRP recovery in injected TAs, which was found to be insufficient to determine a significant increment of alpha-DG glycosylation; 75x 10^3 and 100x 10^3 satellite cells injection doses favoured a significant FKRP positive signal and, consequently, an enhancement of alpha-DG glycosylation.

Actually, these results suggest the existence of a functional window for an efficient rescue of FKRP expression and its recovered role in α-DG glycosylation. The comparable outcomes between 75x 10^3 and 100x 10^3 could be due to the lower survival of intramuscular transplanted cells at high density, so that the number of functional cells did not change significantly between the two conditions. Moreover, also the biochemical analysis performed on contralateral TAs revealed a cell dose-dependent expression of exogenous FKRP, suggesting a first evidence of an exosome-mediated transfer of the glycosyltransferase to distal compartments. As for contralateral TAs α-DG glycosylation, the performed biochemical analysis

showed no significant differences among the three groups of injection and not-injected TAs (data not shown). We hypothesize that the recovery of FKRP expression in these sites is not sufficient to produce an evident increase of the glycosyltransferase functionality and, consequently, α-DG glycosylation.

Unless recent published studies have localized FKRP glycosyltransferase within the Golgi, the endoplasmic reticulum (RE) or, alternatively, as punctate dots diffused in the cytoplasmatic compartment of myofibers [9, 110, 111], IF analysis performed on injected FKRP L276I^{KI} TAs revealed a specific positive signal at the sarcolemma. This observation confirmed previous studies showing FKRP co-localization with α-dystroglycan [114], suggesting a precise function of the glycosyltransferase in the DCG complex and consequently in normal muscle function. Interestingly, we detected two different stainings: one consisting in FKRP+ sarcolemma of cytoplasm GFP negative muscle fibers and another one detecting cytoplasm GFP+ fibers, with perinuclear FKRP+ cells. These results highlighted two alternative mechanisms of the glycosyltransferase expression: the first one determined by engineered satellite cells fusion to receiving myofibers and the second one mediated by exosomes release. The cellular and molecular mechanisms determining exosomes fusion to the plasma membrane of specific target cells are still undetermined, although the events favouring their interactions are starting to emerge. Once secreted, exosomes may interact with specific adhesion molecules on target cells plasma membrane, activating specific intracellular pathways, they may directly associate and fuse to target cells plasma membranes, or alternatively they may undergo a cell uptake via the endocytic pathway. These two last described mechanisms, ensure the release of exosome luminal cargo molecules to the cytosol of target cells. On the basis of this knowledge, FKRP staining on transplanted TAs mirrors the direct fusion of vesicles to plasma membrane, as demonstrated by the localization of a positive signal around muscle membranes.

Additionally, we found TSG-101 positive FKRP-enriched exosomes circulating in all transplanted FKRP L276I^{KI} mice bloodstream. Of note, FKRP signal was detected in the unprocessed plasma sample and exosome-enriched elution fractions, but no band was observed in the exosomes-depleted plasma. Thus, exosomes seemed to act as unique carriers of exogenous FKRP in the bloodstream and promoters of a general improvement of muscles in FKRP L276I^{KI} transplanted mice. By comparing the plasma-derived exosomes isolated from the three groups of injection, we were also able to define a cell-number dependent effect of FKRP expression. Since heart is one of the most compromised tissues in the FKRP L276I^{KI} animal model [120], causing a low endurance and performance for exercise, exosome-mediated FKRP expression and function were evaluated in intramuscularly transplanted FKRP L276I^{KI} mice hearts. FKRP positive signal as well as α-DG increased glycosylation observed exosome-mediated recovery of exogenous FKRP even at distal compartments and underlined once again a cell-dose dependent effect. Of note, exogenous FKRP was found to be more expressed in mice hearts than contralateral TAs.

Despite the increase of α-DG glycosylation observed in the hearts, the recovered expression of FKRP in the contralateral TA muscles was not sufficient to produce an evident rescue of its functionality.

No differences were observed in α-DG glycosylation (neither by western blot, nor by immunofluorescence analysis) between not-injected and 35, 75K and 100K- injected mice groups (data not shown).

This observation seems to be related to exosomes diffusion from the circulation and consequently to the vascularization and blood perfusion of the different muscle tissues. Since the heart is the most blood-perfused system, the impact of FKRP+ exosomes could be reasonably more intense in this compartment. These promising outcomes were reinforced with in vitro experiments using a microfluidic bioreactor, demonstrating an exosome-mediated exogenous FKRP expression kinetic occurring in 24 hours.

Furthermore, like any other enzyme, FKRP could easily and immediately carry out its role once replaced. The outputs obtained from Treadmill and Rotarod functional measurements could be explicated as an overall improvement of cardiac functionality, aerobic capacity and motor recovery, probably mediated by FKRP+ exosomes exerting a cardio-protective effect. Transplanted mice showed an increased performance with an amelioration of rotor capacity, motor recovery, and resistance to eccentric contractions.
Surprisingly, transplanted mice displayed improved functional measurements, FKRP expression, and α-DG glycosylation already after 15 days from LV-FKRP engineered cells. This evidence appears in line with previously reported observations. Some metabolic myopathies, such as Pompe disease, present an enzyme deficiency, which can be balanced by an enzyme replacement therapy (ERT). It was reported that these patients typically need an ERT infusion every 2 weeks, thus underlining an immediate but time-limited enzymatic activity, since within 15 days enzymes are able to completely exert their function. Our strategy, based on a complementary interaction between gene, cell and “cell free” therapy, cannot be simply compared to ERT: a therapeutical approach based on the transplantation of healthy stem cells releasing exosomes carrying functional enzymes may allow to obtain unprecedented benefits by boosting and continuously maintaining the enzymatic levels required for the rescue of a biological functionality [187].

6 CONCLUSIONS

In this study we highlight for the first time the possibility of exploiting exosomal enzymes for addressing a therapeutic need. Exosome-mediated exogenous FKRP transfer to cells lacking the physiological protein function is able to rapidly restore its activity and correct α-DG hypoglycosylation. This exosome-based approach is extremely pioneering and relevant in the plethora of muscular diseases arising from enzymatic defects (α-dystroglycanopathies and metabolic myopathies), rather than structural proteins disruption. In fact, while in this latter case exosomes carrying structural proteins would require time to be functionally re-expressed on muscle membranes and maintain its structure and stability, diseases dependent on enzymatic defects respond quickly to enzymatic function replacement. Moreover, the transplantation of FKRP engineered stem cells would guarantee the continuous release of FKRP-carrying exosomes, thus allowing a long-term supply of the enzyme. Moreover, an intramuscular transplantation would not simply determine a local rescue of protein expression and functionality [57], but also an exosome release that would spread through the bloodstream, providing a systemic effect.

$L276I^{KI}$ mice show no signs of central nervous system damage, thus we omitted to investigate the effect of FKRP+ exosomes in this site.

However, since it is well-known from literature that some CMD disorders present brain abnormalities, such al polymicrogyria of the cerebrum, lissencephaly and hypomyelination, leading to severe to mild mental retardation, it could be interesting to perform supplemental experiments exploiting an appropriate mouse model and evaluate FKRP recovered expression and functionality in the SNC. These experiments would also allow to investigate exosomes capability to cross the blood brain barrier (BBB), after an intramuscular injection.

Moreover, further experiments are necessary to investigate the stability of exosome-transported enzymes, compared to those freely circulating.

Based on previous observations regarding miRNA [188], we hypothesize that enzymes enveloped within exosomal membranes are protected until reaching their target site. It would be also necessary to better examine the long-term beneficial outcomes of this exosome-based approach and to interpret the precise mechanisms of in vivo exosomal FKRP biodistribution. Literature on exosomal biodistribution is still very controversial regarding their kinetics and half-life in the bloodstream. While some pharmacokinetic studies of exosome concentration in the blood suggest that vesicles disappear very quickly, revealing a half-life of approximately 2 minutes [172], other analysis show that intravenously injected exosomes have an in vivo half-life of about 30 min [189] or even of about 24 hours [190].

To irrevocably define exosomes lifetime in vivo after cells release, it should be necessary to establish a labelling method of imaging, following specific criteria: the signal should be stable and sufficient to detect nanoscaled exosomes from background noise and its half-life should be congruous with that of exosomes. Similarly, we have to further investigate the effectiveness of a long term release of exosomes from stem cells, together with the preservation of transplanted stem cells viability. Actually, a precise understanding of cells behaviour following their intramuscular transplantation and the feasibility of maintaining their vitality would be necessary to guarantee a long-lasting release of vesicles.

Overall, obtained data demonstrate that muscular dystrophies associated with α-DG glycosylation defects can be treated by a combined gene and cell therapy aimed at restoring FKRP expression and function. More interestingly, FKRP-carrying exosomes can unexpectedly sustain these strategies, offering the possibility to achieve systemic and general outcomes and to boost the effect of an intramuscular injection.

7 BIBLIOGRAPHY

1. Mercuri, E., et al., *Phenotypic spectrum associated with mutations in the fukutin-related protein gene.* Ann Neurol, 2003. 53(4): p. 537-42.
2. Van Reeuwijk, J., et al., *A homozygous FKRP start codon mutation is associated with Walker-Warburg syndrome, the severe end of the clinical spectrum.* Clin Genet, 2010. 78(3): p. 275-81.
3. Colombo, M., G. Raposo, and C. Thery, *Biogenesis, secretion, and intercellular interactions of exosomes and other extracellular vesicles.* Annu Rev Cell Dev Biol, 2014. 30: p. 255-89.
4. Turturici, G., et al., *Extracellular membrane vesicles as a mechanism of cell-to-cell communication: advantages and disadvantages.* Am J Physiol Cell Physiol, 2014. 306(7): p. C621-33.
5. Tedesco, F.S., et al., *Repairing skeletal muscle: regenerative potential of skeletal muscle stem cells.* J Clin Invest, 2010. 120(1): p. 11-9.
6. Zhu, Q., et al., *Structure of protein O-mannose kinase reveals a unique active site architecture.* Elife, 2016. 5.
7. Aksu, F., et al., *Poster presentations.* Surg Radiol Anat, 2009. 31 Suppl 1: p. 95-229.
8. Kobayashi, Y.M., et al., *Endpoint measures in the mdx mouse relevant for muscular dystrophy pre-clinical studies.* Neuromuscul Disord, 2012. 22(1): p. 34-42.
9. Alhamidi, M., et al., *Fukutin-related protein resides in the Golgi cisternae of skeletal muscle fibres and forms disulfide-linked homodimers via an N-terminal interaction.* PLoS One, 2011. 6(8): p. e22968.
10. Reed, U.C., *Congenital muscular dystrophy. Part I: a review of phenotypical and diagnostic aspects.* Arq Neuropsiquiatr, 2009. 67(1): p. 144-68.
11. Schorey, J.S., et al., *Exosomes and other extracellular vesicles in host-pathogen interactions.* EMBO Rep, 2015. 16(1): p. 24-43.
12. Kirschner, J. and C.G. Bonnemann, *The congenital and limb-girdle muscular dystrophies: sharpening the focus, blurring the boundaries.* Arch Neurol, 2004. 61(2): p. 189-99.
13. Buckingham, M., *Skeletal muscle formation in vertebrates.* Curr Opin Genet Dev, 2001. 11(4): p. 440-8.
14. Aoyama, H. and K. Asamoto, *Determination of somite cells: independence of cell differentiation and morphogenesis.* Development, 1988. 104(1): p. 15-28.

15. Tajbakhsh, S. and M. Buckingham, *The birth of muscle progenitor cells in the mouse: spatiotemporal considerations.* Curr Top Dev Biol, 2000. 48: p. 225-68.

16. Cossu, G. and U. Borello, *Wnt signaling and the activation of myogenesis in mammals.* EMBO J, 1999. 18(24): p. 6867-72.

17. Borycki, A.G., et al., *Pax3 functions in cell survival and in pax7 regulation.* Development, 1999. 126(8): p. 1665-74.

18. Epstein, J.A., et al., *Pax3 modulates expression of the c-Met receptor during limb muscle development.* Proc Natl Acad Sci U S A, 1996. 93(9): p. 4213-8.

19. Punch, V.G., A.E. Jones, and M.A. Rudnicki, *Transcriptional networks that regulate muscle stem cell function.* Wiley Interdiscip Rev Syst Biol Med, 2009. 1(1): p. 128-40.

20. Bajard, L., et al., *A novel genetic hierarchy functions during hypaxial myogenesis: Pax3 directly activates Myf5 in muscle progenitor cells in the limb.* Genes Dev, 2006. 20(17): p. 2450-64.

21. Hu, P., et al., *Codependent activators direct myoblast-specific MyoD transcription.* Dev Cell, 2008. 15(4): p. 534-46.

22. Rawls, A., et al., *Overlapping functions of the myogenic bHLH genes MRF4 and MyoD revealed in double mutant mice.* Development, 1998. 125(13): p. 2349-58.

23. Rudnicki, M.A., et al., *MyoD or Myf-5 is required for the formation of skeletal muscle.* Cell, 1993. 75(7): p. 1351-9.

24. Ishikawa, H., *Fine structure of skeletal muscle.* Cell Muscle Motil, 1983. 4: p. 1-84.

25. Greising, S.M., et al., *Systems biology of skeletal muscle: fiber type as an organizing principle.* Wiley Interdiscip Rev Syst Biol Med, 2012. 4(5): p. 457-73.

26. Ciciliot, S. and S. Schiaffino, *Regeneration of mammalian skeletal muscle. Basic mechanisms and clinical implications.* Curr Pharm Des, 2010. 16(8): p. 906-14.

27. Mann, C.J., et al., *Aberrant repair and fibrosis development in skeletal muscle.* Skelet Muscle, 2011. 1(1): p. 21.

28. Serrano, A.L., et al., *Cellular and molecular mechanisms regulating fibrosis in skeletal muscle repair and disease.* Curr Top Dev Biol, 2011. 96: p. 167-201.

29. Ryall, J.G., J.D. Schertzer, and G.S. Lynch, *Cellular and molecular mechanisms underlying age-related skeletal muscle wasting and weakness.* Biogerontology, 2008. 9(4): p. 213-28.

30. Wynn, T.A., *Cellular and molecular mechanisms of fibrosis.* J Pathol, 2008. 214(2): p. 199-210.

31. Bonniaud, P., et al., *TGF-beta and Smad3 signaling link inflammation to chronic fibrogenesis.* J Immunol, 2005. 175(8): p. 5390-5.

32. Mauro, A., *Satellite cell of skeletal muscle fibers.* J Biophys Biochem Cytol, 1961. 9: p. 493-5.

33. Spencer, M.J., et al., *Helper (CD4(+)) and cytotoxic (CD8(+)) T cells promote the pathology of dystrophin-deficient muscle.* Clin Immunol, 2001. 98(2): p. 235-43.

34. Jankowski, R.J., B.M. Deasy, and J. Huard, *Muscle-derived stem cells.* Gene Ther, 2002. 9(10): p. 642-7.

35. Schultz, E., *Satellite cells in normal, regenerating and dystrophic muscle.* Adv Exp Med Biol, 1985. 182: p. 73-84.

36. Gussoni, E., et al., *Dystrophin expression in the mdx mouse restored by stem cell transplantation.* Nature, 1999. 401(6751): p. 390-4.

37. Jackson, K.A., T. Mi, and M.A. Goodell, *Hematopoietic potential of stem cells isolated from murine skeletal muscle.* Proc Natl Acad Sci U S A, 1999. 96(25): p. 14482-6.

38. Ferrari, G., et al., *Muscle regeneration by bone marrow-derived myogenic progenitors.* Science, 1998. 279(5356): p. 1528-30.

39. Galli, R., et al., *Regulation of neuronal differentiation in human CNS stem cell progeny by leukemia inhibitory factor.* Dev Neurosci, 2000. 22(1-2): p. 86-95.

40. Young, H.E., et al., *Human reserve pluripotent mesenchymal stem cells are present in the connective tissues of skeletal muscle and dermis derived from fetal, adult, and geriatric donors.* Anat Rec, 2001. 264(1): p. 51-62.

41. Qu-Petersen, Z., et al., *Identification of a novel population of muscle stem cells in mice: potential for muscle regeneration.* J Cell Biol, 2002. 157(5): p. 851-64.

42. Peault, B., et al., *Stem and progenitor cells in skeletal muscle development, maintenance, and therapy.* Mol Ther, 2007. 15(5): p. 867-77.

43. Oshima, H., et al., *Differential myocardial infarct repair with muscle stem cells compared to myoblasts.* Mol Ther, 2005. 12(6): p. 1130-41.

44. Payne, T.R., et al., *Regeneration of dystrophin-expressing myocytes in the mdx heart by skeletal muscle stem cells.* Gene Ther, 2005. 12(16): p. 1264-74.

45. Zheng, B., et al., *Prospective identification of myogenic endothelial cells in human skeletal muscle.* Nat Biotechnol, 2007. 25(9): p. 1025-34.

46. Cossu, G. and P. Bianco, *Mesoangioblasts--vascular progenitors for extravascular mesodermal tissues.* Curr Opin Genet Dev, 2003. 13(5): p. 537-42.

47. Guttinger, M., et al., *Allogeneic mesoangioblasts give rise to alpha-sarcoglycan expressing fibers when transplanted into dystrophic mice.* Exp Cell Res, 2006. 312(19): p. 3872-9.

48. Sampaolesi, M., et al., *Cell therapy of alpha-sarcoglycan null dystrophic mice through intra-arterial delivery of mesoangioblasts.* Science, 2003. 301(5632): p. 487-92.

49. Galvez, B.G., et al., *Complete repair of dystrophic skeletal muscle by mesoangioblasts with enhanced migration ability.* J Cell Biol, 2006. 174(2): p. 231-43.

50. Palumbo, R., et al., *Extracellular HMGB1, a signal of tissue damage, induces mesoangioblast migration and proliferation.* J Cell Biol, 2004. 164(3): p. 441-9.

51. Galvez, B.G., et al., *Cardiac mesoangioblasts are committed, self-renewable progenitors, associated with small vessels of juvenile mouse ventricle.* Cell Death Differ, 2008. 15(9): p. 1417-28.

52. Sampaolesi, M., et al., *Mesoangioblast stem cells ameliorate muscle function in dystrophic dogs.* Nature, 2006. 444(7119): p. 574-9.

53. Tedesco, F.S., et al., *Stem cell-mediated transfer of a human artificial chromosome ameliorates muscular dystrophy.* Sci Transl Med, 2011. 3(96): p. 96ra78.

54. Cossu, G., et al., *Intra-arterial transplantation of HLA-matched donor mesoangioblasts in Duchenne muscular dystrophy.* EMBO Mol Med, 2015. 7(12): p. 1513-28.

55. Dellavalle, A., et al., *Pericytes of human skeletal muscle are myogenic precursors distinct from satellite cells.* Nat Cell Biol, 2007. 9(3): p. 255-67.

56. Caplan, A.I., *Why are MSCs therapeutic? New data: new insight.* J Pathol, 2009. 217(2): p. 318-24.

57. Torrente, Y., et al., *Human circulating AC133(+) stem cells restore dystrophin expression and ameliorate function in dystrophic skeletal muscle.* J Clin Invest, 2004. 114(2): p. 182-95.

58. Benchaouir, R., et al., *Restoration of human dystrophin following transplantation of exon-skipping-engineered DMD patient stem cells into dystrophic mice.* Cell Stem Cell, 2007. 1(6): p. 646-57.

59. Torrente, Y., et al., *Autologous transplantation of muscle-derived CD133+ stem cells in Duchenne muscle patients.* Cell Transplant, 2007. 16(6): p. 563-77.

60. Zannettino, A.C., P.J. Psaltis, and S. Gronthos, *Home is where the heart is: via the FROUNT.* Cell Stem Cell, 2008. 2(6): p. 513-4.

61. Hoogduijn, M.J., et al., *Human heart, spleen, and perirenal fat-derived mesenchymal stem cells have immunomodulatory capacities.* Stem Cells Dev, 2007. 16(4): p. 597-604.

62. He, Q., C. Wan, and G. Li, *Concise review: multipotent mesenchymal stromal cells in blood.* Stem Cells, 2007. 25(1): p. 69-77.

63. Jo, Y.Y., et al., *Isolation and characterization of postnatal stem cells from human dental tissues.* Tissue Eng, 2007. 13(4): p. 767-73.

64. Oh, W., et al., *Immunological properties of umbilical cord blood-derived mesenchymal stromal cells.* Cell Immunol, 2008. 251(2): p. 116-23.

65. Pittenger, M.F., et al., *Multilineage potential of adult human mesenchymal stem cells.* Science, 1999. 284(5411): p. 143-7.

66. Lepski, G., et al., *Limited Ca2+ and PKA-pathway dependent neurogenic differentiation of human adult mesenchymal stem cells as compared to fetal neuronal stem cells.* Exp Cell Res, 2010. 316(2): p. 216-31.

67. Liu, Y., et al., *Sox17 is essential for the specification of cardiac mesoderm in embryonic stem cells.* Proc Natl Acad Sci U S A, 2007. 104(10): p. 3859-64.

68. Chivu, M., et al., *In vitro hepatic differentiation of human bone marrow mesenchymal stem cells under differential exposure to liver-specific factors.* Transl Res, 2009. 154(3): p. 122-32.

69. Xie, Q.P., et al., *Human bone marrow mesenchymal stem cells differentiate into insulin-producing cells upon microenvironmental manipulation in vitro.* Differentiation, 2009. 77(5): p. 483-91.

70. Chang, D.J., *The "no-drill" technique of anterior clinoidectomy: a cranial base approach to the paraclinoid and parasellar region.* Neurosurgery, 2009. 64(3 Suppl): p. ons96-105; discussion ons105-6.

71. Rojas, M., et al., *Bone marrow-derived mesenchymal stem cells in repair of the injured lung.* Am J Respir Cell Mol Biol, 2005. 33(2): p. 145-52.

72. Qian, H., et al., *Bone marrow mesenchymal stem cells ameliorate rat acute renal failure by differentiation into renal tubular epithelial-like cells.* Int J Mol Med, 2008. 22(3): p. 325-32.

73. Goncalves, M.A., et al., *Human mesenchymal stem cells ectopically expressing full-length dystrophin can complement Duchenne muscular dystrophy myotubes by cell fusion.* Hum Mol Genet, 2006. 15(2): p. 213-21.

74. Yang, Y.W., et al., *[Experimental study on influence of bone marrow mesenchymal stem cells on activation and function of mouse peritoneal macrophages].* Zhonghua Xue Ye Xue Za Zhi, 2008. 29(8): p. 540-3.

75. Rafei, M., et al., *Mesenchymal stromal cells ameliorate experimental autoimmune encephalomyelitis by inhibiting CD4 Th17 T cells in a CC chemokine ligand 2-dependent manner.* J Immunol, 2009. 182(10): p. 5994-6002.

76. Selmani, Z., et al., *Human leukocyte antigen-G5 secretion by human mesenchymal stem cells is required to suppress T lymphocyte and natural killer function and to induce CD4+CD25highFOXP3+ regulatory T cells.* Stem Cells, 2008. 26(1): p. 212-22.

77. Linero, I. and O. Chaparro, *Paracrine effect of mesenchymal stem cells derived from human adipose tissue in bone regeneration.* PLoS One, 2014. 9(9): p. e107001.

78. Brockington, M., et al., *Mutations in the fukutin-related protein gene (FKRP) cause a form of congenital muscular dystrophy with secondary laminin alpha2 deficiency and abnormal glycosylation of alpha-dystroglycan.* Am J Hum Genet, 2001. 69(6): p. 1198-209.

79. Sparks, S.E., et al., *Congenital Muscular Dystrophy Overview*, in *GeneReviews(R)*, R.A. Pagon, et al., Editors. 1993: Seattle (WA).

80. Mendell, J.R., D.R. Boue, and P.T. Martin, *The congenital muscular dystrophies: recent advances and molecular insights.* Pediatr Dev Pathol, 2006. 9(6): p. 427-43.

81. Lampe, A.K., et al., *Collagen Type VI-Related Disorders*, in *GeneReviews(R)*, R.A. Pagon, et al., Editors. 1993: Seattle (WA).

82. Tetreault, M., et al., *A new form of congenital muscular dystrophy with joint hyperlaxity maps to 3p23-21.* Brain, 2006. 129(Pt 8): p. 2077-84.

83. Mitsuhashi, S., et al., *A congenital muscular dystrophy with mitochondrial structural abnormalities caused by defective de novo phosphatidylcholine biosynthesis.* Am J Hum Genet, 2011. 88(6): p. 845-851.

84. Klein, A., et al., *Differential diagnosis of congenital muscular dystrophies.* Eur J Paediatr Neurol, 2008. 12(5): p. 371-7.

85. Bonnemann, C.G., et al., *Diagnostic approach to the congenital muscular dystrophies.* Neuromuscul Disord, 2014. 24(4): p. 289-311.

86. Smalheiser, N.R. and N.B. Schwartz, *Cranin: a laminin-binding protein of cell membranes.* Proc Natl Acad Sci U S A, 1987. 84(18): p. 6457-61.

87. Ibraghimov-Beskrovnaya, O., V.C. Sheffield, and K.P. Campbell, *Single base polymorphism in the DAG1 gene detected by DGGE and mismatch PCR.* Hum Mol Genet, 1993. 2(11): p. 1983.

88. Taniguchi-Ikeda, M., et al., *Mechanistic aspects of the formation of alpha-dystroglycan and therapeutic research for the treatment of alpha-dystroglycanopathy: A review.* Mol Aspects Med, 2016. 51: p. 115-24.

89. Endo, T., *Glycobiology of alpha-dystroglycan and muscular dystrophy.* J Biochem, 2015. 157(1): p. 1-12.

90. Barresi, R. and K.P. Campbell, *Dystroglycan: from biosynthesis to pathogenesis of human disease.* J Cell Sci, 2006. 119(Pt 2): p. 199-207.

91. Durbeej, M. and K.P. Campbell, *Muscular dystrophies involving the dystrophin-glycoprotein complex: an overview of current mouse models.* Curr Opin Genet Dev, 2002. 12(3): p. 349-61.

92. Bozzi, M., et al., *Functional diversity of dystroglycan.* Matrix Biol, 2009. 28(4): p. 179-87.

93. Dobson, C.M., et al., *O-Mannosylation and human disease.* Cell Mol Life Sci, 2013. 70(16): p. 2849-57.

94. Praissman, J.L. and L. Wells, *Mammalian O-mannosylation pathway: glycan structures, enzymes, and protein substrates.* Biochemistry, 2014. 53(19): p. 3066-78.

95. Yoshida-Moriguchi, T., et al., *SGK196 is a glycosylation-specific O-mannose kinase required for dystroglycan function.* Science, 2013. 341(6148): p. 896-9.

96. Willer, T., et al., *The glucuronyltransferase B4GAT1 is required for initiation of LARGE-mediated alpha-dystroglycan functional glycosylation.* Elife, 2014. 3.

97. Inamori, K., et al., *Dystroglycan function requires xylosyl- and glucuronyltransferase activities of LARGE.* Science, 2012. 335(6064): p. 93-6.

98. Kanagawa, M., et al., *Identification of a Post-translational Modification with Ribitol-Phosphate and Its Defect in Muscular Dystrophy.* Cell Rep, 2016. 14(9): p. 2209-23.

99. Godfrey, C., et al., *Refining genotype phenotype correlations in muscular dystrophies with defective glycosylation of dystroglycan.* Brain, 2007. 130(Pt 10): p. 2725-35.

100. Jimenez-Mallebrera, C., et al., *A comparative study of alpha-dystroglycan glycosylation in dystroglycanopathies suggests that the hypoglycosylation of alpha-dystroglycan does not consistently correlate with clinical severity.* Brain Pathol, 2009. 19(4): p. 596-611.

101. Fukuyama, Y., M. Osawa, and H. Suzuki, *Congenital progressive muscular dystrophy of the Fukuyama type - clinical, genetic and pathological considerations.* Brain Dev, 1981. 3(1): p. 1-29.

102. Cormand, B., et al., *Clinical and genetic distinction between Walker-Warburg syndrome and muscle-eye-brain disease.* Neurology, 2001. 56(8): p. 1059-69.

103. Topaloglu, H., et al., *FKRP gene mutations cause congenital muscular dystrophy, mental retardation, and cerebellar cysts.* Neurology, 2003. 60(6): p. 988-92.

104. MacLeod, H., et al., *A novel FKRP mutation in congenital muscular dystrophy disrupts the dystrophin glycoprotein complex.* Neuromuscul Disord, 2007. 17(4): p. 285-9.

105. Whitmore, C., et al., *The transgenic expression of LARGE exacerbates the muscle phenotype of dystroglycanopathy mice.* Hum Mol Genet, 2014. 23(7): p. 1842-55.

106. Blaeser, A., et al., *Progressive Dystrophic Pathology in Diaphragm and Impairment of Cardiac Function in FKRP P448L Mutant Mice.* PLoS One, 2016. 11(10): p. e0164187.

107. Boito, C.A., et al., *Clinical and molecular characterization of patients with limb-girdle muscular dystrophy type 2I.* Arch Neurol, 2005. 62(12): p. 1894-9.

108. Brockington, M., et al., *Mutations in the fukutin-related protein gene (FKRP) identify limb girdle muscular dystrophy 2I as a milder allelic variant of congenital muscular dystrophy MDC1C.* Hum Mol Genet, 2001. 10(25): p. 2851-9.

109. Brown, S.C., et al., *Abnormalities in alpha-dystroglycan expression in MDC1C and LGMD2I muscular dystrophies.* Am J Pathol, 2004. 164(2): p. 727-37.

110. Esapa, C.T., et al., *Functional requirements for fukutin-related protein in the Golgi apparatus.* Hum Mol Genet, 2002. 11(26): p. 3319-31.

111. Matsumoto, H., et al., *Subcellular localization of fukutin and fukutin-related protein in muscle cells.* J Biochem, 2004. 135(6): p. 709-12.

112. Torelli, S., et al., *Sub-cellular localisation of fukutin related protein in different cell lines and in the muscle of patients with MDC1C and LGMD2I.* Neuromuscul Disord, 2005. 15(12): p. 836-43.

113. Dolatshad, N.F., et al., *Mutated fukutin-related protein (FKRP) localises as wild type in differentiated muscle cells.* Exp Cell Res, 2005. 309(2): p. 370-8.

114. Beedle, A.M., P.M. Nienaber, and K.P. Campbell, *Fukutin-related protein associates with the sarcolemmal dystrophin-glycoprotein complex.* J Biol Chem, 2007. 282(23): p. 16713-7.

115. Lu, P.J., et al., *Mutations alter secretion of fukutin-related protein.* Biochim Biophys Acta, 2010. 1802(2): p. 253-8.

116. Saito, T., et al., *A secreted type of beta 1,6-N-acetylglucosaminyltransferase V (GnT-V) induces tumor angiogenesis without mediation of glycosylation: a novel function of GnT-V distinct from the original glycosyltransferase activity*. J Biol Chem, 2002. 277(19): p. 17002-8.

117. Gerin, I., et al., *ISPD produces CDP-ribitol used by FKTN and FKRP to transfer ribitol phosphate onto alpha-dystroglycan.* Nat Commun, 2016. 7: p. 11534.

118. Vannoy, C.H., et al., *Adeno-associated virus-mediated overexpression of LARGE rescues alpha-dystroglycan function in dystrophic mice with mutations in the fukutin-related protein.* Hum Gene Ther Methods, 2014. 25(3): p. 187-96.

119. Krag, T.O. and J. Vissing, *A New Mouse Model of Limb-Girdle Muscular Dystrophy Type 2I Homozygous for the Common L276I Mutation Mimicking the Mild Phenotype in Humans.* J Neuropathol Exp Neurol, 2015. 74(12): p. 1137-46.

120. Qiao, C., et al., *Muscle and heart function restoration in a limb girdle muscular dystrophy 2I (LGMD2I) mouse model by systemic FKRP gene delivery.* Mol Ther, 2014. 22(11): p. 1890-9.

121. Ackroyd, M.R., et al., *Reduced expression of fukutin related protein in mice results in a model for fukutin related protein associated muscular dystrophies.* Brain, 2009. 132(Pt 2): p. 439-51.

122. Goyenvalle, A., et al., *Functional correction in mouse models of muscular dystrophy using exon-skipping tricyclo-DNA oligomers.* Nat Med, 2015. 21(3): p. 270-5.

123. Wang, B., et al., *A canine minidystrophin is functional and therapeutic in mdx mice.* Gene Ther, 2008. 15(15): p. 1099-106.

124. Wells, D.J., et al., *Expression of human full-length and minidystrophin in transgenic mdx mice: implications for gene therapy of Duchenne muscular dystrophy.* Hum Mol Genet, 1995. 4(8): p. 1245-50.

125. Barresi, R., et al., *LARGE can functionally bypass alpha-dystroglycan glycosylation defects in distinct congenital muscular dystrophies.* Nat Med, 2004. 10(7): p. 696-703.

126. Kanagawa, M., et al., *Impaired viability of muscle precursor cells in muscular dystrophy with glycosylation defects and amelioration of its severe phenotype by limited gene expression.* Hum Mol Genet, 2013. 22(15): p. 3003-15.

127. Xu, L., et al., *Adeno-associated virus 9 mediated FKRP gene therapy restores functional glycosylation of alpha-dystroglycan and improves muscle functions.* Mol Ther, 2013. 21(10): p. 1832-40.

128. Okada, T. and S. Takeda, *Current Challenges and Future Directions in Recombinant AAV-Mediated Gene Therapy of Duchenne Muscular Dystrophy.* Pharmaceuticals (Basel), 2013. 6(7): p. 813-36.

129. Nguyen, H.H., et al., *Overexpression of the cytotoxic T cell GalNAc transferase in skeletal muscle inhibits muscular dystrophy in mdx mice.* Proc Natl Acad Sci U S A, 2002. 99(8): p. 5616-21.

130. Ohtsuka, Y., et al., *Fukutin is prerequisite to ameliorate muscular dystrophic phenotype by myofiber-selective LARGE expression.* Sci Rep, 2015. 5: p. 8316.

131. Bao, X., et al., *Tumor suppressor function of laminin-binding alpha-dystroglycan requires a distinct beta3-N-acetylglucosaminyltransferase.* Proc Natl Acad Sci U S A, 2009. 106(29): p. 12109-14.

132. Miller, M.R., et al., *Downregulation of dystroglycan glycosyltransferases LARGE2 and ISPD associate with increased mortality in clear cell renal cell carcinoma.* Mol Cancer, 2015. 14: p. 141.

133. Annexstad, E.J., I. Lund-Petersen, and M. Rasmussen, *Duchenne muscular dystrophy.* Tidsskr Nor Laegeforen, 2014. 134(14): p. 1361-4.

134. Darin, N., et al., *Inflammation and response to steroid treatment in limb-girdle muscular dystrophy 2I.* Eur J Paediatr Neurol, 2007. 11(6): p. 353-7.

135. Foltz, S.J., et al., *Four-week rapamycin treatment improves muscular dystrophy in a fukutin-deficient mouse model of dystroglycanopathy.* Skelet Muscle, 2016. 6: p. 20.

136. Martin-Rendon, E. and D.J. Blake, *Protein glycosylation in disease: new insights into the congenital muscular dystrophies.* Trends Pharmacol Sci, 2003. 24(4): p. 178-83.

137. Dwek, R.A., *Biological importance of glycosylation.* Dev Biol Stand, 1998. 96: p. 43-7.

138. Spiro, R.G., *Protein glycosylation: nature, distribution, enzymatic formation, and disease implications of glycopeptide bonds.* Glycobiology, 2002. 12(4): p. 43R-56R.

139. Van den Steen, P., et al., *Concepts and principles of O-linked glycosylation.* Crit Rev Biochem Mol Biol, 1998. 33(3): p. 151-208.

140. Wandall, H.H., et al., *The origin and function of platelet glycosyltransferases.* Blood, 2012. 120(3): p. 626-35.

141. Lee-Sundlov, M.M., et al., *Circulating blood and platelets supply glycosyltransferases that enable extrinsic extracellular glycosylation.* Glycobiology, 2017. 27(2): p. 188-198.

142. Pienimaeki-Roemer, A., et al., *Lipidomic and proteomic characterization of platelet extracellular vesicle subfractions from senescent platelets.* Transfusion, 2015. 55(3): p. 507-21.

143. Varki, A., H.H. Freeze, and A.E. Manzi, *Overview of glycoconjugate analysis.* Curr Protoc Protein Sci, 2009. Chapter 12: p. Unit 12 1 12 1 1-8.

144. Palmisano, G., et al., *Characterization of membrane-shed microvesicles from cytokine-stimulated beta-cells using proteomics strategies.* Mol Cell Proteomics, 2012. 11(8): p. 230-43.

145. van der Pol, E., et al., *Classification, functions, and clinical relevance of extracellular vesicles.* Pharmacol Rev, 2012. 64(3): p. 676-705.

146. Thery, C., et al., *Isolation and characterization of exosomes from cell culture supernatants and biological fluids.* Curr Protoc Cell Biol, 2006. Chapter 3: p. Unit 3 22.

147. Tucker, E.M. and J.D. Young, *Biochemical changes during reticulocyte maturation in culture. A comparison of genetically different sheep erythrocytes.* Biochem J, 1980. 192(1): p. 33-9.

148. Johnstone, R.M., *The Jeanne Manery-Fisher Memorial Lecture 1991. Maturation of reticulocytes: formation of exosomes as a mechanism for shedding membrane proteins.* Biochem Cell Biol, 1992. 70(3-4): p. 179-90.

149. Valadi, H., et al., *Exosome-mediated transfer of mRNAs and microRNAs is a novel mechanism of genetic exchange between cells.* Nat Cell Biol, 2007. 9(6): p. 654-9.

150. Lobb, R.J., et al., *Optimized exosome isolation protocol for cell culture supernatant and human plasma.* J Extracell Vesicles, 2015. 4: p. 27031.

151. Tang, Y.T., et al., *Comparison of isolation methods of exosomes and exosomal RNA from cell culture medium and serum.* Int J Mol Med, 2017. 40(3): p. 834-844.

152. Rashed, M.H., et al., *Exosomal miR-940 maintains SRC-mediated oncogenic activity in cancer cells: a possible role for exosomal disposal of tumor suppressor miRNAs.* Oncotarget, 2017. 8(12): p. 20145-20164.

153. Hu, G.W., et al., *Exosomes secreted by human-induced pluripotent stem cell-derived mesenchymal stem cells attenuate limb ischemia by promoting angiogenesis in mice.* Stem Cell Res Ther, 2015. 6: p. 10.

154. Barile, L. and G. Vassalli, *Exosomes: Therapy delivery tools and biomarkers of diseases.* Pharmacol Ther, 2017. 174: p. 63-78.

155. Skog, J., et al., *Glioblastoma microvesicles transport RNA and proteins that promote tumour growth and provide diagnostic biomarkers.* Nat Cell Biol, 2008. 10(12): p. 1470-6.

156. Melo, S.A., et al., *Glypican-1 identifies cancer exosomes and detects early pancreatic cancer.* Nature, 2015. 523(7559): p. 177-82.

157. Chen, L., et al., *Cardiac progenitor-derived exosomes protect ischemic myocardium from acute ischemia/reperfusion injury.* Biochem Biophys Res Commun, 2013. 431(3): p. 566-71.

158. Barile, L., et al., *Extracellular vesicles from human cardiac progenitor cells inhibit cardiomyocyte apoptosis and improve cardiac function after myocardial infarction.* Cardiovasc Res, 2014. 103(4): p. 530-41.

159. Robbins, P.D. and A.E. Morelli, *Regulation of immune responses by extracellular vesicles.* Nat Rev Immunol, 2014. 14(3): p. 195-208.

160. Viaud, S., et al., *Dendritic cell-derived exosomes for cancer immunotherapy: what's next?* Cancer Res, 2010. 70(4): p. 1281-5.

161. Jang, S.C., et al., *Bioinspired exosome-mimetic nanovesicles for targeted delivery of chemotherapeutics to malignant tumors.* ACS Nano, 2013. 7(9): p. 7698-710.

162. Mulcahy, L.A., R.C. Pink, and D.R. Carter, *Routes and mechanisms of extracellular vesicle uptake.* J Extracell Vesicles, 2014. 3.

163. Kooijmans, S.A.A., et al., *Modulation of tissue tropism and biological activity of exosomes and other extracellular vesicles: New nanotools for cancer treatment.* Pharmacol Res, 2016. 111: p. 487-500.

164. Mangeot, P.E., et al., *Protein transfer into human cells by VSV-G-induced nanovesicles.* Mol Ther, 2011. 19(9): p. 1656-66.

165. Cervio, E., et al., *Exosomes for Intramyocardial Intercellular Communication.* Stem Cells Int, 2015. 2015: p. 482171.

166. Yang, C., et al., *Plasma-derived MHC class II+ exosomes from tumor-bearing mice suppress tumor antigen-specific immune responses.* Eur J Immunol, 2012. 42(7): p. 1778-84.

167. Gourlay, J., et al., *The emergent role of exosomes in glioma.* J Clin Neurosci, 2017. 35: p. 13-23.

168. Zhuang, X., et al., *Treatment of brain inflammatory diseases by delivering exosome encapsulated anti-inflammatory drugs from the nasal region to the brain.* Mol Ther, 2011. 19(10): p. 1769-79.

169. Andras, I.E., et al., *Extracellular vesicles of the blood-brain barrier: Role in the HIV-1 associated amyloid beta pathology.* Mol Cell Neurosci, 2017. 79: p. 12-22.

170. Hood, J.L., R.S. San, and S.A. Wickline, *Exosomes released by melanoma cells prepare sentinel lymph nodes for tumor metastasis.* Cancer Res, 2011. 71(11): p. 3792-801.

171. Kharaziha, P., et al., *Tumor cell-derived exosomes: a message in a bottle.* Biochim Biophys Acta, 2012. 1826(1): p. 103-11.

172. Takahashi, Y., et al., *Visualization and in vivo tracking of the exosomes of murine melanoma B16-BL6 cells in mice after intravenous injection.* J Biotechnol, 2013. 165(2): p. 77-84.

173. Wiklander, O.P., et al., *Extracellular vesicle in vivo biodistribution is determined by cell source, route of administration and targeting.* J Extracell Vesicles, 2015. 4: p. 26316.

174. Conboy, M.J. and I.M. Conboy, *Preparation of adult muscle fiber-associated stem/precursor cells.* Methods Mol Biol, 2010. 621: p. 149-63.

175. Schumacher, Y., et al., *Dysregulated CRTC1 activity is a novel component of PGE2 signaling that contributes to colon cancer growth.* Oncogene, 2016. 35(20): p. 2602-14.

176. Ge, X., J. Yu, and H. Jiang, *Growth hormone stimulates protein synthesis in bovine skeletal muscle cells without altering insulin-like growth factor-I mRNA expression.* J Anim Sci, 2012. 90(4): p. 1126-33.

177. Lagana, M. and M.T. Raimondi, *A miniaturized, optically accessible bioreactor for systematic 3D tissue engineering research.* Biomed Microdevices, 2012. 14(1): p. 225-34.

178. Li, P., et al., *Progress in Exosome Isolation Techniques.* Theranostics, 2017. 7(3): p. 789-804.

179. Herbst, R., et al., *Aberrant development of neuromuscular junctions in glycosylation-defective Large(myd) mice.* Neuromuscul Disord, 2009. 19(5): p. 366-78.

180. Jaffe, A., et al., *Gene therapy for children with cystic fibrosis--who has the right to choose?* J Med Ethics, 2006. 32(6): p. 361-4.

181. Negroni, E., et al., *In vivo myogenic potential of human CD133+ muscle-derived stem cells: a quantitative study.* Mol Ther, 2009. 17(10): p. 1771-8.

182. Gicquel, E., et al., *AAV-mediated transfer of FKRP shows therapeutic efficacy in a murine model but requires control of gene expression.* Hum Mol Genet, 2017. 26(10): p. 1952-1965.

183. Keramaris-Vrantsis, E., et al., *Fukutin-related protein localizes to the Golgi apparatus and mutations lead to mislocalization in muscle in vivo.* Muscle Nerve, 2007. 36(4): p. 455-65.

184. Moldovan, L., et al., *Analyzing the circulating microRNAs in exosomes/extracellular vesicles from serum or plasma by qRT-PCR.* Methods Mol Biol, 2013. 1024: p. 129-45.

185. Martins, V.R., M.S. Dias, and P. Hainaut, *Tumor-cell-derived microvesicles as carriers of molecular information in cancer.* Curr Opin Oncol, 2013. 25(1): p. 66-75.

186. Coumans, F.A.W., et al., *Methodological Guidelines to Study Extracellular Vesicles.* Circ Res, 2017. 120(10): p. 1632-1648.

187. Holbeck-Brendel, M. and B.K. Poulsen, *Treatment with enzyme replacement therapy during pregnancy in a patient with Pompe disease.* Neuromuscul Disord, 2017.

188. Zhang, J., et al., *Exosome and exosomal microRNA: trafficking, sorting, and function.* Genomics Proteomics Bioinformatics, 2015. 13(1): p. 17-24.

189. Lai, C.P., et al., *Dynamic biodistribution of extracellular vesicles in vivo using a multimodal imaging reporter.* ACS Nano, 2014. 8(1): p. 483-494.

190. Lai, C.P., et al., *Visualization and tracking of tumour extracellular vesicle delivery and RNA translation using multiplexed reporters.* Nat Commun, 2015. 6: p. 7029.

SCIENTIFIC PRODUCTS

- Meregalli M, Farini A, Sitzia C, Beley C, Razini P, Cassinelli L, Colleoni F, **Frattini P**, Santo N, Galbiati E, Prosperi D, Tavelli A, Belicchi M, Garcia L, Torrente Y. Stem Cell-Mediated Exon Skipping of the Dystrophin Gene by the Bystander Effect. *Current Gene Therapy,* 2015. 15(6), p. 563 - 571
- **Frattini P**, Villa C, De Santis F, Meregalli M, Belicchi M, Erratico S, Bella P, Raimondi MT, Lu Q, Torrente Y. Autologous intramuscular transplantation of engineered satellite cells induces exosome-mediated systemic expression of Fukutin-related protein and rescues disease phenotype in a murine model of limb-girdle muscular dystrophy type 2I. *Human Molecular Genetics*, 2017. 26(19):3682-3698.

CONGRESSES

- **Stem Cell Research Italy (SCRI),** 28th-30th May 2014. **Poster presentation**: ‘’Full-Length Dysferlin Expression Driven by Engineered Human Dystrophic Blood-Derived CD133+ Stem Cells’’ ; **P. Frattini**, M. Meregalli, C. Navarro, C. Sitzia, A. Farini, E. Montani, P. Razini, L. Cassinelli, M. Belicchi, D. Parazzoli, L. Garcia, Y. Torrente. ***AWARD FOR BEST POSTER PRESENTATION***.

- **Myology,** 14th-18th March 2016. **Poster presentation:** ‘’FKRP rescue in blood-derived 133+ cells isolated from patients affected by Congenital Muscular Dystrophies’’; **P. Frattini**, F. De Santis, P. Razini, S. Erratico, M. Meregalli and Y. Torrente.

RINGRAZIAMENTI

Dopo tre lunghi e intensi anni finalmente il momento è arrivato: scrivere queste frasi di ringraziamento sarà il tocco finale della mia tesi.
Questi quattro anni in laboratorio sono stati per me un periodo di profondo apprendimento, non solo scientifico, ma anche personale.
Quello che ho appreso, più di ogni altra cosa, è che la ricerca scientifica non è solo un lavoro, ma una passione da affrontare con estrema dedizione, in grado di regalare tante soddisfazioni, quante frustrazioni.
Vorrei in primo luogo ringraziare il Prof. Giacomo Comi, tutore del mio lavoro di tesi, per la sua disponibilità.
Un particolare ringraziamento va al Prof. Yvan Torrente, per avermi dato l'opportunità di svolgere il dottorato nel laboratorio di Cellule Staminali, ma soprattutto per avermi cresciuta lungo questo percorso.
Un ''grazie'' vorrei dedicarlo alla Dott.ssa Chiara Villa, che più di ogni altro ha contribuito alla stesura di questa tesi, nonostante tutte le difficoltà incontrate, spero di essere stata per lei una valida ''prima studentessa PhD''.
Grazie a tutti i miei colleghi e agli studenti che in questi anni hanno lasciato il loro segno in laboratorio e in me, siete stati una seconda famiglia!
Tra tutti, Pamela. Per l'aiuto che ho trovato in lei quotidianamente. Per la sua forza, la grinta, la motivazione, nel lavoro e nella vita. Sei stata per me un esempio.
…Ai miei genitori e mia sorella, per il supporto che mi hanno dato nonostante quest'anno di difficoltà. Nessun problema è insormontabile, se alle spalle c'è l'unione di una famiglia.
…A Luca, il mio braccio destro e la mia forza. Per il sostegno che mi ha dato, credendo in me più di chiunque altro. Per il suo modo ammirevole di vivere e affrontare le difficoltà con il sorriso…e alla sua famiglia, che in questi sei anni è stata anche un po' la mia.

...Ai miei amici, nominarli tutti sarebbero troppi! In particolare a Laura, Ada, Giulia, Elena e Paola. Per le nostre serate e le nostre risate, studiate ad hoc per non lasciarmi mai sola nei momenti di sconforto!
…Agli amici del maneggio, per le bellissime giornate trascorse insieme a cavallo e la semplicità con cui condividiamo questa passione!
…Agli amici del sub, soprattutto a Cinzia, che mi ha permesso di scoprire questo mondo nuovo, insegnandomi a credere in me stessa e a cercare sempre di superare i miei limiti e le mie paure.

Mi sento di concludere questi ringraziamenti citando una delle più celebri frasi di Einstein, poiché perfettamente riflette lo spirito con cui, giorno dopo giorno, ho affrontato questo mio percorso:

Le tre regole di lavoro:
1. Esci dalla confusione, trova semplicità.
2. Dalla discordia, trova armonia.
3. Nel pieno delle difficoltà, risiede l'occasione favorevole